MICROCOPY RESOLUTION TEST CHART

NATIONAL BUREAU OF STANDARDS-1963-A

USAFA-TR-83-2

AIR FORCE ACADEMY
Aeronautics Digest – Spring/Summer 1982

MARCH 1983
Final Report

APPROVED FOR PUBLIC RELEASE: DISTRIBUTION UNLIMITED

Department of Aeronautics
Dean of the Faculty
United States Air Force Academy
Colorado 80840

83 05 18 075

COVER:
The cover shows the Lockheed SR-71 reconnaissance aircraft in flight.
This aircraft represents one of the many very successful programs
completed by the Advanced Development Products Division (known as the
"Skunk Works") of the Lockheed California Company under the leadership of
C.L. "Kelly" Johnson. In this issue Mr. Johnson's successor, Mr. Ben
Rich, discusses the philosophy of advanced aircraft design and development
that has made the "Skunk Works" so successful.

Editorial Review by Capt James M. Kempf, Department of English
USAF Academy, Colorado 80840

Thomas E. McCann, Lt. Colonel, USAF
Director of Research and Continuing Education
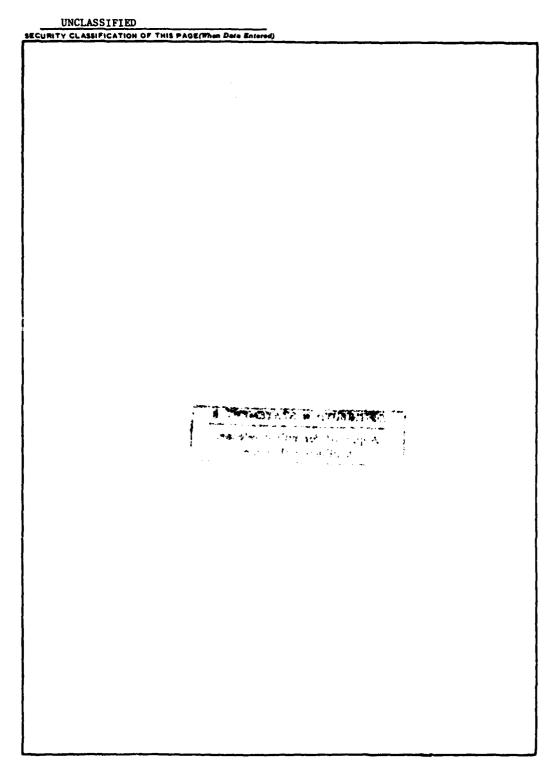
REPORT DOCUMENTATION PAGE	READ INSTRUCTIONS BEFORE COMPLETING FORM	
1. REPORT NUMBER USAFA-TR-83-2	2. GOVT ACCESSION NO. AD-A12 82 48	3. RECIPIENT'S CATALOG NUMBER
4. TITLE (and Subtitle) Air Force Academy Aeronautics Digest Spring/Summer 1982	5. TYPE OF REPORT & PERIOD COVERED Final Report	
	6. PERFORMING ORG. REPORT NUMBER	
7. AUTHOR(s) EDITORS: J. DeJongh, A.M. Higgins, J.M. Kempf, E.J. Jumper, M. Arends	8. CONTRACT OR GRANT NUMBER(s)	
9. PERFORMING ORGANIZATION NAME AND ADDRESS Department of Aeronautics United States Air Force Academy, CO 80840	10. PROGRAM ELEMENT, PROJECT, TASK AREA & WORK UNIT NUMBERS	
11. CONTROLLING OFFICE NAME AND ADDRESS	12. REPORT DATE March 1983	
	13. NUMBER OF PAGES 162	
14. MONITORING AGENCY NAME & ADDRESS(if different from Controlling Office)	15. SECURITY CLASS. (of this report)	
	15a. DECLASSIFICATION DOWNGRADING SCHEDULE	

16. DISTRIBUTION STATEMENT (of this Report)

DISTRIBUTION STATEMENT A

Approved for public release;
Distribution Unlimited

17. DISTRIBUTION STATEMENT (of the abstract entered in Block 20, if different from Report)

18. SUPPLEMENTARY NOTES

19. KEY WORDS (Continue on reverse side if necessary and identify by block number)

Aerodynamics, Propulsion, Thermodynamics, Wind Tunnel, Aeronautical
History, Engineering Education, Supersonic Flow, Wave Drag

20. ABSTRACT (Continue on reverse side if necessary and identify by block number)

This Digest covers unclassified research in aeronautics performed
at the United States Air Force Academy during the six months ending
15 August 1982. This report includes technical papers in the
specific areas of aerodynamics, propulsion, experimental
instrumentation, engineering education, and aeronautical history.

PREFACE

This report is the ninth issue of the Air Force Academy Aeronautics Digest* Our policy is to print articles which represent recent scholarly work by students and faculty of the Department of Aeronautics, members of other departments of the Academy and the Frank J. Seiler Research Laboratory, researchers directly or indirectly involved with USAFA-sponsored projects, and authors in fields of interest to the USAFA.

In addition to complete papers, the Digest includes, when appropriate, abstracts of lengthier reports and articles published in other formats. The editors will consider for publication contributions in the general field of Aeronautics, including:

> Aeronautical Engineering
> > Aerodynamics
> > Flight Mechanics
> > Propulsion
> > Structures
> > Instrumentation
> Fluid Dynamics
> Thermodynamics and Heat Transfer
> Biomechanics
> Engineering Education
> Aeronautical History

Papers on other topics will be considered on an individual basis. Contributions should be sent to:

> Editor, Aeronautics Digest
> DFAN
> US Air Force Academy, Co 80840

*The first eight issues of the Digest can be ordered from the Defense Technical Information Center (DTIC), Cameron Station, Alexandria, VA 22324. Use the following AD numbers: Aeronautics Digest - Spring 1978, ADA060207; Aeronautics Digest - Fall 1978, ADA069044; Aeronautics Digest - Spring 1979, ADA075419; Aeronautics Digest - Fall 1979, ADA085770; Aeronautics Digest - Spring/Summer 1980, ADA093378; Aeronautics Digest - Fall/Winter 1980, ADA108338; Aeronautics Digest - Spring/Summer 1981, ADA112421; Aeronautics Digest - Fall/Winter 1981, ADA119168.

CONTENTS

SECTION I

Aerodynamics

THE SUPERSONIC AREA RULE AND A PROPOSED SIMPLIFICATION

Eric J. Jumper*

Abstract

This paper outlines the development of the supersonic area rule from
theory to application. Then a simplification to the rule is introduced
which greatly reduces the complexity involved in using the full supersonic
area rule to predict wave drag increments. Finally, the results of
applying the modified rule to an F-15 aircraft configured with near-axis
conformal pallets are described.

I. Introduction

In supersonic flight drag is due to three separate phenomena. The
first two are the same as in subsonic flight: skin-friction drag (i.e.,
viscous drag) and pressure drag due to separated flow. In supersonic
flight the third phenomenon is known as wave drag, which is due to the
difference in pressure between regions of the flow separated by shock or
expansion waves. These waves emanate from flow boundaries (for example,
body surfaces) and may intersect with waves from other boundaries causing
interference effects. These interference effects further complicate an
already complicated analysis problem.

In 1956 Jones (Ref. 1) published a method of predicting wave drag
that included the interference effects. This method was similar in form
to the transonic area rule and was, therefore, christened the supersonic
area rule. Since the appearance of Jones' report, aerodynamicists have
exploited the supersonic area rule to determine wave-drag effects for
aircraft of various geometries and to determine the wave-drag effects of
changes in geometry such as fuselage shape and wing location. In 1957
Nelson and Welsh (Ref. 2) used a Fourier-series method for applying the
supersonic area rule in an extensive comparison between predicted results
obtained by using the rule and experimental data obtained for the same
configurations in wind-tunnel tests. They found that the rule provided

*Major, USAF, Associate Professor, Department of Aeronautics and
Astronautics, Air Force Institute of Technology, Wright Patterson AFB,
Ohio

predictions of wave drag which were reasonably close to those obtained in the wind tunnel. Then in 1963 Harris (Ref. 3) published a report describing a computer program written by Boeing Company that made possible the general application of the supersonic area rule for predicting wave drag. With the availability of high-speed computers, the Boeing program, or derivatives of it, came into standard use in larger and more extensive aerodynamic prediction and design programs such as that by Baals, Robins, and Harris (Ref. 4).

Aerodynamic prediction programs are useful not only in the design phase of planning a new airplane but also in understanding the effect of changes to existing aircraft configurations, such as adding wing stores, or enlarging a turret. While programs like the one written by Boeing are generally available and are, in fact, used in conjunction with wind-tunnel tests in the final stages of the design process, they are seldom used for early-management decisions or in system design studies. The main reason for this is that these computer programs require large computers and complicated input parameters. Further, the configurations to be considered might be quite numerous. These factors add up to an extremely expensive exercise.

If the supersonic area rule could be adapted for use on a small computer, it would greatly benefit early-management decisions and system design studies. However, the supersonic area rule, in its present form, is not suited for use on smaller computers because of large core storage requirements and the long computation time necessary. Looking at some specific applications of the area rule might indicate ways in which the rule could be streamlined to make it compatible with small computers.

One example of a program-management decision that could be aided by using the supersonic area rule is the placement of a near-fuselage-axis store or equipment pod. This decision might involve numerous candidate

locations chosen for other than aerodynamic reasons, such as structural
considerations. The use of the area rule would limit the number of
configurations to be studied further in wind-tunnel tests and/or in more
extensive analytic studies. Because this application involves changing an
existing configuration, much is already known about the original airplane
and only drag increments, due to locating the pod or to minor changes in
the pod shape at the same location, are of interest to the analyst

The supersonic area rule would also be helpful in system design
studies; however, these studies often determine volume requirements rather
than specific configurations. For example, the study might examine the
aerodynamic performance trade-off of adding some new avionics package
which can be accommodated only by adding volume to the fuselage of an
existing aircraft. If the envelope of the aircraft includes supersonic
flight, the supersonic area rule would clearly be helpful. However, these
system studies include many considerations other than predicting the
wave-drag effect, making the large computer-time requirement of the
supersonic area rule prohibitive. Further, the supersonic area rule
requires detailed information about a specific configuration and, as
mentioned above, the only configuration information which is likely to be
available is the volume requirement.

In both the management-decision example and the system-design-study
application, the requirement for precision in the wave-drag prediction is
relaxed, and the theoretician is given considerable license in modifying
the supersonic area rule to streamline its use. From a user's point of
view, the most important modifications to the supersonic area rule would
be those which would simplify the formulation of the input data describing
the aircraft configuration; however, modifications which reduce process
time and core storage requirements of the associated computer program are

4

also important and, in the end, may be the deciding factor in whether the
method is used.

This paper describes the supersonic area rule and a modification to
it which greatly simplifies its use and computer requirements. A program
that incorporates the modified area rule is also described. The results
of using the supersonic area rule and the modified rule are compared for a
number of aircraft configurations including an F-15 for which wind-tunnel
data had been collected with and without a near-fuselage-axis protuberance
in place.

II. Supersonic Area Rule

A. Theory

Suppose we consider an airplane in a steady supersonic flow whose
surfaces are inclined to the freestream by only a small amount. The
ideal-fluid flow field around the airplane is then amply described by the
linearized potential equation

$$\beta^2 \phi_{xx} - \phi_{yy} - \phi_{zz} = 0 \tag{1}$$

where $\beta^2 = M_\infty^2 - 1$, M_∞ is the freestream Mach number, ϕ is the velocity
potential, and the subscripts refer to differentiation in the streamwise
direction, x, and the two other orthonormal coordinates, y and z, of
cartesian three-space. Lomax (Ref. 5) showed that the general solution of
Eqn. (1) for the wave-drag coefficient, C_{D_w}, for a lifting or non-lifting
airplane is given by

$$C_{D_w} = \frac{1}{2\pi} \int_0^{2\pi} C_{D_w} (\theta) \, d\theta \tag{2}$$

where

$$C_{D_W}(\theta) = -\frac{1}{2\pi q S_b}\left\{\int_0^L\int_0^L S''(\xi)\ln\left|\frac{x}{L}-\frac{\xi}{L}\right|d\xi dx\right.$$

$$-\int_0^L\int_0^L\left[S''(\xi)\frac{\beta}{2q}\frac{df}{dx}+S''(x)\frac{\beta}{2q}\frac{df}{d\xi}\right]\ln\left|\frac{x}{L}-\frac{\xi}{L}\right|d\xi dx \tag{3}$$

$$+\int_0^L\int_0^L\frac{\beta^2}{4q^2}\frac{df}{d\xi}\frac{df}{dx}\ln\left|\frac{x}{L}-\frac{\xi}{L}\right|d\xi dx\left.\right\}$$
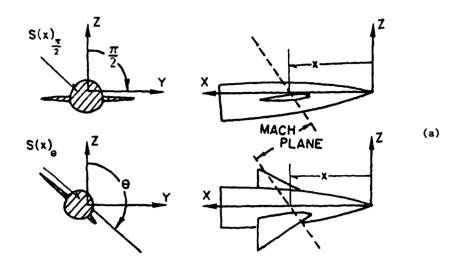
In Eqns. (2) and (3) θ is measured from a fixed coordinate relative to the freestream and indicates the orientation of a plane tangent to a Mach cone for M_∞ whose angle of inclination, μ, is $\sin^{-1}(1/M_\infty)$. S_b is some reference area and q is the reference pressure, one-half the density times the freestream velocity squared ($\frac{1}{2}\rho V_\infty^2$). To define the area $S(x)$, let the x-axis of a cartesian coordinate system be fixed parallel to the freestream with its origin at the nose (or most forward point) of the aircraft, and let a Mach plane of orientation θ intersect the x-axis at a point x. Then $S(x)$ is defined as the projection, normal to the x-axis, of the area formed by the intersection of the Mach plane and the aircraft. Figure 1a shows $S(x)$ at two orientation angles, $\pi/2$ and an arbitrary angle, θ. In Eqn. (3), f is the net force conormal to the stream direction and the θ direction (see Figure 1b), computed by a closed integration of the pressure around the surface, σ, cut by the Mach plane.

One might think of the coefficient of drag given in Eqn. (2) as consisting of the two parts given in Eqn. (4):

$$C_{D_W} = C_{D_O} + C_{D_L} = \frac{1}{2\pi}\left[\int_0^{2\pi}C_{D_O}(\theta)d\theta+\int_0^{2\pi}C_{D_L}(\theta)d\theta\right] \tag{4}$$

where the $C_{D_O}(\theta)$ consists of the first term on the right side of Eqn. (3) and $C_{D_L}(\theta)$ consists of the last two terms of Eqn. (3). It is clear that
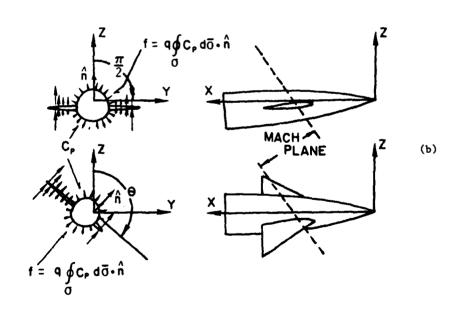
Figure 1.   Geometric Descriptions Employed in Computing the Wave-Drag: (a)
Forward Projection of the Airplane Section Cut by the Mach
Plane at Location x at Two Roll Angles $\pi/2$ and θ and (b)
Formation of the Net Conormal Force Term, f

only C_{D_L} (θ) contains terms requiring knowledge of the pressure distribution on the surface of the airplane. Although the subscript L on the term is slightly misleading, Lomax (Ref. 5) points out that when the orientation of θ is such that the positive net conormal force f is pointing up at 90 degrees to the freestream, f represents the net section lift. Thus, the terms of C_{D_L} (θ) do in a way resemble drag due to a "lift" of sorts.*

The supersonic area rule as described by Jones (Ref. 1) gives the formula for the approximate coefficient of drag as

$$C_{D_w} = \frac{1}{4\pi^2 q S_b} \int_0^{2\pi} \left[\int_0^L \int_0^L S''(\xi) \, S''(x) \, \ln \left| \frac{x}{L} - \frac{\xi}{L} \right| \, d\xi dx \right] d\theta \qquad (5)$$

where S(x) is defined in a similar way as for Eqn. (3).** Comparing Eqn. (5) to Eqn. (4) shows that the supersonic area rule is simply the C_{D_o} term of Lomax's more general expression which, you recall, was subject only to the limitations of linearized theory. As Nelson and Welsh (Ref. 2) demonstrated and Lomax (Ref. 5) himself pointed out, the C_{D_L} term of Eqn. (4) represents the limiting factor to the correctness of the supersonic area rule, Eqn. (5), even within the framework of linearized theory.

One cannot help but notice the striking resemblance of Eqn. (5) to von Karman's slender-body result for a closed (or constant radius at x=L) body of revolution (Ref. 6) that gives the wave-drag coefficient as

$$C_D = \frac{1}{2\pi q S_b} \int_0^L \int_0^L A''(\xi) \, A''(x) \, \ln \left| \frac{x}{L} - \frac{\xi}{L} \right| \, d\xi dx \qquad (6)$$

---

*In general, even nonlifting configurations will have non-zero $C_{D_L}(\theta)$'s.
**Jones suggests using the areas cut by the Mach planes; however, Nelson and Welsh (Ref. 2) found that using the same definition for S(x) as in Eqn. (3) gave better results.

where $A(x)$ is the cross-sectional area of the body of revolution. We may write the integrand of Eqn. (5) as

$$C_{D_w}(\theta) = \frac{1}{2\pi q S_b} \int_0^L \int_0^L S''(\xi) \, S''(x) \, \ln \left| \frac{x}{L} - \frac{\xi}{L} \right| \, d\xi dx \tag{7}$$

A comparison of Eqn. (7) to Eqn. (6) suggests an interpretation of Eqn. (7) as the von Karman coefficient of drag for an "equivalent" body of revolution for a given family of Mach planes of θ orientation. In this interpretation S of the θ Mach planes appears to simply replace the A of Eqn. (6). It is in this light that Jones (Ref. 1) presented the supersonic area rule. It is important to remember, however, that it is C_{D_L} of Eqn. (4) which forms the limitation of the area rule and not the restriction to von Karman's integral formula, which requires that the body be closed (or constant radius at $x=L$), for example.

If we were to examine a closed body of revolution at zero angle of attack, it is interesting that the slender-body theory, Eqn. (6), leads to a coefficient of drag which is independent of Mach number. In this case, $C_{D_o}(\theta)$ of Eqn. (7) is independent of θ so that C_{D_o} equals $C_{D_o}(\theta)$. Additionally, as Lomax pointed out (Ref. 5), this case would lead to the symmetry properties that

$$S''(x,\theta) = S''(x, -\theta) \tag{8}$$

and

$$\frac{df}{dx}(\theta) = -\frac{df}{dx}(-\theta) \tag{9}$$

so that the first term of C_{D_L} would become identically zero. Further, since there is no net streamwise-normal force, the second term must also be zero. For the body-of-revolution problem, then, it would appear that the supersonic area rule takes into account wave-drag changes with Mach number due to thickness distribution that are not accounted for in slender-body theory.

9

B. Application

In order to obtain a wave-drag computation within the framework of linearized theory, one would need a complete description of the pressure distribution on the surface of a given airplane; having that pressure distribution, however, would lead directly to the drag by means of a surface integration. With the exception of some simple configurations, pressure information this complete requires extensive computation, perhaps based on paneling techniques, and having that information obviates the need for employing Eqn. (3). Lacking this information the supersonic area rule, Eqn. (5), has been employed to obtain an approximation to C_{D_w}. As Lomax (Ref. 1) and Nelson and Welsh (Ref. 2) pointed out, there are aircraft configurations for which C_{D_L} (the term which limits the accuracy of the supersonic area rule) is not small. But for supersonic aircraft of conventional form Baals, Robins, and Harris (Ref. 4) have shown that the area rule gives good results.

In practice, numerical computer algorithms are used to carry out the integrations in Eqn. (5). One of the first widely known algorithms was that written by Boeing Company in the 1960s. I believe that it is fair to say that by today's standards the Boeing program seems crude. Nonetheless, the Boeing program served as the point of departure for many of today's algorithms. As described by Harris (Ref. 3) the Boeing method calculates $C_D(\theta)$ for each of a finite number of θ's by numerically integrating Eqn. (7) using the equivalent body of revolution determined by the projection on an axis-normal plane of the section area cut by the Mach plane oriented at the roll angle θ. Sufficient θ's are chosen $\Delta\theta$ apart so that θ goes through 360 degrees. C_{D_w} is then computed by averaging all $C_D(\theta)$'s.

A major problem in building such a computational algorithm is in describing the geometry of the airplane. Computer-interactive-graphics

methods have made this problem a simpler one than it once was from the operator's point of view, but this simplification was paid for at the price of both algorithm and computer hardware sophistication (Ref. 4).

III. Modification of the Supersonic Area Rule

It might at first seem ludicrous to suggest a modification to the area rule that is less sophisticated than the published works of the 1960s. The modification proposed here, however, is for the user who is without access to large computers and operates with little or no interactive graphics capability. If we add to these constraints the demand for a simple input capability, it is clear that some modification to the supersonic area rule is needed if it is to be used.

The modification I adopted was to construct a simple equivalent body of revolution based on planes cut normal to the fuselage axis. It is this equivalent body of revolution to which the area rule is then applied. This means that Eqn. (7) need only be applied and numerically integrated once for each Mach number of interest. Further, the algorithm for constructing new equivalent bodies of revolution at each Mach number becomes almost trivial when applied to a body of revolution. In addition, the input requirement is satisfied by a simple area distribution which, if not readily available, is simple to construct. And finally, any protuberance to be added to an existing aircraft may be specified as a simple additive area at applicable axial fuselage locations, thus making it ideal for systems studies where these areas may be the extent of the information available.

A. Previous Work

This modification is not without precedent. Harris (Ref. 3) described a similar technique for simplifying the description of the

fuselage in the early Boeing program; however, authors, when speaking of
the supersonic area rule, have not been so bold as to collapse the entire
wing structure, tail structure, etc. onto a single body of revolution. No
doubt investigators along the way have done so, but I found no mention of
this in the literature.

Hall (Ref. 7) performed a beautiful piece of experimental work
dealing with the transonic area rule. In this work he compared drag data
taken from actual aircraft configurations to drag data taken from
equivalent body-of-revolution models for Mach numbers up to 1.3. The
results are quite marvelous. Hall's conclusion was that the simple
equivalent bodies of revolution were able to predict drag rise of the
airplane configurations to within 15 percent. Selected results of Hall's
study are given in Figures 2, 3, and 4.
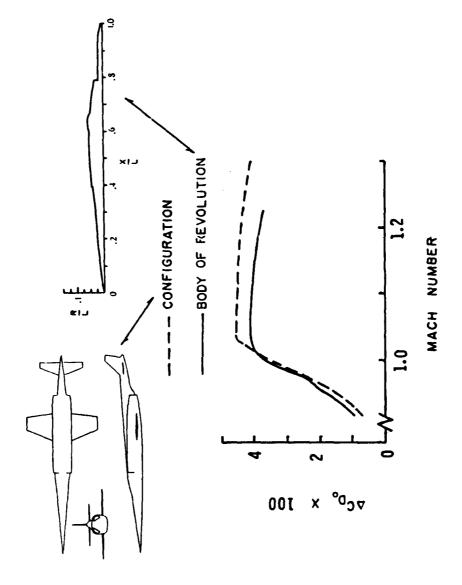
Since the proposed modification to the supersonic area rule is the
exact (within the framework of linearized theory) computation for a body
of revolution, Hall's work tends to justify the use of the simplified
supersonic area rule. Further, because the simplified area rule is
proposed for use within the context of the introduction, a qualitative
result, based on its use for analysis of near-axis protuberances, seems
strengthened by Hall's results.

IV. Computer Program

A. Numerical Integration
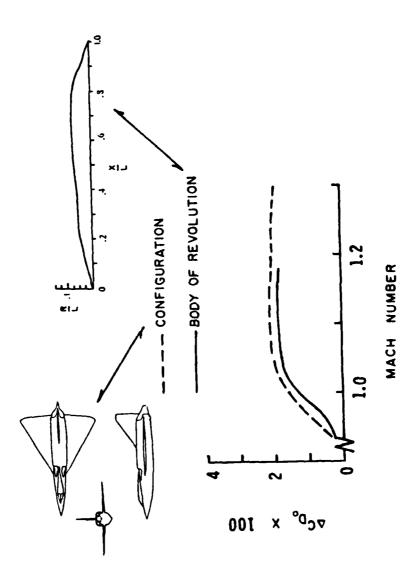
A computer program was written to numerically integrate Eqn. (7)
by dividing the axis into a number of small segments of length Δx_i. Let
us assume that we have an axial distribution of Mach-plane areas $S(x,M)$
(the methods I used to arrive at this distribution will be discussed
later) at the appropriate Mach number, M. The numerical integration of
Eqn. (7) was carried out using the following simple algorithm:
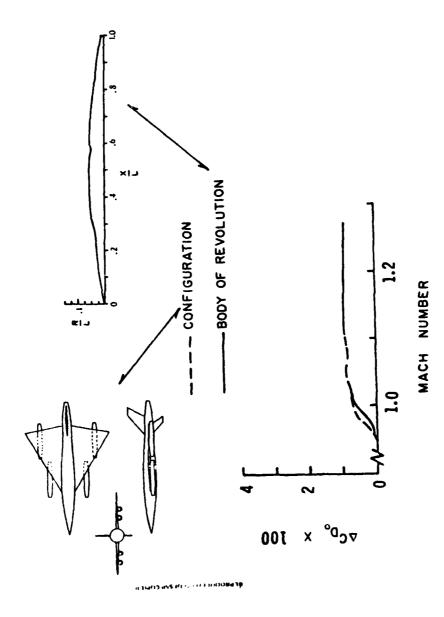
Figure 2. Experimental Drag Rise Comparison for the Aircraft
Configuration and the Body of Revolution. Drag Based on Wing
Planform Area

Figure 3. Experimental Drag Rise Comparison of the Aircraft Configuration and the Body of Revolution. Drag Based on Wing Planform Area

Figure 4. Experimental Drag Rise Comparison of the Aircraft Configuration and the Body of Revolution. Drag Based on Wing Planform Area

$$
C_{D_w} = -\frac{1}{2\pi q S_b} \left\{ \sum_{i=1}^{n} S_i{''} \Delta x_i \left[\sum_{j=1}^{i-1} (S_j{''} \ln \left| \frac{x_i}{L} - \frac{\xi_j}{L} \right| \Delta \xi_j) \right. \right.
$$

$$
+ 2S_i{''} L \left| (\frac{x_i}{L} - \frac{\xi_{i-1}}{L}) \ln (\frac{x_i}{L} - \frac{\xi_{i-1}}{L}) - (\frac{x_i}{L} - \frac{\xi_{i-1}}{L}) \right| \tag{10}
$$

$$
\left. \left. + \sum_{j=i+1}^{n} (S_j{''} \ln \left| \frac{x_i}{L} - \frac{\xi_j}{L} \right| \Delta \xi_j) \right] \right\}
$$

The summation was broken up and an analytic expression used at i=j to avoid the singularity in the natural logarithm as x approaches ξ (i.e., i=j).

Because the goal of writing the program included making the input format as simple as possible, the expected input format was a simple tabulation of the axial location and cross-sectional area of the airplane configuration. Although the number of locations chosen would affect the accuracy of the numerical integration (this point will be discussed later), a more complex problem arises from the fact that Eqn. (10) requires the second derivative of the area schedule at each axial location, be it the original area schedule or the Mach-plane area schedule. Several schemes for dealing with this problem were tried, including fitting the area schedule with a cubic spline which provided a continuous area distribution as well as continuous first and second derivatives. The cubic spline, however, turned out to be the source of large errors. I finally settled on a five-point nested average of simple differences to obtain the approximation for the required derivatives.

Starting with the area distribution, a range of five slopes surrounding a given axis location was averaged to arrive at a first derivative value for that point. The same procedure was again used to calculate the second derivative from the calculated first derivative table. Each axial location was handled in this manner except the extreme

ends of the body where a five-point range was not available. In these two

regions progressively smaller slope-averaging ranges were used.

B. Mach-Plane Area Distribution

By far the greatest computational simplification comes as a

consequence of the method of initially describing the airplane

configuration as a simple tabulation of cross-sectional area. Any

algorithm for determining equivalent Mach-plane area need only deal with a

body of revolution, and this at zero incidence. The first consequence is

that the Mach-plane area need only be calculated once for each Mach

number, because the axial symmetry leads to the same area for every roll

angle θ (taken with respect to the body axis). Secondly, again because of

symmetry, only half the area need be investigated, i.e., $0 \leq \phi \leq 180$ degrees,

where ϕ defines the radius location of the forward-normal projection of

the Mach-plane area (see Figure 5).
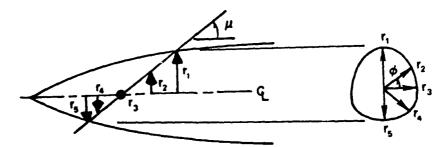
Figure 5. Geometric Description for Computation of the Radii of the New
Mach-plane Body of Revolution Applied to a Simple Body of
Revolution

One hundred and eighty-one such radii were determined corresponding to

equal $\Delta\phi$ of one degree.

It is possible to perform this operation in two-dimensional space.

It can be shown that an angle ϕ for the Mach-plane, as shown in Figure 5,

is related to γ in the two-dimensional plane of Figure 6 by the following

relationship:

17

$$\tan\gamma = \tan(\mu)/\sin\phi \qquad\qquad (11)$$
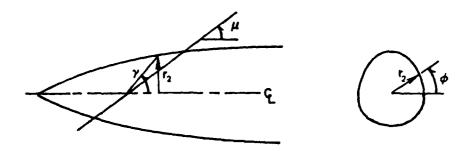
Figure 6. Relation between ϕ and γ

By using the two-dimensional plane technique ϕ was chosen at one-degree increments through a total of π radians (180 degrees) and the corresponding γ's were used to determine the appropriate radii of the forward-normal Mach-plane projection (i.e., r_1, r_2, etc. of Figure 5) at each value of x. The area for each pie slice between adjacent radii was determined and added to the other slice-shaped areas. This gave the area of half the Mach-plane projection. The total area was obtained by multiplying by two.

The intersection of the line at an angle γ and the radius of the body of revolution was determined by marching to the right when the axis system was laid out as in Figure 5 (or to the left if ϕ was less than 0) in increments of Δx; computing the height of the y-leg of the triangle determined by the γ-angle ray, x marching distance and the height, y; and comparing the height with the radius at that location. Once the radius had been exceeded, an iterative process was used to let y approach the linear interpolated r to within some small predetermined amount.

V. Results

A. Computer Storage and Process Time

The storage requirement is dependent upon the method of inputing the original area distribution and the manner of manipulating the various quantities in the program; however, with little effort a program incorporating the algorithm of the last section can be made to fit into a computer with 32K words of storage (8-bit words). The driving influence is the number of axial locations chosen. One hundred axial locations gave sufficient resolution for most area configurations.

Process time varied with the number of axial points chosen. For a program written in Fortran and executed on a Harris 500 computer, the times were less than half a minute for 50 points, approximately a minute and a half for 100 points, and approximately 6 minutes for 200 points. These are the process times to determine the wave-drag coefficient of a given configuration for one Mach number. Clearly, there is an advantage to staying near 100 points in terms of both accuracy and execution time considerations.

B. Controls

As mentioned earlier, Figures 2, 3, and 4 represent a set of controls, in an experimental rather than an analytic sense, which serves as a justification for the use of the method; however, it is of interest to explore the method further. In order to investigate the sensitivity of the method for determining the best location to place a protuberance of known volume and shape, I performed a wind-tunnel test of a basic body of revolution which could change configurations so as to place a known protuberance in two locations on the body. Then the same configurations were analyzed using the computer program, and the analytical results compared to the wind-tunnel data.

A brass model, the pieces of which are shown in Figure 7, was constructed so that it allowed for interchanging the protuberance location.
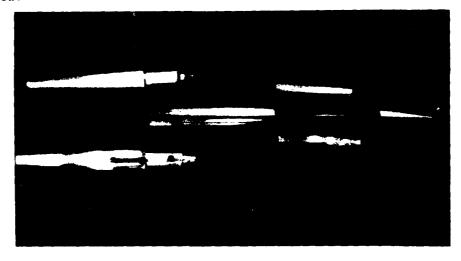
Figure 7.   Wind-Tunnel Model Showing the Various Parts Which Made the Configuration Changes Possible

The basic body was a parabolic (single-arch) body of revolution, ten inches long, whose radius in inches, r, versus axial position in inches, x, is described by the equation

$$r = (0.225 - 0.01875x)x \tag{12}$$

A two-inch long, football-shaped protuberance was added to the body of revolution, in one case at x=2 inches and in the second case at x=7 inches.   The radius of the protuberance in inches, r_p, versus axial location along the protuberance in inches, ℓ, is given by the equation

$$r_p = (0.8 - 0.4\ell)\ell \tag{13}$$

Each of these configurations was tested at four Mach numbers (1.2, 1.67, 2.45, and 3.02) in the one-foot square test section of the trisonic wind tunnel at the United States Air Force Academy.   This tunnel has been described in detail previously (Ref. 8).   Schlieren photographs of the three configurations typical of all runs are shown in Figure 8.   These

Figure 8.   Schlieren Photographs of Three Wind-Tunnel Model Configurations

photographs show that the flow remained attached and indicate that differences in drag should be due to wave-drag differences.
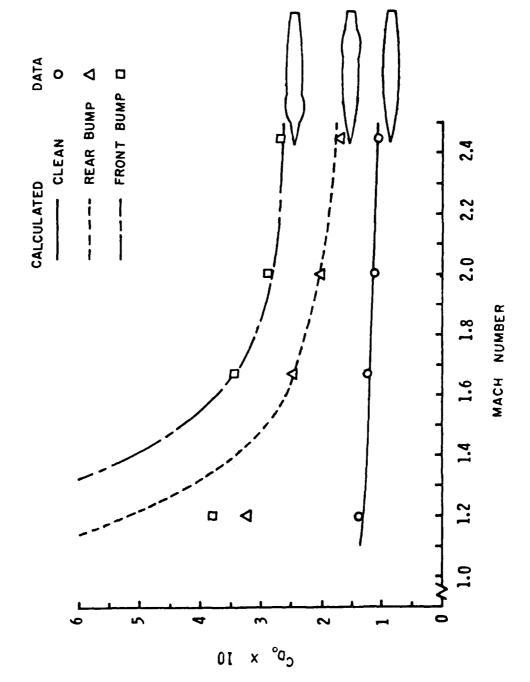
The results are shown in Figure 9 along with the predicted performance, predicted using the simplified-area-rule program. The method does seem to be able to judge the best location for a given protuberance, as demonstrated for these configurations.

The demonstrated ability of the method to discriminate the best location of a given protuberance must be attributed to the supersonic area rule, since the test involved a body of revolution for which the simplification is identical to the rule.

In order to further exercise the method and the program, I tested three model configurations originally studied by Nelson and Welsh (Ref. 2). I chose models 1, 4, and 5 from Ref. 2 for the following reasons: (a) model 1 was a simple body of revolution for which the program should give results identical to the standard supersonic area rule; (b) model 4 represented an example of moderately large areas located far off axis for which the supersonic area rule did a good job of predicting the experimental wave drag; and (c) model 5 represented an extreme case of large areas located far off axis for which even the supersonic area rule began to fail. These models are described in detail in Ref. 9 and summarized briefly in Table 1.

The results of the comparison are shown in Figure 10. Notice that both the simplified and complete area rule give identical results for the body of revolution -- as they should. Model 4 shows that the area rule predicts the data very closely, while the simplified area rule is off by as much as 20 percent at M=1.1, but is within 7 percent by M=1.5. For model 5 it is clear that even the area rule is unacceptable, and the simplified area rule is worse.
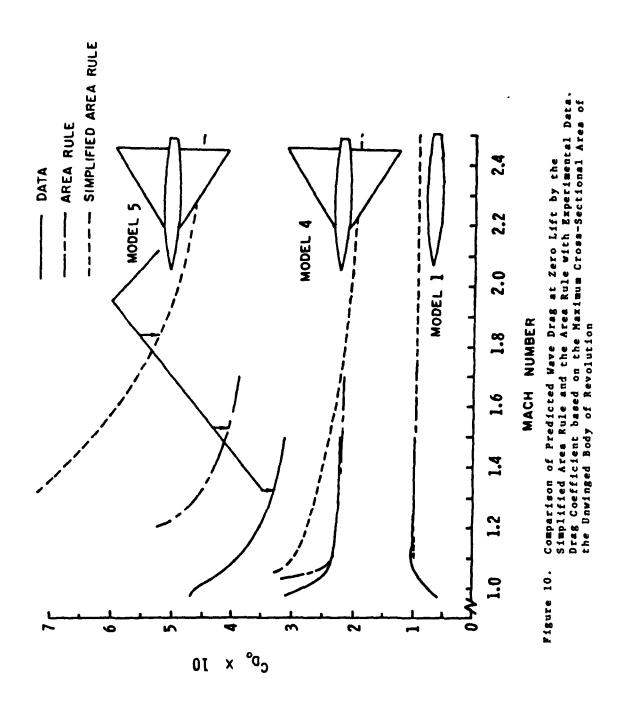
Figure 9. Comparison of Predicted Wave Drag at Zero Lift to the Predicted Wave Drag. Drag Coefficient Based on Maximum Cross-Sectional Area of the Unmodified Body of Revolution.

Table 1 Summary of Model Characteristics

Model	Designation	Body Type	Body Fineness Ratio d/ℓ	Maximum Thickness Location	Wing Type	Wing Leading Edge Sweep
1	Wingless	Parabolic body of revolution	0.10	42%		
4	Delta Wing	Parabolic body of revolution	0.10	42%	NACA 65A003	60°
5	Delta Wing	Parabolic body of revolution	0.10	42%	NACA 65A006	60°

Figure 10. Comparison of Predicted Wave Drag at Zero Lift by the
Simplified Area Rule and the Area Rule with Experimental Data.
Drag Coefficient based on the Maximum Cross-Sectional Area of
the Unwinged Body of Revolution

It should be noted that in those cases where the supersonic area rule gives good results, the simplification does a fair job. Further note that this is the total drag, and the intended use of the simplification is to give an estimate of drag increments due to minor configuration changes.

C. Application to the F-15

The preceding section represented a set of what might be termed controls but did not enable me to decide the usefulness of the simplified method for applications which fall under the stated purpose of the introduction. In this section the actual and predicted effect of adding near-axis protuberances to the basic clean F-15 will be examined. Since some wind-tunnel data exists for the McDonnell-Douglas FAST PACK fuel pallets, these have been selected for examination (Ref. 10). Figure 11 shows the location of the left pallet on the F-15. Figure 12 gives the area distributions (with and without the pallets) used for the computations.

First, the area distribution for the clean F-15 was used to obtain the coefficient of drag. Then the distribution was modified to account for the additional area due to the conformal pallets. (Conformal means that the added body is designed to blend with the main body so as to reduce undesirable aerodynamic characteristics such as flow separation, which can increase drag.) The curve in Figure 13 was obtained by subtracting the without-pallet configuration results from the with-pallet results. In this case the simplified area rule more closely predicted the data than did the area rule.

VI. Conclusions

In this paper I have presented the theory and application of a modified supersonic area rule. Although the modification is applied to a
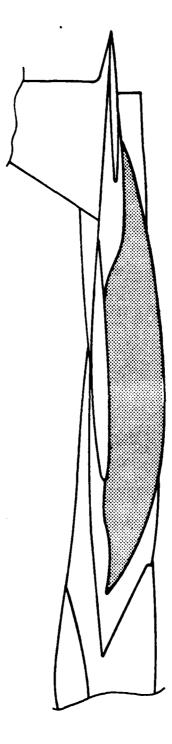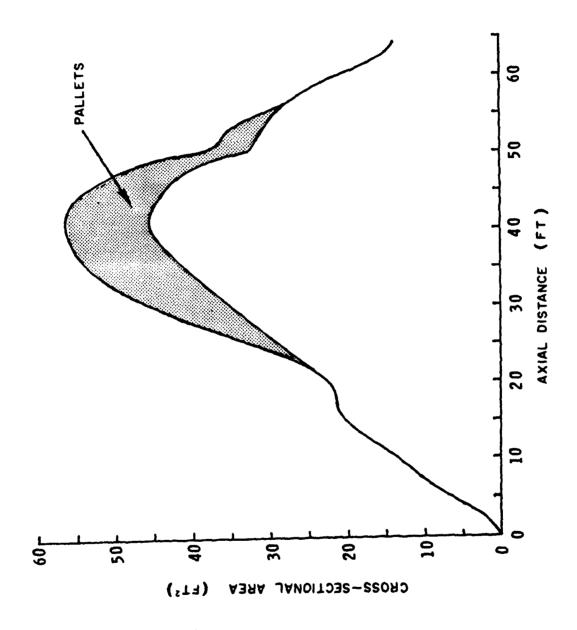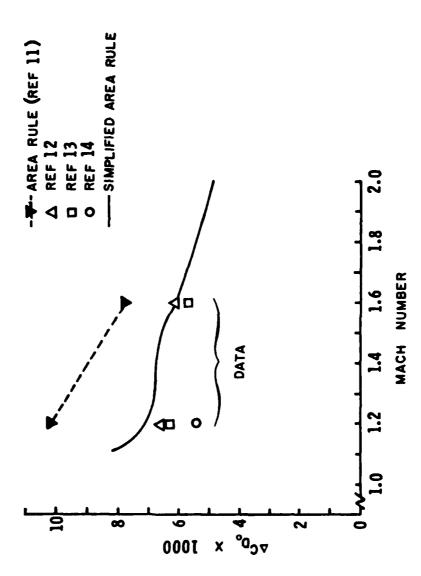
Figure 11. Location of the Left Fast Pack Pallet under the Wing and along the Fuselage of the F-15. Pallet Shown Shaded

Figure 12. Area Distribution of the F-15 with and without the Fast Pack Pallets Attached

Figure 13. Incremental Drag Due to Adding the Fast Pack Fuel Pallets.
Drag Coefficient Based on Wing Planform Area (608 sq. ft. –
see Ref. 2)

single example, it appears to lead to acceptable results when used for the express purpose of obtaining drag increments due to adding near-axis protuberances to existing aircraft configurations. Further, the cases examined for the purpose of providing a set of controls seem to indicate that the modification to the supersonic area rule yields relatively good predictions of the total wave drag in those cases where the unmodified area rule also yields good results. This result exceeds the expectations of the modification.

There is no doubt that the merit of the modification presented here needs further study before receiving general wide-scale approval. The results of this study, however, do seem to indicate that this modification to the supersonic area rule would prove very useful in systems studies and early-management decisions. Therefore, I recommend its use, since employing an approximation to the supersonic area rule is better than not exploiting the area rule at all.

VII Epilogue

In preparing Figure 13 for this paper I was struck by how well the modified supersonic area rule predicted the data when dealing with drag increments. I thought that there might be something inherent in the method which uncoupled the area increments from the base area distribution and that this might might be demonstrated mathematically. To this end I expanded Eqn. (10), including the difference schemes, to see if there might be a way in which nonlinearities were somehow compensating for one another. I found that there was still a strong nonlinear coupling term which linked the additional protuberance area to the original configuration area. Based on this cursory analysis I must conclude that the agreement demonstrated in Figure 13 is only by chance better than that determined by the full supersonic area rule. That is to say, the

modification approximates the full area rule and in general one would expect that the supersonic area rule forms the limitation of how accurate one would expect results to be, and the modification will approximate this solution. This question, however, might warrant further study.

Acknowledgement

References

1. Jones, R.T., "Theory of Wing-Body Drag at Supersonic Speeds," RM A55A18a, 1955, NACA.

2. Nelson, R.L. and Welsh, C.J., "Some Examples of the Transonic and Supersonic Area Rule," TN D-446, NASA (Supersedes RM L56D11, 1957, NACA).

3. Harris, R.V., "An Analysis and Correlation of Aircraft Wave-Drag," TM X-947, 1964, NASA.

4. Baals, R.V., Robins, A.W., and Harris, R.V., "Aerodynamic Design Integration of Supersonic Aircraft," Journal of Aircraft, Vol. 7, No. 5, Sept-Oct, 1970, pp. 385-394.

5. Lomax, H., "The Wave Drag of Arbitrary Configurations in Linearized Flow as Determined by Areas and Forces in Oblique Planes," RM A55A18, NACA, 1955.

6. Liepman, H.W. and Roshko, A., Elements of Gas Dynamics, John Wiley & Sons, New York, 1957, pp. 235-239.

7. Hall, J.R., "Comparison of Free-Flight Measurements of Zero-Lift Drag Rise of Six Airplane Configurations and Their Equivalent Bodies of Revolution at Transonic Speeds," RM-L53J21a, 1954, NACA.

8. Davis, M.W., Icardi, S.E., Gallington, R.W., and Wright, J.A., "Flow Quality Improvements in the USAFA Trisonic Tunnel," STA Paper, Proceedings of the 51st Meeting of the Supersonic Tunnel Association, Burbank, Calif., 1979.

9. Morrow, J.D. and Nelson, R.L., "Large-Scale Flight Measurements of Zero-Lift Drag of 10 Wing-Body Configurations at Mach Numbers from 0.8 to 1.6," RM L52D18a, 1953, NACA.

10. Lemley, C.E., Triplett, W.E., Verhoff, A., "Aerodynamic Interference due to Optical Turrets," Flight Dynamics Laboratory Report, AFWAL-TR-80-3058, Air Force Wright Aeronautical Laboratories, Sept, 1978,

11. Calculations performed using NASA wave-drag program described in Ref. 3. Results reported in Ref. 10, p. 79.

12. Meyer, W.L., "Summary of Results of Series XI Polysonic Wind Tunnel Tests on 4.5 Percent Scale Model of the Model 199A-PSWT Test #366," Report MDC 4589, Dec, 1976, McDonnell-Douglas Aircraft Company, St. Louis, Missouri.

13. Meyer, W.L., "Summary of Results of Series XI Polysonic Wind Tunnel Test on 4.7 Percent Scale Model of Model 199A-PSWT Test #361," Report on MDC A4405, Sept 1976, McDonnell-Douglas Aircraft Company, St. Louis, Missouri.

14. Riley, D.R., "Results of F-15 CFT Store Station Wind Tunnel Test with MK-82 Low-Drag General Purpose and MK-84 Laser-Guided Bombs," Report MDC A5907, April, 1979, McDonnell-Douglas Aircraft Company, St. Louis, Missouri.

SECTION II

Propulsion

J69-T-25 TURBOJET CYCLE ANALYSIS

Robert E. Boyle, Jr.*

Abstract

Numerous test runs of the J69-T-25 turbojet engine have been made at
the Aeronautics Laboratory of the United States Air Force Academy over the
past 25 years. However, the test data -- specifically the nominal values
of thrust, specific fuel consumption, and compressor and turbine
efficiencies -- have not been readily accessible. To correct this
situation, this paper makes the data available in a comprehensive
reference. Since the instructor or researcher will be provided with
sufficient information for planning purposes, needless engine runs will be
prevented.

Two analyses of the data were produced. The first is a simplified
analysis based on assumptions that make the determination of engine
performance parameters less complicated. This provides a basic
understanding of the engine operation while reducing the amount of data
reduction required. Only two simplifying assumptions are made in the
second analysis; thus the determination of engine operating parameters is
more accurate but more complicated.

The simplified analysis yields results that are within 10 percent of
the experimental values, demonstrating that nominal values can be
predicted with a less sophisticated approach. This analysis lends itself
nicely to demonstrating the principles of the turbojet engine to a basic
engineering class. The rigorous analysis, on the other hand, provides an
adequate description of what actually occurs during engine operation and
could be used in more advanced courses on jet engine design.

I.   Introduction

Teledyne J69-T-25 turbojet engines are used by the United States Air

Force as power plants on T-37 trainers, as the booster engines on the

C-123J cargo aircraft, and in the MA1A air cart to supply air for starting

certain jet aircraft. Two of these enggines are mounted in test cells at

the Aeronautics Laboratory of the USAF Academy. Their primary purpose is

to demonstrate to Aeronautical Engineering students the principles of

turbojet engines and the operation of specific engine components. By

indicating nominal values of thrust, fuel flow, and turbine and compressor

efficiencies, this paper will aid instructors who demonstrate the

performance of these engines in classroom situations.

Figure 1 shows a schematic of the J69-T-25 turbojet engine and the

---

*Captain, USAF, Associate Professor of Aeronautics, DFAN

stations of particular interest in this development.

STA   STA   STA   STA   STA   STA
T   2   3   4   5   6
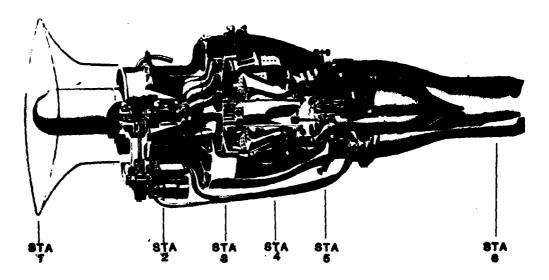
Figure 1.   Cutaway of J69-T-25 Showing Stations of Particular Interest

Two different analyses of the engine performance are produced. The first

analysis, which is used in the Department of Aeronautics core course,

makes several simplifying assumptions. The first of these assumptions is

that the mass flow into the engine is equal to the mass flow exiting the

engine. This is true only ᶠ ⁺he mass flow of the fuel is ignored. It is

also assumed that the mechanical efficiency of the engine is unity. This

assumption implies that there are no frictional or mechanical linkage

losses involved in the operation of the compressor-turbine combination.

It also ignores any power loss due to the operation of accessories such as

the fuel pump, the oil pump or the generator. The pressure loss in the

combustor is assumed to be negligible. The validity of this assumption,

which affects the calculation of turbine efficiencies, will be examined

using the experimental data. The nozzle is assumed to be adiabatic; this

assumption will also be examined in the experimental analysis. The values

of the specific heat at constant pressure, C_p, and ratio of specific

heats, γ, are assumed to be constant throughout the engine. The high temperatures attained as well as change in composition of the gas in the combustor and turbine will affect the accuracy of this assumption. Since the velocity of the flow at the turbine exit is assumed to be negligible compared to nozzle exit velocity, the static temperature at station 5 is equal to the total temperature there or $T_5 = T_{05}$. It is also assumed that the exit nozzle is perfectly expanded, i.e., exit pressure is just equal to atmospheric pressure. Since the Mach number at the exit can be shown to be subsonic at all RPM settings, this assumption is accurate. Also inherent in a static thrust analysis is the fact that the total pressure and temperature at the entrance of the compressor is just equal to atmospheric values. With the low entrained velocities in the inlet, the changes in total properties are, in fact, negligible. The assumptions are therefore:

(1) Mass flow rate into the engine equals the mass flow out of the engine ($\dot{m}_{in} = \dot{m}_{out}$), i.e., the mass flow rate of the fuel is assumed to be negligible ($\dot{m}_f \cong 0$)

(2) Mechanical efficiency of unity ($\eta_m = 100\%$)

(3) No pressure loss in combustor ($P_{04} = P_{03}$)

(4) Adiabatic nozzle ($T_{06} = T_{05}$)

(5) C_p and γ are constant throughout the engine
$$(C_p = .24 \frac{Btu}{lbm\ R}, \ \gamma = 1.4)$$

(6) Velocity at the turbine exit is much less than nozzle exit velocity ($V_5 \ll V_6$)

(7) Perfectly expanded nozzle ($P_6 = P_{atm}$)

(8) Total pressure and total temperature in the inlet are assumed constant, i.e., $P_{02} = P_{atm}$, $T_{02} = T_{atm}$. This is only true for a stationary engine with no losses in the inlet.

(9) The air and fuel-air mixture are assumed to be perfect

gases ($P = \rho RT$)

The more rigorous approach, which is taken in the Aero majors' courses, uses only the static thrust assumption (no. 8) and the perfect gas assumption (no. 9). This approach better describes what actually occurs in the engine and, therefore, should produce a more accurate analysis of component performance. Throughout this paper the engine parameters for both analyses will be compared.

II. Test Apparatus

The Teledyne J69-T-25 engine, designed in 1956, is very similar to the original turbojet designs. It consists of a centrifugal compressor, an annular combustor, an axial flow turbine, and an exhaust nozzle of fixed exit area. A Bell-mouth nozzle has been added at the inlet to allow steady, one-dimensional air flow to be delivered to the compressor and to permit an accurate determination of the mass flow entering the engine. See Figure 2 for the location of the Bell-mouth on the engine.

BELL MOUTH INLET
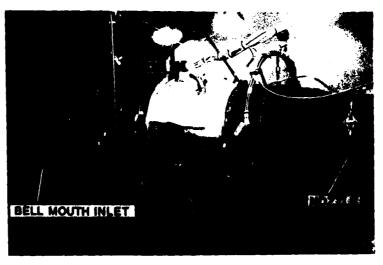
Figure 2. Picture of J69-T-25 Engine, Bell-mouth inlet,
and Instrumentation

Table 1
TEST CELL MEASUREMENTS

PARAMETER	SYMBOL	DIMENSIONS
Engine Thrust	F	lbf
Fuel Flow	$\dot{m}_f$	lbm/hr
Atmospheric Pressure	P_{atm}	in. Hg
Dynamic Pressure in Bell-mouth ($P_{atm} - P_2$)	ΔP	in. H_2O
Total Pressure at Compressor Entrance	P_{02}	psi
Total Pressure at Compressor Exit	P_{03}	psi
Total Pressure at Turbine Exit	P_{04}	psi
Total Pressure at Nozzle Exit	P_{06}	in. Hg
Total Temperature at Compressor Inlet	T_{02}	^0F
Total Temperature at Compressor Exit	T_{03}	^0F
Total Temperature at Turbine Exit	T_{05}	^0F
Total Temperature at Nozzle Exit	T_{06}	^0F
Percent of Maximum Engine RPM	%RPM	%
Actual Engine RPM	RPM	revolutions per minute

Table 1 shows the parameters measured during our test runs. The temperatures in the engine were measured using thermocouples implanted in pitot tubes. T_{02} was measured by a single probe at the inlet. T_{03} was measured by a single probe located at the compressor exit. T_{04} was not

measured. Although measurement of this temperature by means of

thermocouples is possible, the failure rate, as well as the number of

probes required to accurately measure T_{04} make it economically attractive

to calculate the turbine inlet temperature analytically. T_{05} was measured

by a total of 24 probes mounted radially in a 6 x 4 configuration as shown

in Figure 3.

ENGINE CROSS SECTION
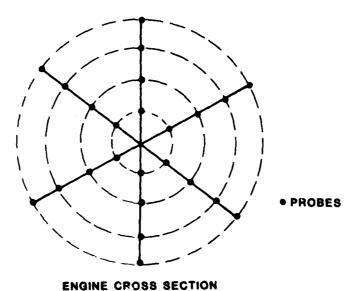
Figure 3. Probe Arrangement for Measurement of T_{05}

T_{06} is measured at the nozzle exit by eight probes mounted radially.

Pressures were measured at different locations using static ports or pitot

tubes. In some locations multiple pressure ports were used and the

measured pressures were averaged. P_2 was measured using four static

pressure ports mounted radially at the throat of the Bell-mouth and is

used to determine ΔP, the difference between the total pressure and the

static pressure at the throat. P_{03} was measured by one probe located at

the compressor exit. P_{04} was measured by two probes located at the

turbine entrance. P_{06} was measured by six probes mounted radially at the

nozzle exit. The engine's thrust was measured with a lead cell mounted
at the base of the test stand.

An oil pump, a fuel pump, and an engine generator are the only
accessories driven by the engine. The power required to operate these
engine accessories is included in the mechanical efficiency, η_m, used in
the majors' courses. The value of η_m is .96 for the majors' analysis
and 1.0 in the simplified core course analysis.

III. Analytical Approach

The thrust of a turbojet engine can be determined analytically by
using a momentum balance on a control volume surrounding the engine. If a
one-dimensional, steady flow is assumed to enter and leave the engine, the
thrust can be represented as

$$F = \dot{m}_6 V_6 - \dot{m}_1 V_1 + A_6 (P_6 - P_1) \tag{1}$$

where F is the thrust of the engine. If the nozzle is perfectly expanded
for all RPM settings, then $P_6 = P_1 = P_{atm}$. Also, this analysis is a
determination of thrust for a stationary turbojet engine, i.e., static
thrust, so the inlet velocity is essentially zero ($V_1 \approx 0$). The resulting
thrust equation, then, is simply

$$F = \dot{m}_6 V_6 \tag{2}$$

where $\dot{m}_6$ is the mass flow out of the engine and V_6 is the velocity at the
nozzle's exhaust. The mass flow and velocity at the nozzle exit are not
easily measured during engine operation, so Eqn. (2) must be altered to
include known parameters. One form of this equation is

$$F = \dot{m}_1 (1+f) \left[2C_{pt} T_6 \left\{ \left(\frac{P_{06}}{P_6} \right)^{\frac{\gamma_t - 1}{\gamma_t}} - 1 \right\} \right]^{\frac{1}{2}} \tag{3}$$

where f is the fuel-air ratio ($\dot{m}_f/\dot{m}_I$). For the core course thrust calculation, Eqn. (3) reduces to

$$F = \dot{m}_I \left[2C_p \, T_6 \left\{ \left(\frac{P_{06}}{P_6}\right)^{\frac{\gamma-1}{\gamma}} - 1 \right\} \right]^{\frac{1}{2}} \qquad (4)$$

since the fuel flow is neglected ($\dot{m}_f = 0$) and the mass flow out of the engine is assumed to be equal to the inlet mass flow.

It is clear from Eqn. (4) that both C_p and γ affect the calculation of engine thrust. No appreciable change in these two parameters is encountered in the inlet or compressor due to the relatively low temperature changes encountered there. Thus, they are assumed to be constant up to the combustor. These values are: $\gamma_c = 1.4$, $C_{pc} = .24 \frac{Btu}{lbm\ R}$. In the simplified analysis these parameters are assumed to be constant throughout the engine regardless of the temperature. In the majors' course analysis, the variation with temperature is taken into account by assuming that γ and C_p are constant after the combustion process but with new values $\gamma_t = 1.35$ and $C_{pt} = .264 \frac{Btu}{lbm\ R}$. The subscript "t" is usually used to denote the values of and C downstream of the combustor. Later, another calculation of theoretical thrust is discussed in which the values of and C are varied in the turbine and nozzle.

Isentropic and polytropic efficiencies of the compressor and turbine are very important to any jet engine analysis. The isentropic efficiency is one way of measuring the amount of power lost due to the entropy produced during the compression or expansion of the flow. In other words, we compare an actual device to an ideal or the best possible adiabatic device. For example,

$$\eta_c = \frac{ideal\ power\ required}{actual\ power\ required} \qquad (5)$$

or

$$\eta_c = \frac{T_{03S} - T_{02}}{T_{03} - T_{02}} \tag{6}$$

where

$$T_{03S} = T_{02} \left(\frac{P_{03}}{P_{02}}\right)^{\frac{\gamma_c - 1}{\gamma_c}} \tag{7}$$

Here the subscript "s" refers to the conditions obtained in an ideal (reversible and adiabatic or isentropic) device. For the turbine,

$$\eta_t = \frac{\text{actual power produced}}{\text{ideal power produced}} \tag{8}$$

or

$$\eta_t = \frac{T_{04} - T_{05}}{T_{04} - T_{05S}} \tag{9}$$

where

$$T_{05S} = T_{04} \left(\frac{P_{05}}{P_{04}}\right)^{\frac{\gamma_t - 1}{\gamma_t}} \tag{10}$$

The polytropic efficiency of the compressor, e_c, is defined as the ratio of the ideal work of compression to the actual work of compression for a differential pressure change. It is needed during the early engine design phase to determine the required stages of compression. This determination is made easier because the polytropic efficiency is essentially constant throughout the compressor. It can be shown for the the compressor, for example, that, with entropy production,

$$\frac{T_{03}}{T_{02}} = \left(\frac{P_{03}}{P_{02}}\right)^{\frac{\gamma_c - 1}{\gamma_c}} e^{-\Delta S/R} \tag{11}$$

where Δs is entropy produced and R is the gas constant (Ref. 5). If this pressure change is analyzed differentially, i.e. the total change is divided into many small increments of pressure change, Eqn. (11) can be represented as

$$\frac{T_{03}}{T_{02}} = \left(\frac{P_{03}}{P_{02}}\right)^{\frac{\gamma_c - 1}{\gamma_c e_c}} \qquad (12)$$

In other words, we are replacing the entropy production term, which can vary significantly from point to point in the compressor, with a term which is easily determined and remains practically constant throughout the compressor. The polytropic efficiency of the turbine, e_t, can be determined from the following relation:

$$\frac{T_{04}}{T_{05}} = \left(\frac{P_{04}}{P_{05}}\right)^{\frac{(\gamma_t - 1)e_t}{\gamma_t}} \qquad (13)$$

IV. Results

Two test runs of the J69-T-25 turbojet engine on 8 July 1982 produced the data used in this report. Table 2 shows the average values of the data taken for the two runs, while Table 3 lists the absolute values of these same temperatures and pressures, and Table 4 gives operating parameters calculated from the variables in Table 3.

The actual mass flow into the engine inlet was determined from the P measured in the Bell-mouth (Ref. 7) and is tabulated in Table 4 for various engine RPM (Ref. 1). The fuel-air ratio, determined from the air mass flow calculated at the inlet and the measured fuel flow, is also listed. The Mach number at the engine's exit, M_6, is tabulated in Table 4 along with the calculated value of turbine inlet temperature, T_{04}. The determination of T_{04} will be discussed later. The variation of the

isentropic and polytropic efficiencies of the turbine and compressor as a function of RPM tabulated in Table 4 are plotted in Figures 4 and 5.
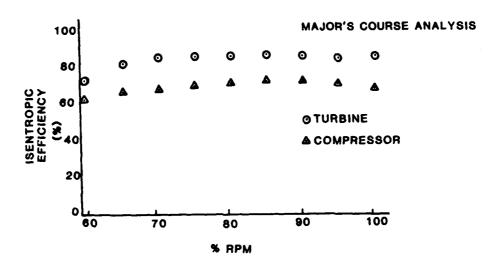
Figure 4. Isentropic Efficiency of Compressor and Turbine vs. RPM
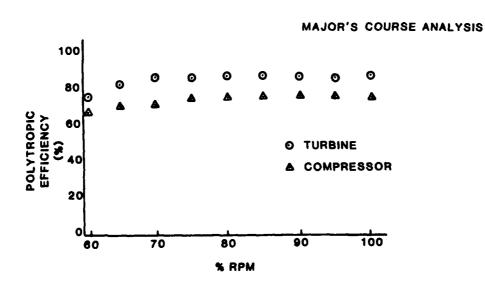
Figure 5. Polytropic Efficiency of Compressor and Turbine vs. RPM

Table 2

AVERAGE OF DATA TAKEN FOR 2 TEST RUNS

% RPM	ΔP(in H₂O)	P_{03}(psig)	P_{04}(psig)	P_{05}(in Hg)	P_{06}(in Hg)	T_{03}(F)	T_{05}(F)	T_{06}(F)	F (lbf)	* $\dot{m}_f$
60	2.95	7.13	6.95	2.93	2.63	178	976	948	158	327
65	3.7	8.88	7.95	3.6	3.25	198	964	945	191	360
70	4.7	10.88	9.75	4.53	4.05	220	935	923	239	392
75	6.0	13.38	12.05	5.65	5.05	241	914	893	294	429
80	7.28	16.0	14.28	6.9	6.2	264	928	895	356	482
85	8.85	19.0	16.98	8.43	7.78	290	962	910	430	546
90	10.45	22.13	20.0	10.18	9.45	317	1010	947	513	622
95	12.4	25.75	23.88	12.38	11.52	347	1082	994	615	720
100	14.28	29.13	26.83	15.0	13.82	379	1174	1060	730	846

P_{atm} = 23.31 in Hg

T_{atm} = 64 degrees F

*mass flow rate, m_f, in lbm/r

Table 3

ENGINE OPERATING PARAMETERS REDUCED FROM DATA IN TABLE 2

% RPM	RPM	P_{03}(psia)	P_{04}(psia)	P_{05}(psia)	P_{06}(psia)	T_{03}(R)	T_{05}(R)	T_{06}(R)
60	12785	18.57	18.4	12.89	12.74	638	1436	1408
65	13900	20.32	19.4	13.22	13.05	658	1424	1405
70	15070	22.32	21.2	13.67	13.44	680	1395	1383
75	16280	24.82	23.5	14.22	13.93	701	1374	1353
80	17325	27.45	25.72	14.84	14.5	724	1388	1355
85	18410	30.45	28.42	15.59	15.27	750	1422	1370
90	19320	33.57	31.45	16.45	16.09	777	1470	1407
95	20375	37.20	35.32	17.53	17.11	807	1542	1454
100	21318	40.57	8.27	18.82	18.24	839	1634	1520

Table 4

ENGINE OPERATING PARAMETERS DETERMINED FROM TABLE 3

% RPM	$\dot{m}_{air}$ (lbm/s)	f	η_c Eqn. (6)	e_c Eqn. (12)	T_{04} (R) Eqn (14)	T_{04} (R) Eqn (15)	η_t Eqn (9)	e_t Eqn. (13)	M_6	F_{major} (lbf) Eqn. (3)	F_{core} (lbf) Eqn. (4)
60	7.07	.0128	.684	.702	1542	1550	.78	.772	0.4	158.6	161.5
65	7.93	.0126	.694	.720	1549	1558	.85	.846	0.44	196.6	194.4
70	8.89	.0122	.796	.732	1541	1551	.88	.875	0.49	241.3	240.7
75	10.04	.0119	.734	.760	1539	1551	.878	.871	0.55	297.6	299.6
80	11.0	.0122	.745	.773	1575	1588	.895	.886	0.60	356.8	361.3
85	12.13	.0125	.748	.780	1633	1648	.898	.889	0.67	435.6	444.2
90	13.13	.0132	.747	.780	1706	1723	.894	.886	0.73	518.5	533.1
95	14.26	.014	.742	.780	1806	1825	.88	.87	0.79	620.1	645.7
100	15.26	.0154	.724	.768	1927	1949	.904	.896	0.86	728.3	761.6

Notice the fairly constant values of e_c above 70 percent RPM. Thus e_c behaves as expected. The isentropic efficiency of the compressor peaked at about 90 percent RPM indicating the desired cruise operating point for the engine. Figure 6 shows the different turbine efficiencies obtained from the two analyses. The relatively large difference occurs because
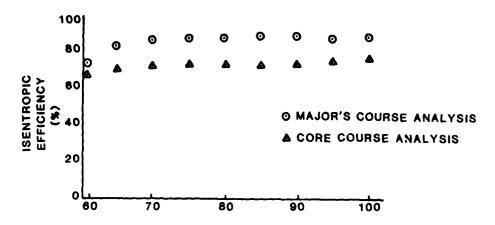
Figure 6. Comparison of Isentropic Turbine Efficiencies from the Two Analyses

the pressure drop in the burner yields a turbine inlet pressure lower than that assumed in the core-course analysis. Because of this lower pressure the related ideal temperature drop is lower than originally predicted, resulting in higher turbine efficiencies than those obtained from the core analysis. T_{04} was not measured but was calculated using a power balance between the compressor and turbine. A mechanical efficiency of 96 percent was assumed in the majors' course analysis. This efficiency takes into account not only frictional losses but also the power required to drive the engine accessories, as previously mentioned. For example,

$$\underbrace{\dot{m}_1 C_{pc}(T_{03} - T_{02})}_{\text{work of compressor}} = \eta_m \underbrace{\dot{m}_6 C_{pt}(T_{04} - T_{05})}_{\text{work of turbine}} \tag{14}$$

47

These parameters are also corrected to sea level as shown in the figures.
Figure 9 shows the comparison of measured thrust to those values
determined by the two analyses. The corrected sea-level thrust is
approximately 8.5 percent less than the original engine data (Ref. 6).
This is probably due to the deterioration of the engine components over
the past 25 years. Figure 10 shows the thrust specific fuel consumption
(TSFC) as a function of RPM.
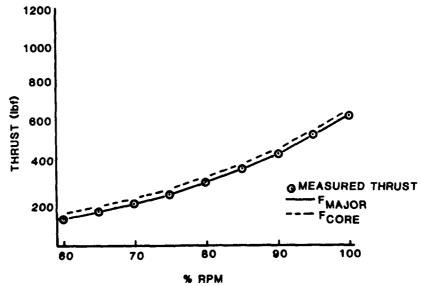
Figure 9. Comparison of Calculated to Measured Thrust
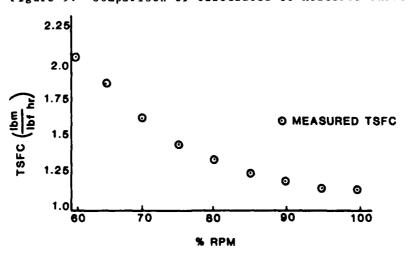
Figure 10. Thrust Specific Fuel Consumption vs. RPM

For the core course T_{04} calculation, Eqn. (15) reduces to

$$T_{04} = T_{03} + T_{05} - T_{02} \qquad (15)$$

since $C_{pc} = C_{pt}$, $\eta_m = 1$, and $\dot{m}_1 = \dot{m}_6$. As previously mentioned, these calculated values of T_{04} for both core and majors' calculations are listed in Table 4. Thrust and fuel flow are shown as a function of engine RPM in Figures 7 and 8.
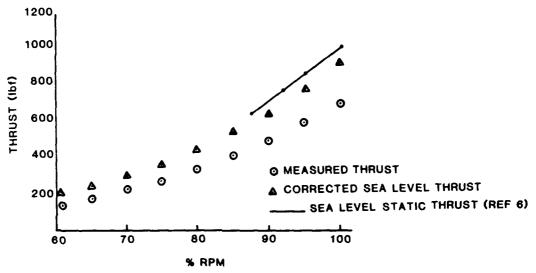
Figure 7. Measured and Corrected Sea Level Thrust vs. RPM
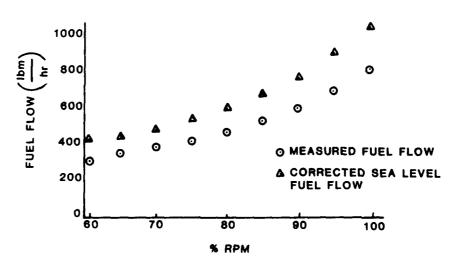
Figure 8. Measured and Corrected Sea Level Fuel Flow vs. RPM

49

In the present engine, at the altitude of the Academy, the minimum TSFC occurs at 100 percent. When corrected to sea level the minimum occurs at approximately 95 percent. The sea level TSFC indicates almost no shift in the original sea level data produced by the engine manufacturer.

V.   Conclusions

The simplified analysis gives a thrust within 4 percent of the measured value as shown in Figure 9. This apparently good prediction is due to compensating errors introduced by the assumptions. For example, the adiabatic nozzle assumption requires the use of T_{05} instead of the lower T_{06}. This causes a higher T_6, a higher V_6, and, therefore, a predicted thrust higher than that in the majors' analysis. On the other hand, the core analysis does not consider the mass flow of the fuel in the thrust calculation. This results in a predicted thrust lower than that of *the majors' analysis.* These two assumptions result in an accurate thrust prediction (see Table 4).

The two analyses show large differences in their predictions of turbine efficiencies. This is due to the core analysis assumption that there is no pressure loss in the combustor. The isentropic efficiency is calculated using and ideal, isentropic temperature at the turbine exit. This ideal temperature depends on the pressure loss in the turbine. The pressure at the turbine inlet is assumed to be higher than it actually is, resulting in a T_{05S} lower than it should be, as shown by Eqn. (10). Using Eqn. (9) one can see that a lower η_t results. The turbine isentropic efficiency should be inherently higher than that in the compressor due to their modes of operation. The compressor is centrifugal, causing large entropy changes, while the axial flow turbine accomplishes its task more efficiently. The polytropic and isentropic efficiencies in the turbine, as expected, are very similar because the turbine is single stage. One

must also consider that the polytropic efficiency of the compressor may be meaningless in that e_c is used to determine stages of compression during engine design. The centrifugal compressor, by its very nature, is not staged.

An analysis was completed to determine the effect on thrust of variation of γ_t and C_{pt} with temperature at the turbine inlet, the turbine exit, and the nozzle exit. This resulted in no more than 0.1 percent difference in thrust. The assumption that $\gamma_t = 1.35$ and $C_{pt} = .264 \frac{Btu}{lbm\ R}$ and that they are constant downstream of the burner is, therefore, quite adequate for this analysis.

The turbine inlet temperature was almost constant below 80 percent RPM. This is due to the fact that the fuel air ratio is nearly constant in this range. As f then increased toward stoichiometric ($f_{st} = 0.066$) the turbine inlet temperature also increased. The turbine exit temperature showed a decrease and then an increase at higher RPM because, as the engine RPM increased, the amount of work required by the turbine continually increased. Since T_{04} was constant at first, T_{05} must decrease (work of the turbine is proportional to $T_{04} - T_{05}$). As T_{04} rose, T_{05} also increased at higher RPM.

Despite its somewhat inaccurate calculations, caused by the many restrictive assumptions, the simplified core-course analysis provides a basic understanding of the turbojet engine for the non-Engineering general student. The majors' course analysis is much less restrictive and provides a more accurate description of the actual component operating parameters. This approach is necessary for the Aero Propulsion student to gain the more sophisticated background necessary for a propulsion design course.

2. James, R.N., "Aircraft Gas Turbine Engine Analysis," Unpublished Text, Department of Aeronautics, USAF Academy, Colorado, 1972.

3. Oates, G.C. "Notes on Rockets and Airbreathing Engines," Transcript from lectures presented at USAF Academy during the Fall semester 1975.

4. Hill, P. and Petersen, C. Mechanics and Thermodynamics of Propulsion, Addison-Wesler, 1970.

5. Kuethe, A. and Chow, C. Foundations of Aerodynamics, John Wiley and Sons, 1976.

6. AFG3, Vol. I, Mar. 1976.

7. Reagan, M., Thornley, P., Higgins, A. "An Improved Method for Calculation of Static Thrust for the USAFA J-85/13 Turbojet Engine," Aeronautics Digest, USAFA Spring/Summer 1981.

Symbols

A_1	inlet frontal area
A_6	exhaust nozzle exit area
C_{pc}	specific heat at constant pressure ahead of combustor
C_{pt}	specific heat at constant pressure aft of combustor
$\dot{m}_1$	mass flow rate into compressor
$\dot{m}_6$	mass flow rate from nozzle exit
$\dot{m}_f$	mass flow rate of fuel
M_6	Mach number at the exit
P_{02}	total pressure at compressor entrance
P_{03}	total pressure at compressor exit
P_{04}	total pressure at turbine entrance
P_{05}	total pressure at turbine exit
P_{06}	total pressure at nozzle exit
T_{02}	total temperature at compressor entrance
T_{03}	total temperature at compressor exit
T_{04}	total temperature at turbine entrance
T_{05}	total temperature at turbine exit
T_{06}	total temperature at nozzle exit
η_m	mechanical efficiency of compressor-turbine combination
γ_c	ratio of specific heats ahead of combustor
γ_t	ratio of specific heats aft of combustor
η_c	isentropic efficiency of compressor
η_t	isentropic efficiency of turbine
e_c	polytropic efficiency of compressor
e_t	polytropic efficiency of turbine

References

1. Shannon, Hiram W., Performance Calculations for T53 and T55 Gas Turbine Engines, Corpus Christi Army Depot, 22 October 1976.

ROUGHNESS EFFECTS IN AXIAL FLOW COMPRESSORS:
AN EMPIRICAL MODEL

R.J. Stiles*

Abstract

This paper presents an empirical model, taken from recent technical literature, which can be used to compute both the compressor airfoil surface finish required to create a hydrodynamically smooth fluid flow through an axial flowjet engine compressor and the effects of changes in airfoil surface finish on compressor efficiency. Standard surface roughness measurements and the problems associated with using those measurements in the model are also discussed. To illustrate its use, the model has been applied to the compression sections of three Air Force gas-turbine engines: the TF33-PW-7, the F100-PW-100, and the J85-GE-5H.

I.   Introduction

In recent years rapidly escalating fuel costs have created renewed

interest among aircraft gas-turbine engine designers in the effects of

compressor airfoil surface finish on turbine engine performance. There is

some experimental data which shows that reduced roughness in compressor

components can result in improved compressor efficiency which, in turn,

will yield lower thrust specific fuel consumption (TSFC) and lower exhaust

gas temperature (EGT) for the engine (Refs. 1 through 3). Since current

Air Force fuel consumption is approximately 3.6 billion gallons per year,

even a small reduction in TSFC for the engines which consume most of that

fuel can result in substantial cost savings. One manufacturer of smooth

coatings for compressor components has suggested that the application of

his product to J57, TF33, and J79 engines could yield an average 1.5

percent reduction in TSFC for those engines; that would save as much as

200 million gallons of fuel over a six year period (Ref. 4). Since high

EGT is a primary life-limiting factor for the materials in a jet engine,

lower EGT should result in lower engine maintenance and replacement costs

over a period of time.

The objective of this paper is to describe and illustrate an

empirical model developed by Schaffler (Ref. 3) which can be used to

_____

*Major, USAF, Aero Propulsion Laboratory

estimate the effect of airfoil surface finish on axial compressor
performance. The model permits designers to calculate the airfoil surface
finish required to obtain maximum available compressor efficiency at a
given compressor operating point (specified by pressure ratio and
corrected speed) and aircraft mission point (specified by Mach number and
altitude). Also, the model can be used to estimate changes in compressor
efficiency associated with changes in airfoil surface finish. This
information can then be used in an engine cycle analysis to determine
changes in TSFC and EGT.

The discussion that follows begins with a definition of surface
roughness and provides some background information concerning the
difficulty of measuring roughness in a given material. Then, after the
empirical model is presented, its use is illustrated by application to the
compression sections of three Air Force engines: the TF33-PW-7, the
F100-PW-100, and the J85-GE-5H.

II. Definition and Measurement of Roughness

Surface roughness is defined as the "fine irregularities in the
repetitive or random deviations from the intended surface contour" of a
given material (Ref. 5). There are a variety of surface measurements that
can be made to characterize a material surface in terms of its roughness
(see Ref. 5 for examples), but a measurement called the arithmetic average
roughness, Ra, is most commonly used. As illustrated in Figure 1, Ra is
the arithmetic average of deviations from a mean line through the surface
profile. It is defined by the equation

$$Ra = \frac{1}{L} \int_{X=0}^{X=L} |y| dx \qquad (1)$$

55

where y is the ordinate of the curve of the profile and L is the sampling length.
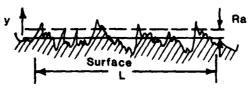
Figure 1.   Nomenclature for Determining the Arithmetic Average Roughness

While it is relatively easy to measure various physical characteristics of a material's surface, determination of the relationship between the measured characteristic and fluid flow behavior over the surface is more difficult. In fluid mechanics surface roughness is often specified in terms of "equivalent roughness," a concept which has its basis in systematic and extensive experiments performed by Nikuradse (Ref. 6) and which is symbolized by the parameter k_s. Roughness on the inside of a pipe will reduce the fluid flow rate through the pipe for a given pressure gradient along the length of the pipe. This loss can be quantified by a parameter, λ, called the resistance coefficient of pipe flow (see Ref. 7, page 79). In Nikuradse's experiments, sand grains of a uniform height, k_s, were applied (as closely packed as possible) to the inside surface of a circular pipe of a given radius, R, and λ was measured for a range of values, k_s, R, and pipe Reynolds numbers. For a particular Reynolds number range the flow in the pipe can be characterized as "completely rough" (see Ref. 7, page 580 for a complete definition of this term), and λ is found to agree very closely with values given by Eqn. (2).

$$\lambda = \frac{1}{(2 \log \frac{R}{k_s} + 1.74)^2} \tag{2}$$

A surface is said to have an equivalent sand roughness of k_s if the measured value of λ for flow over the surface is equal to the value of λ computed using Eqn (2) with the value for k_s. Equivalent sand roughness
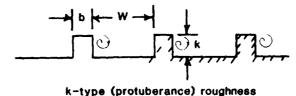
for a particular surface depends on the shape, height, and distribution of surface irregularities (or roughness elements). Figure 2, taken from Ref. 7, page 587, provides a summary of some equivalent sand roughness measurements made by Schlichting.
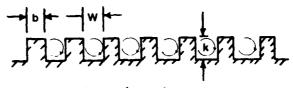
No	item	dimensions	D [cm]	d [cm]	k [cm]	k_s [cm]
1			4	0.41	0.41	0.093
2			2	0.41	0.41	0.344
3	spheres		1	0.41	0.41	1.26
4			0.6	0.41	0.41	1.56
5			densest arrgt.	0.41	0.41	0.257
6			1	0.21	0.21	0.172
7			0.5	0.21	0.21	0.759
8	spherical segments		4	0.8	0.26	0.031
9			3	0.8	0.26	0.049
10			2	0.8	0.26	0.149
11			densest arrgt.	0.8	0.26	0.365
12	cones		4	0.8	0.375	0.059
13			3	0.8	0.375	0.164
14			2	0.8	0.375	0.374
15	'short' angles		4	0.8	0.30	0.291
16			3	0.8	0.30	0.618
17			2	0.8	0.30	1.47

Figure 2. Equivalent Sand Roughness for Various Roughness Types (from Boundary-Layer Theory by Dr. Hermann Schlichting, translated by Dr. J. Kestin. Copyright (c) 1968, McGraw-Hill, Inc. Used with the permission of McGraw-Hill Book Company)

Note from Figure 2 that the ratio of roughness element spacing, D, to roughness element height, k, appears to be an important factor influencing equivalent sand roughness; that is, increasing the ratio D/k for a given surface reduces k_s for that surface.

If the ratio D/k is large, the roughness is said to be k-type or protuberance roughness, while if the ratio D/k is small, the roughness is said to be d-type or cavity roughness. These types of roughnesses are illustrated in Figure 3. An experimental study by Perry et al (Ref. 8) showed that turbulent boundary layer flow is significantly different for surfaces with cavity roughness than it is for surfaces with protuberance roughness for the same height of roughness elements.

k-type (protuberance) roughness

d-type (cavity) roughness

Figure 3. k-type and d-type Roughness

Surfaces of compressor blades and vanes contain a variety of peak (or cavity) shapes and a broad spectrum of peak (or cavity) densities and heights. As noted by Schaffler (Ref. 3), the Ra value of a given surface may not be indicative of the hydrodynamic character of the surface. The effect of surface roughness is felt in turbulent flow when the roughness elements penetrate the laminar sublayer of the turbulent boundary layer. It is conceivable that three surfaces could have equal Ra values and yet could have significantly different effects on the boundary layer flow. In Figure 4, surface (a) has a series of moderate deviations from the mean line with no pronounced peaks or cavities. Surface (b) is quite smooth with occasional pronounced peaks, and surface (c) is a mirror image of (b). Suppose that all protuberances are contained in the laminar sublayer

58

USAFA-TR-83-2

of the boundary layer over surface (a) while the peaks penetrate the
laminar sublayer in case (b). Then (b) should produce a significantly
greater effect on the flow than (a). Surface (c) probably would not
affect the flow in the same way that surface (b) would. Clearly, Ra is an
inadequate measure of "effective roughness," k_e. Effective roughness is a
parameter with a known relationship to flow losses and boundary layer
behavior.
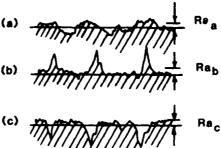
Figure 4. Three Different Surfaces of Equal Ra

Attempts have been made to determine a meaningful expression for the
effective roughness of aircraft engine compressor stage airfoil surfaces.
Schaffler (Ref. 3) has defined an effective roughness parameter k_S:

$$k_S = \overline{y}_{peak} - \overline{y}_{groove} \tag{3}$$

where $\overline{y}_{peak}$ = the arithmetic mean of the 10 highest peaks/millimeter and
$\overline{y}_{groove}$ = the arithmetic mean of the 10 deepest grooves/millimeter. By
performing a number of measurements on compressor blade surfaces,
Schaffler developed the correlation between k_S and Ra shown in Eqn. (4).

$$k_S = 8.9 \text{ Ra} \tag{4}$$

Koch and Smith (Ref. 9) also derived a relationship between
equivalent sand roughness, k_s, and Ra when they measured the ratios k_s/k
and Ra/k for a series of sandpapers. They found that

$$\frac{k_s/k}{Ra/k} = \frac{k_s}{Ra} = 6.2 \tag{5}$$

Eqns. (4) and (5) are of the form

$$k_e = f(Ra) \tag{6}$$

Both Schaffler and Koch and Smith obtained a relation for effective roughness as a function of only Ra, as shown in Eqn. (6). Relationships of this form are used in actual practice (and will be used in the model presented below), because they are currently the best interpretation of available data. From experiments which were discussed above, however, it is known that effective roughness depends on a number of geometric characteristics of the surface, that is, effective roughness can be written in the form of Eqn. (7). The precise form of Eqn. (7) is not known.

$$k_e = f(Ra, \text{ peak density, peak shape, k or d-type, etc.}) \tag{7}$$

A series of systematic experiments would be required to obtain a better expression for effective roughness in terms of measurable surface characteristics and, as suggested by Schaffler, a more accurate specification of Eqn. (7) would provide a significant contribution to our understanding of roughness effects in compressors.

III. A Model for Calculating the Effect of Surface Finish on Axial Compressor Performance in an Aircraft Engine

A. Approach

The model is intended to provide a means for estimating changes in compressor performance which result from changes in blade or vane surface roughness. The flow of the working fluid in a multistage compressor is exceedingly complex, and thus it would be very difficult to base the model on the details of the interactions between individual airfoils and the viscous flow passing over them. It is possible, however, to proceed from the assumption that each stage of a compressor, or the compressor as a whole, can be treated as a control system, so that the integrated effect

60

of detailed interactions between the flow and the airfoils is modeled.
That approach is taken here. Viscous losses in the compressor result in a
temperature rise which is greater than that for isentropic compression
between the compressor inlet and exit total pressures. Since the loss
mechanism stems from the viscous nature of the flow, we examine compressor
efficiency as a function of Reynolds number (the ratio of inertia forces
to viscous forces in the flow) with airfoil surface finish as a parameter.
With proper definition compressor efficiency can be made independent of
the overall compressor ratio, so that results of analyses for compressors
with different pressure ratios can be directly compared. The measure of
compressor efficiency that allows this direct comparison is polytropic
efficiency (this term is defined in Ref. 10). Polytropic efficiency is
used throughout this work. The discussion which follows is based largely
on the work of Schaffler (Ref. 3).

B. Efficiency versus Reynolds Number

Reynolds number effects in axial flow compressors have been
studied extensively. Refs. 11, 12 and 3, and 13 provide examples of test
results of cascade, single stage, and multistage turbomachines,
respectively. I have drawn several conclusions from a review of the data
in these references:

First, for a given compressor operating point (specified by pressure
ratio and corrected speed), as Reynolds number (based on first rotor blade
mean chord) is varied from low to high values, two critical values are
observed: a lower critical Reynolds number, $Re_{crit\ L}$, and an upper critical
Reynolds number, $Re_{crit\ U}$.

Second, below $Re_{crit\ L}$, compressor efficiency increases rapidly with
increasing Reynolds number.

Third, above $Re_{crit\ U}$, compressor efficiency does not change with Reynolds number and is a function of the effective roughness only.

Fourth, between $Re_{crit\ L}$ and $Re_{crit\ U}$ the relationship between ζ and Re can be represented by the equation

$$1 - \eta = K\ Re^{-n} \tag{8}$$

where K – proportionality constant and n is a Reynolds number sensitivity parameter. Figure 5 illustrates conclusions 1 through 4.
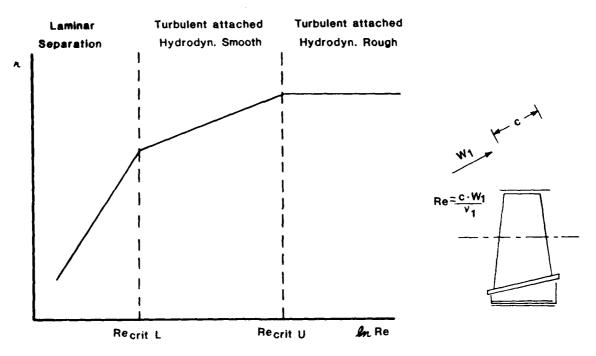
Figure 5. Compressor Performance -- η versus Re (for Given PR and N/ θ)

The poor compressor performance in the region below $Re_{crit\ L}$ is attributed to laminar separation. In this region the laminar boundary layer on a compressor blade contains insufficient energy to overcome the adverse pressure gradient impressed on it by the outer flow, and it separates. Compressor flow is thus reduced, and viscous losses increase sharply. Additional information concerning this region below $Re_{crit\ L}$ may he found in Ref. 3 and will not be discussed further here.

In the region between $Re_{crit\ L}$ and $Re_{crit\ U}$, the flow is turbulent and remains attached. When all surface protuberances are contained within the laminar sublayer of the turbulent boundary layer, the flow is called "hydrodynamically smooth." Losses are independent of roughness so long as all roughness elements are contained in the laminar sublayer. With increasing Reynolds number in this region, the turbulent velocity profile becomes fuller and the thickness of the laminar sublayer is reduced. As roughness elements begin to penetrate this layer, the losses become a function of Reynolds number _and_ roughness.

Above $Re_{crit\ U}$, the flow is still turbulent and attached, but most roughness elements penetrate the laminar sublayer and losses become a function of the roughness only. This region is called "hydrodynamically rough." Note that η increases with Reynolds number until the flow becomes hydrodynamically rough. Thus, roughness provides a constraint on best possible compressor efficiency (at a given compressor operating point).

Schaffler (Ref. 3) has experimentally demonstrated the three regions of compressor behavior described above with five- and six-stage compressors (Figure 6, taken from Ref. 3). Also, he has noted that the "curl over" region (a transition region between hydrodynamically smooth and hydrodynamically rough flow in which ζ is a function of both roughness and Reynolds number) occurs over a small Reynolds number range.

The effect of changing airfoil roughness is shown schematically in Figure 7. Also note that data showing this same effect is presented in Figure 6. Increasing surface roughness reduces the efficiency level at which the flow becomes hydrodynamically rough. Given the compressor operating Reynolds number, Re_{op}, and the η versus Re curve for various surface finishes, it is possible to estimate compressor performance changes associated with changes in surface finish and the surface finish required for best possible performance at that operating point (i.e.
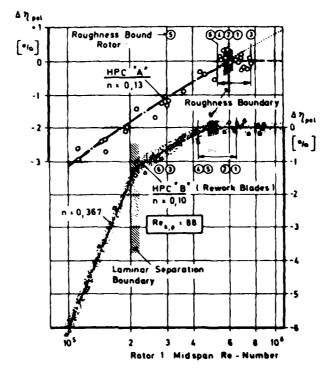
Figure 6.   Effect of Reynolds Number and Surface Roughness on Polytropic
Efficiency of Two Six-Stage Compressors (Figure 5 of Ref. 3)
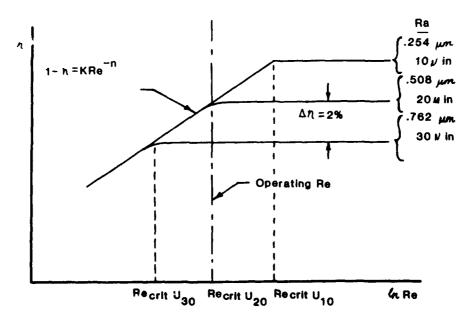
Figure 7.   Effect of Surface Roughness on Compressor Efficiency

hydrodynamically smooth flow). Consider the situation shown in Figure 7.

For the given operating Reynolds number, surface finishes (in terms of Ra)

better than .508μm (20 μin.), would provide no performance improvement.

However, if surface finish is .762 μm (30μin.) and can be reduced to .508μm

(20μin.), then compressor efficiency should improve by two percent as a

result of that change. Note that the curve of η versus Re for

hydrodynamically smooth and rough flow is defined by the parameters n and

$Re_{crit\ U}$. The procedure for estimating these two parameters will be

discussed below.

C. Critical Roughness Reynolds Number

To determine $Re_{crit\ U}$, the point of transition from

hydrodynamically smooth to hydrodynamically rough flow on the η versus Re

curve must be found. This transition will occur when roughness elements

on the surface protrude through the laminar sublayer of the turbulent

boundary layer flow over the surfaces. The size of the roughness elements

for which this will occur has been related to the equivalent sand

roughness parameter by a series of experiments with rough flat plates.

These experiments have led to the definition of the "critical roughness

Reynolds number," Re_{k_s}. This is a Reynolds number based on equivalent

sand roughness that defines the transition from smooth to rough flow

described above. Schlichting (Ref. 7) presents the following simple

formula applicable to fully turbulent flow over a rough flat plate:

$$Re_{k_s} = k_s \frac{W_1}{\nu} \le 100 \qquad (9)$$

where k_s is equivalent sand roughness. W_1 is the relative velocity of

flow past the plate, and ν is the kinematic viscosity. Eqn. (9) means

that for a rough flat plate with Re_{k_s} less than 100, the flow is

hydrodynamically smooth. As suggested by Koch and Smith (Ref. 9), flow

conditions in an operating compressor may be significantly different from

those of flat plate flow (i.e. strong adverse pressure gradient, laminar and turbulent boundary layer, and unsteady flow) and therefore Eqn. (9) should be modified for use in compressors. They recommend

$$k_S \frac{W_1}{\nu} \leq 90 \tag{10}$$

where k_S is 6.2 Ra. Schaffler's experimental results (Ref. 3) showed

$$k_S \frac{W_1}{\nu} \leq 88 \text{ (electrochemically machined blades)} \tag{11}$$

$$k_S \frac{W_1}{\nu} \leq 135 \text{ (ground blades)} \tag{12}$$

where k_S is 8.9 Ra. Not that Eqns. (10) through (12) can be written in the form

$$k_e \frac{W_1}{\nu} = k_e \frac{R_e}{c} \leq E \tag{13}$$

where k_e is the effective roughness, Re/c is the Reynolds number per unit length (based on stage relative velocity and blade chord), and E is the empirically determined constant as in the right hand sides of Eqns. (9) to (12). Considering the equal sign in Eqn. (13), rearranging and taking logarithms yields

$$\ln(k_e) = \ln(E) - \ln(Re/c) \tag{14}$$

This result is shown graphically in Figure 8 for a general (unspecified) value of E. The equation is a straight line on logarithmic axes. The region below the diagonal $\left[\text{Eqn. (14)}\right]$ is hydrodynamically smooth $[\eta = f(n, Re)]$ f(n,Re) and that above the diagonal is hydrodynamically rough $[\eta = f(k_e)]$ The bar represents the distribution of stage Reynolds number divided by blade mean chord length, c, (Re/c). This must be determined for the compressor with known surface finish at a given operating point (pressure ratio and corrected speed) and aircraft mission point (Mach number, M, and altitude, h).
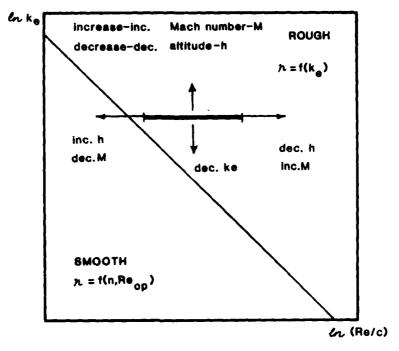
Figure 8. Hydrodynamically Rough and Smooth Regions

The location of the Re/c distribution changes (for the same compressor operating point) as the mission changes; high altitude and low Mach number shift the distribution to the left and low altitude and high Mach number shift it to the right in Figure 8. Changes in surface finish move the Re/c distribution in the vertical direction in Figure 8. Best possible compressor performance (at a given operating point) occurs when the Re/c distribution is in the hydrodynamically smooth region. It is not known with certainty how many stages of a multistage compressor must be hydrodynamically rough before the whole compressor behaves as rough; Schaffler's data (Ref. 3) indicates approximately 60 percent of the total number of stages.

Using Eqn. (13), it is possible to determine $Re_{crit\ U}$. Note that when the equal sign applies in Eqn. (13),

$$E \frac{c}{k_e} = \frac{Rek_e}{c} \frac{c}{k_e} = Re \qquad (15)$$

where c/k_e is the ratio of blade chord to effective roughness for a stage. So, for a given value of E, and with a knowledge of c/k_e for each compressor stage, $Re_{crit\ U}$ is computed as follows:

$$Re_{crit\ U} = \frac{1}{Z} \sum_{i=1}^{Z} E\left(\frac{c}{k_\epsilon}\right)_i \qquad (16)$$

where Z = number of compressor stages. This is simply the average, over all machine stages, of the stage Reynolds number corresponding to the transition from hydrodynamically smooth to rough flow.

D. Reynolds Number Sensitivity Parameter

To determine the Reynolds number sensitivity parameter, n, recall that below $Re_{crit\ U}$, η and Re are related by Eqn (8), which is

$$1 - \eta = K\ Re^{-n} \qquad (8)$$

Wassell (Ref. 14) has developed an empirically based correlation for the determination of n. He examined η versus Re for 20 different compressors over a broad range of Reynolds number. He assumed that

$$n = p \cdot q \qquad (17)$$

where p depends on the mean Mach number level in the compressor and q is a function of compressor geometry. Schaffler (Ref. 3) compared experimental values of n with those found from the Wassell correlation and found good agreement. Refer to Ref. 13 for details of the use of the Wassell correlation.

E. Calculation of Efficiency Change

If the value of n for the compressor and values of $Re_{crit\ U}$ for various surface roughnesses are known (corresponding to a given compressor operating point), then curves of η versus Re can be generated for the various roughnesses. For hydrodynamically smooth flow, we have Eqn. (8):

$$1 - \eta = K\ Re^{-n} \qquad (8)$$

So, with respect to reference values, η_{ref} and Re_{ref}, we may write

$$\frac{1-\eta}{(1-\eta)_{ref}} = \left(\frac{Re}{Re_{ref}}\right)^{-n} \tag{18}$$

If we take logarithms and then exponentials of each side we obtain

$$1 - \eta = (1-\eta)_{ref} \, \exp\left[-n \, \ln\left(\frac{Re}{Re_{ref}}\right)\right] \tag{19}$$

Then, defining $\Delta\eta$ as

$$\Delta\eta = \eta_{ref} - \eta \tag{20}$$

we obtain
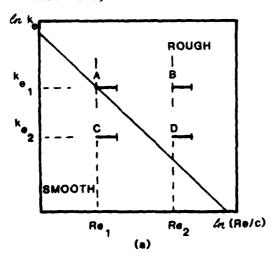
$$\Delta\eta = (1-\eta)_{ref} \left\{\exp\left[-n \, \ln\left(\frac{Re}{Re_{ref}}\right)\right] - 1\right\} \tag{21}$$

Eqn (21) can be used to compute the compressor efficiency change between two values of $Re_{crit\ U}$ corresponding to two different roughnesses. Recall that $Re_{crit\ U}$ is computed by Eqn. (16).

F. Relationship between η versus Re and K versus Re/c Curves.

Figure 9 shows how the results of the preceding sections can be used to estimate the effects of surface roughness on compressor efficiency.
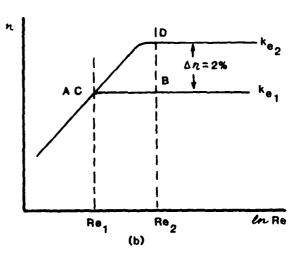
Figure 9. Relationship between k versus Re/c and η versus Re

In part (a) of Figure 9, Re/c distributions corresponding to two operating
Reynolds numbers (Re$_1$ and Re$_2$) and two roughnesses (ke$_1$ and ke$_2$) are
shown. The bar represents the distribution of Re/c for the compressor.
Corresponding operating Reynolds numbers and roughnesses are shown in part
(b). Consider a compressor operating at point B (roughness = K$_{e_1}$).
Reducing the Re/c distribution to point A (by increasing altitude, for
example) produces no change in η because the Re/c distribution stays in
the hydrodynamically rough region. Reducing roughness from B to D
produces a two percent increase in η at the same operating Reynolds number
even though the flow is still hydrodynamically rough at D. Now consider
moving from D to C by reducing the operating Reynolds number. As shown in
part (a), the Re/c distribution soon enters the smooth region and then η
decreases according to $1- \eta = k \, Re^{-n}$ as shown in part (b).

G. Model Summary

Eqns. (7), (13), (16), (17), and (21) constitute the empirical
model for estimating roughness effects in axial flow compressors. They
are repeated here for convenience.

$$k = f(Ra, \text{ peak density, peak shape, k- or d-type, etc.}) \qquad (7)$$

$$k_e \, \frac{Re}{c} \leq E \qquad (13)$$

$$Re_{crit \, U} = \frac{1}{Z} \sum_{i=1}^{Z} E\left(\frac{c}{k_e}\right)_i \qquad (16)$$

$$n = p \cdot q \text{ where p and q are determined by the method of Ref. 14} \qquad (17)$$

$$\Delta \eta = (1-\eta)_{ref} \left\{ \exp\left[-n \, \ln\left(\frac{Re}{Re_{ref}}\right)\right] - 1 \right\} \qquad (21)$$

Until further data becomes available, I recommend the use of Schaffler's results in Eqns. (7) and (13). Thus, Eqns. (4) and (11) are used in the illustrative examples in the next section so that

$$k_e = 8.9 \text{ Ra} \tag{22}$$

$$k_e = \frac{Re}{c} \leq 88 \tag{23}$$

IV. Application of the Model

A. Choice of the Application

In this section, results are presented from the application of the empirical model to the compression sections of three Air Force Engines: the TF33-PW-7, the F100-PW-100, and the J85-GE-5H. The surface finishes required for hydrodynamically smooth flow at various mission points are estimated. Also, the changes in compressor efficiency, which could be achieved by reducing airfoil roughness to that for hydrodynamically smooth flow, are computed.

The TF33-PW-7 was chosen for three reasons: first, it is a primary Air Force fuel user, second, other studies of airfoil surface finish have been performed on this or similar engines (Refs. 1 and 2), and third, it is a transport engine with a well-defined mission profile. The F100-PW-100 was chosen because it is a fighter engine representing relatively current technology. The J85-GE-5H was chosen because of its potential use in a roughness effects test in the Aero Propulsion Laboratory's Compressor Research Facility. A J85 test rig has been procured for facility checkout and it will be used as a vehicle for testing roughness effects.

B. TF33-PW-7

The TF33-PW-7, 7A is used to power the USAF C-141 fleet. The engines were first delivered in 1964 and are currently consuming about 600

million gallons of fuel per year (Ref. 15). Table 1 shows an aggregate mission for the C141B; it is a statistical representation of 23 different missions including training, exercise, airlift, and contingency flight profiles (Ref. 15).

TABLE 1				
AGGREGATE MISSION FOR C141B				
	Altitude Feet	M	Power	Time Minutes
Takeoff	Sea Level	0.15	Max. T/O	6.0
Climb	(1)	(1)	NR	16.0
Cruise	37,000	0.74	75-80% NR	203.0
Descent	(2)	(2)	Idle	21.0
Approach and Land	500'	0.2	30% MR	18.0
Taxi (In and Out)	0	0	Idle	25.0
			TOTAL	289.0

(1) 250 Kts to 10,000 Ft., 280 Kts to 0.7 M
    Fuel Increased 50% to Reflect Touch & GO & GO Around Training
(2) Reverse Climb Path

MR= Military Rated
NR= Normal Rated

Note that the aircraft is in the cruise condition for 70 percent of total mission time. The empirical model for roughness effects can be applied for any given aircraft mission point (M and altitude) and compressor operating point. Only the cruise condition is considered here since it is the major portion of the aggregate mission.

Figure 10 shows the distribution of Reynolds number per unit length (Re/c) for the compression section of this engine at M = 0.75 and h =

35,000 feet, with an assumed Ra of 1.778 μm (70 μ in). This is a
conservatively high Ra from field measurements.
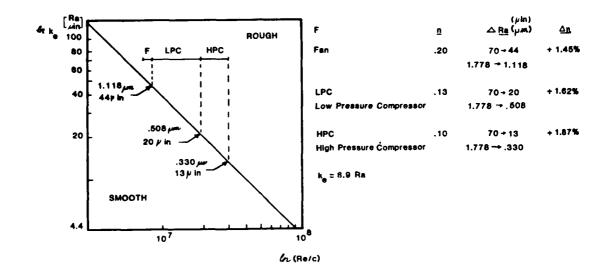
Figure 10. Re/c Distribution for TF33-PW-7 -- Cruise Mission

Note that the fan, low pressure compressor (LPC), and high pressure
compressor (HPC) are all in the hydrodynamically rough region. Also, note
the values of n, which were computed using the Wassell correlation for
each component. These components would have to be smoothed to Ra = 1.118,
.508, and .330 μm, respectively, in order for the flow to be completely in
the hydrodynamically smooth region. Component efficiency changes
corresponding to a reduction from Ra = 1.778μm to these levels are 1.45
percent, 1.62 percent, and 1.87 percent. An Aero Propulsion Laboratory
analysis of the TF33-PW-7 for similar efficiency changes yielded an
approximate 1.5 percent reduction in TSFC at the cruise thrust level.
This result is consistent with the experimental data of Refs. 1 and 2.

73

C. F100-PW-100

The F100-PW-100 is used in the F-15 aircraft. In contrast to the TF33, the F100 is required to operate over an extensive range of flight conditions. The aggregate mission for the F100 in the F-15 has more elements and is more complex than that for the TF33. Figure 11 illustrates the effect of Mach number and altitude on the distribution of Reynolds number per unit length for the compression section of this engine.
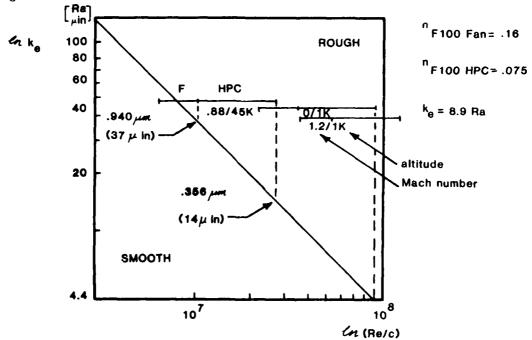
Figure 11. Re/c Distribution for F100-PW-100 -- Various Missions

The M = .88, h = 45,000 feet condition represents a ferry mission, while the low altitude mission demonstrates the high values of Re/c (and corresponding low values of Ra required for hydrodynamically smooth flow) which can occur during F100 operation. Given the amount of time spent at each altitude/Mach number condition in the aggregate mission, the corresponding Re per unit length, and the model described in this paper,

it is possible to estimate an aggregate TSFC reduction which would result
from changes in compressor airfoil surface finish. No further analysis or
discussion will be presented here, since the primary purpose of this
example is to illustrate Mach number and altitude effects on compressor
Re/c distributions.

D. J85-GE-5H

A J85-GE-5H compressor is being used to verify the operation of
the Aero Propulsion Laboratory's Compressor Research Facility. This
compressor will be used for an investigation of roughness effects on J-85
compressor efficiency. The Compressor Research Facility provides
compressor inlet pressure control (atmospheric to approximately 2 psia),
so performance for a range of Reynolds numbers can be examined.
Production J85 blades and vanes have a surface roughness of approximately
Ra = .508 μm. A parametric variation of surface finish will be used in
this test in an attempt to isolate and measure roughness effects on
efficiency independent of other influences. Figure 12 shows the Re/c
distributions for a J-85 compressor (at design conditions) over a range of
inlet pressures and surface roughnesses. Figure 13 shows curves of
efficiency versus Reynolds number corresponding to the roughness levels in
Figure 12. Note that the range of surface roughnesses and inlet pressures
suggested in Figure 13 provides ample opportunity for investigation of the
transition from hydrodynamically smooth to rough flow in the J85
compressor. This example has been provided to illustrate the application
of the empirical model in forecasting test results for a planned
Compressor Research Facility test.

V.   Conclusion

This paper has provided an explanation of some of the problems
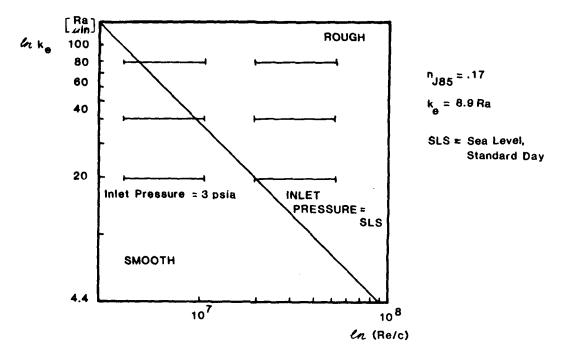
Figure 12.   Re/c Distributions for J85 Compressor -- Various Inlet
Pressures and Surface Roughnesses
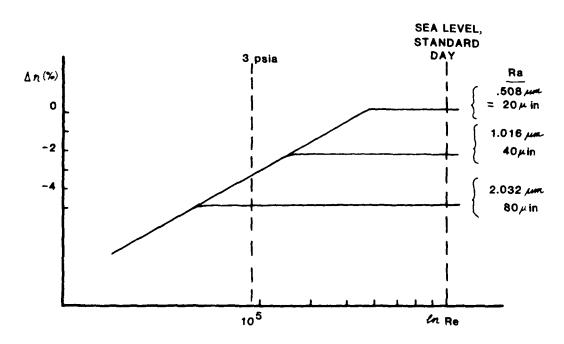
Figure 13.   Efficiency versus Re Corresponding to Figure 12

associated with surface roughness measurement and a description of an
empirical model which can be used to estimate the effect of airfoil
surface finish changes on axial compressor performance. It must be
emphasized that compressor efficiency changes, which are calculated
through the use of this model, must be treated as estimates; much more
experimental data is required for "calibration" of the model. However,
this model is useful in that it provides insight into the problems of
estimating airfoil surface finish effects on compressor efficiency. The
relationship between measured surface properties and effective roughness
is of primary importance and the understanding of that relationship
requires additional investigation.

Symbols

English Symbols

b	roughness element width in k- and d-type roughness
c	blade/vane chord length
d	roughness element width
D	peak spacing
E	empirical constant in equation (13)
EGT	exhaust gas temperature
h	altitude
k	roughness element height
k_e	effective roughness
k_s	equivalent sand roughness
k_S	roughness defined by Eqn. (3)
K	proportionality constant
L	sampling length in Ra definition
M	Mach number
n	Reynolds number sensitivity parameter

N	engine speed
p	parameter used to define n; $n = p \cdot q$
PR	pressure ratio
q	parameter used to define n; $n = p \cdot q$
R	pipe radius
Ra	arithmetic average roughness
Re	Reynolds number (usually based on midspan of first rotor)
Re_{k_s}	critical roughness Reynolds number
Re_{op}	Re corresponding to the compressor operating point and aircraft mission conditions
$Re_{crit\,L}$	lower critical Reynolds number based on first rotor blade mean chord
$Re_{crit\,U}$	upper critical Reynolds number based on first rotor blade mean chord
TSFC	thrust specific fuel consumption
W_1	roughness element spacing in k- and d-type roughness
W	relative velocity
y	ordinate or curve of roughness profile
$\bar{y}_{peak}$, $\bar{y}_{groove}$	see definition of k , Eqn. (3)
z	number of stages in turbomachine

Greek Symbols

η	polytropic efficiency
μ	kinematic viscosity
θ	temperature ratio - used in corrected speed $N\sqrt{\theta}$
λ	flow loss coefficient (pipe flow)

Subscripts

i   denotes i^{th} stage of turbomachine

ref   reference values of η and Re

References

1. Pratt & Whitney Aircraft Surface Roughness Analysis, Curve No. 317563, Pratt and Whitney Aircraft, Dec 77.

2. Ross, E., The Silver Streak Effort, Oklahoma City Air Logistics Center (OC-ALC/MA) Aug 79.

3. Schaffler, A., "Experimental and Analytical Investigation of the Effects of Reynolds Number and Blade Surface Roughness on Multistage Axial Flow Compressors." Transactions of the ASME Journal of Engineering for Power, Vol 102, No. 1, Jan 1980, pp. 5-13.

4. United States Air Force Process 5375 Briefing, April 9, 1980, SermeTel, Inc.

5. Surface Texture. (ANSI B46.1-1978), American Society of Mechanical Engineers, NY, 1978.

6. Nikuradse, J., "Stromungsgesetze in rauhen Rohren." Forsch. Arb. Ing.-Wes. No. 361 (1933).

7. Schlichting, H. Boundary Layer Theory, McGraw-Hill, New York, Sixth Ed., 1968.

8. Perry, A.E., Schofield, W.H., Joubert, P.N., "Rough Wall Turbulent Boundary Layers." Journal of Fluid Mech, Vol 37, Part 2, 1969, pp. 383-413.

9. Koch, C.C. and Smith, L.H., Jr., "Loss Sources and Magnitudes in Axial-Flow Compressors." ASME Journal of Engineering for Power, Vol 98, No. 3, Jul 1976, pp. 41-424.

10. Oates, Gordon C., ed., The Aerothermodynamics of Aircraft Gas Turbine Engines, AFAPL-TR-78-52, July 1978, Chapter 6.

11. Ainley, D.G. and Smith, A.G., Some Notes Concerning the Influence of Reynolds Numbers on Axial Compressor and Turbine Performance. Aeronautical Research Council, Report No. 13775, 1951.

12. Neustein, J., "Low Reynolds Number Experiments in an Axial Flow Turbomachine." ASME Journal of Engineering for Power, Vol 86, No. 3, Jul 1964, pp. 257-295.

13. Lowrie, B.W., The Influence of Reynolds Number on Axial Compressors - A Correlation of Data within Rolls-Royce. Rolls-Royce Ltd Internal Report No. RCR 90086, 1966.

14. Wassell, A.B., "Reynolds Number Effects in Axial Compressors." ASME Journal of Engineering for Power. Vol 90, No. 2, Apr 1968, pp. 143-156.

15. A Feasibility Study on Improving the Thrust Specific Fuel Consumption for the TF33-P-7 Engines, Pratt and Whitney Aircraft Group, FP80-840, 18 Aug 80.

AN EXAMPLE OF UNCERTAINTY ANALYSIS IN COMPRESSOR TESTING

R.J. Stiles* and C.A. Boedicker**

Abstract

This paper presents an overview of the most fundamental and important concepts in uncertainty analysis, a technique which can be used by a test engineer to estimate the accuracy of measured data and values that are calculated from measured data. Some of the results of an uncertainty analysis which was accomplished for a turbine engine compressor test are used to illustrate the analysis procedure and results. Also, the benefits of doing an uncertainty analysis as part of a test are briefly discussed.

I.   Introduction

Performance indices and aerothermodynamic parameters that are used to assess the performance of turbine engine components are based upon measurements of basic quantities like pressure, temperature, force, and position. Values for these basic quantities are obtained by processes that inevitably yield measurement error (i.e., the difference between the true value of the quantity of interest and the value indicated by a particular measurement process). Furthermore, if a performance index is computed as a function of measured values, then the effect of measurement error is to introduce error in the performance index itself; the measurement error propagates through the performance calculation.

Uncertainty analysis is a procedure that can be used before a test to estimate the maximum measurement errors that can reasonably be expected for particular measurement processes and the effects of these errors on calculated parameters, which are derived from the measured values. In order to conduct a meaningful evaluation of a turbine engine component, it is necessary to understand, and often to minimize, the sources of error in both measured and computed values.

Our objective in writing this paper is to provide an overview of the fundamentals of uncertainty analysis and to present some results from an

*Major, USAF, AFWAL Aero Propulsion Laboratory
**C1C, USAF Academy

uncertainty analysis which was performed for the test of a centrifugal
compressor at the AFWAL (Air Force Wright Aeronautical Laboratories) Aero
Propulsion Laboratory's Compressor Research Facility (CRF),
Wright-Patterson AFB, Ohio. Ref. 1 presents a complete description of the
CRF. We have not written a step-by-step procedure for accomplishing an
uncertainty analysis; the interested reader should see Ref. 2 for that
kind of information. This overview of a specific application of
uncertainty analysis and the accompanying examples are intended to
illustrate the utility of the analysis procedure and results.

II   Compressor Flowpath and Performance Calculations

The Garrett Turbine Engine Company has designed and manufactured a
variable-geometry centrifugal compressor (Figure 1), which will be tested
at the CRF.

Figure 1.   Variable-Geometry Centrifugal Compressor

At its design operating speed (23,000 RPM), this compressor produces a
pressure ratio of 8:1 in a single stage and has an airflow rate of
approximately 11.34 Kg/sec (25 lbm/sec). The test is designed to
demonstrate the effects of variable inlet guide vanes and variable
diffuser area on centrifugal compressor performance. Analysis has shown
that near-design levels of compressor ratio and efficiency can be
maintained over a broad range of flow rate by properly adjusting the
variable geometry hardware. The ability to modulate airflow in a turbine
engine by simple geometry changes is quite useful. For example, in a
turbofan application the variable-geometry compressor, when coupled with a
variable-geometry turbine, would provide variable engine bypass ratio by
changing core airflow. Bypass ratio could then be adjusted to minimize
fuel consumption for a range of flight conditions.

A cross-section of the compressor flowpath, with measurement station
designation, is shown in Figure 2.
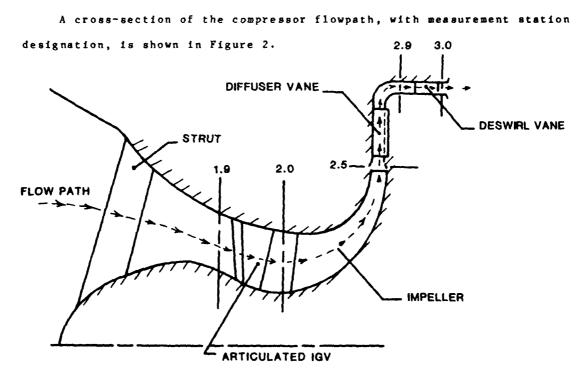
Figure 2. Compressor Flowpath and Station Designation

More than 300 individual measurement probes have been installed in this
compressor and 20 different measured values M_j (j=1,20) along the flowpath
are used in the calculation of 65 performance and aerothermodynamic
parameters C_i (i=1,65). Measured values of pressures and temperatures at
a specific measurement station along the flowpath are derived from an
arithmetic average of the measurements from individual probes
circumferentially distributed (with respect to the flow) at that station.
A detailed description of all of the measurements and calculations
associated with this test is outside the scope of this paper. Discussions
of specific measurements and calculations are presented where appropriate
in the sections that follow.

III. Uncertainty Analysis Overview

In this section we overview the most fundamental and important
concepts in uncertainty analysis. The interested reader should refer to
the many books and journal articles concerning uncertainty analysis for
additional details (Refs. 2 through 5, for example). We have followed the
methodology of Refs. 2 and 5 in the information presented here.

"Measurement error" is the difference between a measured value and
the true value, as defined by the National Bureau of Standards (NBS), of
the quantity being measured (Ref. 2). "Measurement uncertainty" is the
maximum measurement error that might reasonably be expected; uncertainty
is a measure of accuracy. The problem in uncertainty analysis is to
construct an uncertainty interval which limits measurement error.

Assuming that there are no gross errors in the measurement (i.e.,
human error or instrument malfunctions), then there are two components of
measurement error: (1) precision (random) error and (2) bias (fixed)
error.

A. Precision Error

If a particular measurement process is repeated many times, one will find that the results can be plotted in a frequency distribution, as illustrated in Figure 3.
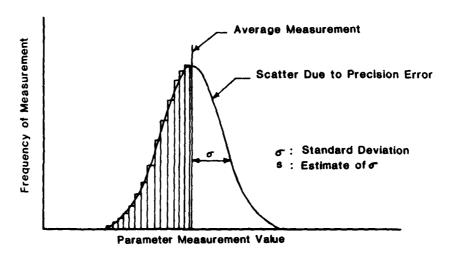
Figure 3. Precision Error

The frequency distribution will usually be a normal one, the consequence of random errors from a number of independent influences in the measurement system. Precision error is the variation between repeated measurements; the standard deviation (σ) of the frequency distribution is used as a measure of this error. Also, for finite sample size, the statistic S is used to calculate an estimate of the standard deviation. S is called the precision index and is calculated as follows.

$$S = \sqrt{\frac{\sum_{i=1}^{N} (X_i - \bar{X})^2}{N-1}} \qquad (1)$$

where N = number of measurements represented in the frequency distribution and $\bar{X}$ = average value of the individual measurements X_i.

It is particularly significant to note that the precision error can be reduced by making many measurements of the same variable. The standard deviation of the mean of "n" independent measurements is equal to $1/\sqrt{n}$ times the standard deviation of the frequency distribution for a single measurement. Therefore, the use of redundant instrumentation and/or multiple measurements over a period of time for values which must be known accurately is very important in turbine engine testing. It is important to distinguish between N and n. N corresponds to the number of data scans one uses to arrive at a single measured value of the parameter of interest. The symbol n refers to either the number of times the measurement is obtained over a period of time or the number of redundant measurements of the same parameter.

B. Bias Error

The second component of measurement error, bias error, is significantly more difficult to estimate than precision error. Bias error (sometimes called systematic error) is constant during a test and, therefore, averaging repeated measurements does not affect the bias. Bias can only be determined by comparing a measured value with the true (NBS) value of the quantity being measured. Known bias is normally determined by a calibration procedure in which a measurement instrument is compared (and corrected) so that it agrees with a standard instrument over the measurement range. However, after elimination of the known bias, unknown bias remains, and it must be estimated as part of the uncertainty analysis. In most cases, the data engineer must use his judgment to estimate an upper limit on the unknown bias error; i.e., he must specify the "bias limit, B." Note that the estimate of bias error does not have a statistical basis as does the estimate of precision error. Figure 4

illustrates the bias and precision error that combine too form measurement
error.
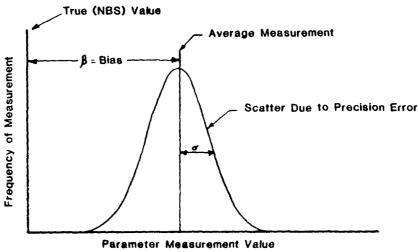
Figure 4. Bias and Precision Error

C. Combining Elemental Error Sources

As part of an uncertainty analysis, one must develop estimates of
bias and precision errors for each measured quantity. Before this can be
done, though, the measurement process must be defined. Specifically, the
test procedure, instrumentation type, and number of sensors must be known.
Then estimates of bias and precision errors for measurement subprocesses
(i.e., calibration, data acquisition, and data recoding) can be made. The
elemental estimates for the subprocesses are then combined by
root-sum-square (as in Eqns. (2) and (3) to give bias limit and precision
index estimates for individual measurements.

$$S = \sqrt{S^2_{calib} + S^2_{data\ acq} + S^2_{data\ rec}} \qquad (2)$$

$$B = \sqrt{B^2_{calib} + B^2_{data\ acq} + B^2_{data\ rec}} \qquad (3)$$

87

D. Combining Bias and Precision -- Measurement Uncertainty

It is convenient to combine the estimates of bias and precision error into a single number (i.e., measurement uncertainty), which can be interpreted simply as the largest error one should reasonably expect for a given measurement. A more rigorous statement of the meaning of uncertainty is not possible because it is the combination of a statistic (precision) and a judgment (bias). At best, we can say that the measurement uncertainty estimate provides a number that is analogous to a confidence interval. The author of Ref. 5 suggests calculation of measurement uncertainty by the equation

$$U_{99} = \pm (B + t_{95} S) \tag{4}$$

where B is the bias limit, S is the precision index, and t_{95} is the 95th percentile point for the two-tailed Students t-distribution. The t_{95} value depends on sample size; it decreases with increasing sample size and has a lower limit of 1.96. For sample sizes of 30 or more, $t_{95} = 2$ is often used in Eqn. (4). Note that the effect of t is to inflate U_{99} and thus reduce the risk of underestimating S when a small sample is used to calculate S. The subscript 99 on U indicates (loosely) a 99 percent confidence level for the uncertainty computed from Eqn. (4). Figure 5 illustrates the concept of measurement uncertainty.

E. Uncertainty of Calculated Values

Measurement uncertainties, which are computed using Eqns. (2) through (4) propagate through calculations involving those measurements. One can estimate the effect of measurement uncertainty on a given calculated value by expanding the calculated value (which is a function of j measurements) in a Taylor Series. It can be shown that the precision and bias errors of a computed value are (for a first-order Taylor Series expansion)

$$S_{C_i} = \sqrt{\sum_j \left(\frac{\partial C_i}{\partial M_j} S_{M_j}\right)^2} \tag{5}$$

$$B_{C_i} = \sqrt{\sum_j \left(\frac{\partial C_i}{\partial M_j} B_{M_j}\right)^2} \tag{6}$$

where the subscripts on S and B pertain to the i_{th} computed value (C_i) and the jth measured value (M_j). Details for the derivation of Eqns. (5) and (6) are given in Appendix B of Ref. 2. The uncertainty of calculated values can be determined using Eqn. (4).

Note that in order to determine the bias limit and precision index (and then the uncertainty) of a computed value, the partial derivatives $\partial C_i/\partial M_j$ in Eqns. (5) and (6) must be known. For a few simple calculations one may be able to compute the partial derivatives analytically. However, in most experiments in which many calculations and measurements are involved, it is more convenient to use a numerical procedure to estimate these terms. For the test that is the subject of this paper, there were 65 calculations involving 20 independent measured values. The partials $\partial C_i/\partial M_j$ (sometimes called the in nce coefficient matrix) were computed using the first order approximation.

$$\frac{\partial C_i}{\partial M_j} = \frac{C_i' - C_i'}{M_j' - M_j} \tag{7}$$

where C_i is derived from the nominal set of measurements and C_i' is derived from a measurement set with all nominal values except M_j, which is M_j' and is one percent higher than its nominal value. Note that the terms given by Eqn. (7) will, in general, have dimensions. It is desirable to be able to review the influence coefficient matrix to determine the most significant terms, but this is not possible unless all

the terms have the same dimensions or are dimensionless. Therefore, we
chose to alter the influence coefficient matrix as follows.
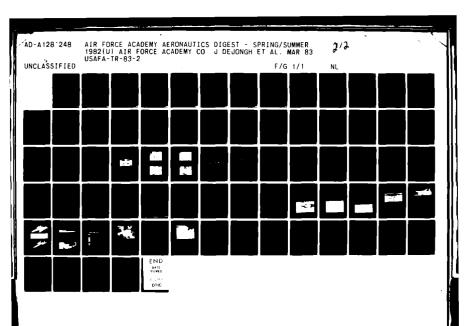
$$\text{Dimensionless Influence Coefficient} = \frac{\partial C_i}{\partial M_j} \cdot \frac{M_j}{C_i} = \frac{(C_i' - C_i)/C_i}{(M_j' - M_j)/M_j} \tag{8}$$

Since M_j' is always one percent greater than M_j , influence coefficients
in the form of Eqn. (8) give the percentage change in C_i corresponding to
a one percent change in M_j. Also, influence coefficients in dimensionless
form can be used in Eqns. (5) and (6) as long as bias and precision errors
are expressed as percentages.

IV. Results and Illustrative Examples

    We have chosen to present the results of the centrifugal compressor
uncertainty analysis for only 10 of the 65 calculated parameters involving
10 (of the total 20) different measurements, since our objective is only
to illustrate the analysis procedure and results. Table I lists these 10
measurements and also gives estimated bias limits and precision indices
(percent of reading) for the measurements.

    Figure 6 is the dimensionless influence coefficient matrix for the 10
measurements and 10 calculations we have chosen to highlight. Values in
each row are the percentage change in the calculated value (at the far
left of each row) corresponding to a one percent change in the measurement
directly above the value. One can compare magnitudes of the values in
each row to find the most important measurements affecting a calculation.
Comparing magnitudes of the values in each column shows w..ich calculated
parameters are most affected by a given measurement. The influence
coefficient matrix is a valuable tool, not only for determining important
measurements, but also for direct estimates of the effects of measurement
changes. It is important to note that the influence coefficients in

MICROCOPY RESOLUTION TEST CHART
NATIONAL BUREAU OF STANDARDS-1963-A

Measurement
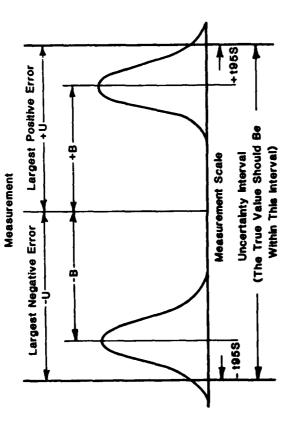
Figure 5. Measurement Uncertainty (Ref. 5)

Table I

COMPRESSOR MEASUREMENTS AND THEIR BIAS AND PRECISION ERRORS

Measurement*	P_T 19	T_T 20	W	N	T_T 30	P_S 25	P_S 29	P_T 29	P_T 30	SH
No. of Sensors	10	10	1	1	32	8	8	32	32	1
Bias Error (%)	0.16	0.215	0.50	0.0	0.215	0.16	0.16	0.16	0.16	0.20
Precision Error (%)**	0.15	0.054	0.25	0.0016	0.054	0.33	0.50	0.50	0.50	0.054

*See Figure 6 for definitions of the measurement names.
**For a single sensor.

MEASURED VALUES

	P_T 19	T_T 20	W	N	T_T 30	P_S 25	P_S 29	P_T 29	P_T 30	SH
AM 19	-0.126E 01	0.642E 00	0.128E 01	0.0	0.0	0.0	0.0	0.0	0.0	0.479E-02
AM 20	-0.133E 01	0.677E 00	0.136E 00	0.0	0.0	0.0	0.0	0.0	0.0	0.493E-02
BETA 20	0.478E 00	-0.430E 00	-0.485E 00	0.372E 00	0.0	0.0	0.0	0.0	0.0	-0.288E-02
RM 20	-0.324E 00	-0.221E 00	0.335E 00	0.788E 00	0.0	0.0	0.0	0.0	0.0	-0.112E-02
AM 25	-0.832E-04	-0.160E 01	0.129E 01	-0.104E 01	0.176E 01	-0.126E 00	0.0	0.0	0.0	0.591E-02
ALPH 25	0.0	-0.348E 00	-0.237E 00	-0.361E 00	0.446E 00	0.236E 00	0.0	0.0	0.0	0.776E-03
BETA 25	0.0	-0.359E 01	-0.610E 00	-0.403E 01	-0.431E 01	0.611E 00	0.0	0.0	0.0	-0.187E-01
P_T 25	0.122E-02	-0.227E 01	0.188E 00	-0.151E 01	0.261E-01	0.813E 00	0.0	0.0	0.0	-0.687E-02
AM 29	-0.895E-03	-0.368E-02	0.142E-03	0.448E-02	-0.125E-01	0.102E-02	-0.893E 01	0.819E 01	0.0	-0.977E-03
ETAAD	-0.630E 00	0.204E 01	0.0	0.0	-0.206E 01	0.0	0.0	0.0	0.632E 00	-0.335E-02

AM 19 — Mach Number - Station 19*
AM 20 — Mach Number - Station 20
BETA 20 — Relative Flow Angle - Station 20
RM 20 — Relative Mach Number - Station 20
AM 25 — Mach Number - Station 25
ALPH 25 — Absolute Flow Angle - Station 25
BETA 25 — Relative Flow Angle - Station 25
P_T 25 — Total Pressure - Station 25
AM 29 — Mach Number - Station 29
ETAAD — Adiabatic Efficiency

P_T 19 — Total Pressure - Station 19
T_T 20 — Total Temperature - Station 20
W — Airflow Rate
N — Mechanical Speed (RPM)
T_T 30 — Total Temperature - Station 30
P_S 25 — Static Pressure - Station 25
P_S 29 — Static Pressure - Station 29
P_T 29 — Total Pressure - Station 29
P_T 30 — Total Pressure - Station 30
SH — Specific Humidity

*See Figure 2 for station designation.

Figure 6. Influence Coefficient Matrix

92

Figure 6 are valid for only one set of measured variables. In this case
they correspond to conditions at 100 percent compressor design speed.

Table II lists the 10 calculated parameters along with the expected
uncertainties in these values (expressed as a percentage). The
uncertainties were derived using equations (4) through (6), the
measurement errors shown in Table I, and the influence coefficients in
Figure 6. These values are only valid at 100 percent design speed; at
other speeds we would expect changes in the influence coefficients and
thus the measurement uncertainty values.

We now present two examples that serve to clarify and illustrate the
use of the results shown in Tables I and II and Figure 6.

A. Example 1: Mach Number Calculations

There are four Mach number calculations represented in Figure 6
(not including the relative Mach number calculation RM20); they are AM19,
AM20, AM25, and AM29. Referring to the measurement station in Figure 2,
note that these are the Mach number values before the inlet guide vanes,
before the impeller, before the diffuser, and after the diffuser/90 degree
bend, respectively. The calculated Mach numbers are of interest both in
themselves, to indicate compressibility of the flow, and as elements used
in additional calculations. For example, the total pressure loss across
the inlet guide vanes (IGVs) depends on IGV angle and (to a lesser extent)
AM19. The calculations of AM20 and AM25 are necessary for the
determination of flow velocity components at stations 2.0 and 2.5,
respectively. AM29 is used to calculate static temperature at station
2.9, which is used, in turn, to calculate diffuser efficiency.

The calculation of these Mach numbers provides a useful example of
the influence of calculation procedure on the uncertainty of calculated
values AM19, AM20, and AM25 are all calculated using measured or computed

Table II

UNCERTAINTIES OF THE CALCULATED VALUES

Calculation*	AM 19	AM 20	BETA 20	RM 20	AM 25	ALPH 25	BETA 25	P_T 25	AM 29	ETAAD
Uncertainty (%)	1.34	1.41	0.52	0.35	0.62	0.35	0.17	1.00	5.40	0.79

*See Figure 6 for definitions of the calculation names.

total pressure and total temperature at the station of interest along with the continuity equation. Using these total properties and the equation (Ref. 6)

$$\frac{W\sqrt{T_T}}{P_T \, C_D \, A \, C\alpha} = \sqrt{\frac{\gamma}{R}} \; M \left[1 + \frac{\gamma-1}{2} M^2 \right]^{-\left[\frac{\gamma+1}{2(\gamma-1)}\right]} \tag{9}$$

where W is airflow, T_T is total temperature, P_T is total pressure, C_D is discharge coefficient, A is area, α is flow swirl angle, γ is the ratio of specific heats of the flow, and M is Mach number, one can solve for M by an iterative procedure if α is known. Note that at station 2.5, α is not known, so that Euler's Turbine equation is used together with Eqn. (9) to solve iteratively for AM25 and α. (Euler's Turbine equation is obtained by applying conservation of energy and the momentum equation to a stream tube past a rotor blade. For more information see Ref. 7, pages 10 to 13 or pages 17 to 22.)

AM29 is calculated from measured static and total pressure values at station 2.9 using the isentropic relationship (Ref. 6)

$$\frac{P_T}{P_S} = \left(1 + \frac{\gamma-1}{2} M^2 \right)^{\gamma/\gamma-1} \tag{10}$$

where P_S is static pressure. Solving for M yields

$$M = \left\{ \frac{2}{\gamma-1} \left[\left(\frac{P_T}{P_S} \right)^{\frac{\gamma-1}{\gamma}} - 1 \right] \right\}^{\frac{1}{2}} \tag{11}$$

We note from Figure 6 that the influence coefficients for AM29 corresponding to the measurements PS29 and PT29 are the largest coefficients in the matrix. It is interesting to examine the partial derivatives of Eqn. (11) with respect to P_S and P_T. Expressions for these partial derivatives are

$$\left.\frac{\partial M}{\partial P_S}\right|_{P_T} = -\frac{1}{\gamma P_S} \sqrt{\frac{1}{\frac{2}{\gamma-1}\left[\left(\frac{P_T}{P_S}\right)^{\frac{\gamma-1}{\gamma}} - 1\right]}} \left(\frac{P_T}{P_S}\right)^{\frac{\gamma-1}{\gamma}} \qquad (12)$$

and

$$\left.\frac{\partial M}{\partial P_T}\right|_{PS} = \frac{1}{\gamma P_S} \sqrt{\frac{1}{\frac{2}{\gamma-1}\left[\left(\frac{P_T}{P_S}\right)^{\frac{\gamma-1}{\gamma}} - 1\right]}} \left(\frac{P_T}{P_S}\right)^{-\frac{1}{\gamma}} \qquad (13)$$

Dimensionless influence coefficients corresponding to Eqns. (12) and (13) are derived by multiplying (12) and (13) by $(P_S/M)_{nominal}$ and $(P_T/M)_{nominal}$, respectively. Also note from Eqns. (12) and (13) that

$$\frac{P_T}{M} \left.\frac{\partial M}{\partial P_T}\right|_{P_S} = -\frac{P_S}{M} \left.\frac{\partial M}{\partial P_S}\right|_{P_T} \qquad (14)$$

The change in the influence coefficients in (14) with P_S/P_T (or Mach number) is shown in Figure 7.
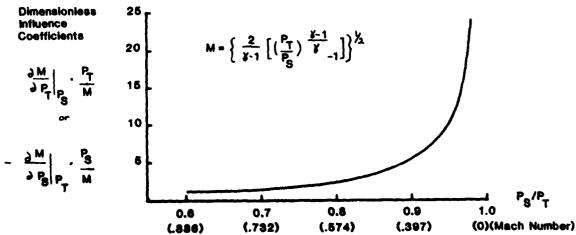
Figure 7. Influence Coefficients versus Mach Number for the Given Equation

We can conclude from Eqns. (12) through (14) and Figure 7 that a Mach number calculation using Eqn. (11) is _quite_ sensitive to errors in P_T or

P_S, particularly for low, subsonic Mach numbers. Therefore, it is not surprising to observe in Table II that the uncertainty of the calculated value AM29 is significantly larger than that for AM19, AM20, or AM25. The important lesson in this example is that calculation procedure may have a strong influence on the accuracy of a computed value. If an engineer has several options for calculation procedure, he should consider the accuracy of the result in selecting the best option.

B. Example 2: Compressor Efficiency

Compressor efficiency is one of the most important calculated values used to characterize the performance of the machine; it can have a very significant influence on the performance of the turbine engine. We have said in an earlier section that the values in the influence coefficient matrix depend upon the magnitudes of the measured values (i.e., the influence coefficient values will vary with compressor speed). In this example we show how the uncertainty of compressor efficiency varies with compressor speed, and why it is particularly difficult to make an accurate determination of compressor efficiency at low speed.

Compressor efficiency is calculated from measured pressures and temperatures at the compressor inlet and exit. Assuming an average value of the ratio of specific heats for the compressor, $\bar{\gamma}$, adiabatic efficiency can be calculated using the equation

$$\eta = \frac{\left(\dfrac{P_{T30}}{P_{T19}}\right)^{\frac{\bar{\gamma}-1}{\bar{\gamma}}} - 1}{\dfrac{T_{T30}}{T_{T19}} - 1} \tag{15}$$

Taking partial derivatives of Eqn. (15) with respect to P_{T30}, P_{T19}, T_{T30}, and T_{T19},

$$\frac{\partial \eta}{\partial P_{T30}} = \left[\frac{(\bar{\gamma}-1)/\bar{\gamma}}{P_{T19}}\left(\frac{P_{T30}}{P_{T19}}\right)^{-\frac{1}{\bar{\gamma}}}\right] \Bigg/ \left(\frac{T_{T30}}{T_{T19}} - 1\right) \tag{16}$$

$$\frac{\partial \eta}{\partial P_{T19}} = \left[-\frac{(\bar{\gamma}-1)/\bar{\gamma}}{P_{T19}}\left(\frac{P_{T30}}{P_{T19}}\right)^{\frac{\bar{\gamma}-1}{\bar{\gamma}}}\right] \Bigg/ \left(\frac{T_{T30}}{T_{T19}} - 1\right) \tag{17}$$

$$\frac{\partial \eta}{\partial T_{T30}} = \left\{-\frac{\left[\left(\frac{P_{T30}}{P_{T19}}\right)^{\frac{\bar{\gamma}-1}{\bar{\gamma}}} - 1\right]}{T_{T19}}\right\} \Bigg/ \left(\frac{T_{T30}}{T_{T19}} - 1\right)^2 \tag{18}$$

$$\frac{\partial \eta}{\partial T_{T19}} = \left\{\frac{T_{T20}}{T_{T19}^2}\left[\left(\frac{P_{T30}}{P_{T19}}\right)^{\frac{\bar{\gamma}-1}{\bar{\gamma}}} - 1\right]\right\} \Bigg/ \left(\frac{T_{T30}}{T_{T19}} - 1\right)^2 \tag{19}$$

The dimensionless influence coefficients corresponding to Eqns. (16) through (19) are

$$\frac{\partial \eta}{\partial P_{T30}} \cdot \left(\frac{P_{T30}}{\eta}\right)_{nom}, \frac{\partial \eta}{\partial P_{T19}} \cdot \left(\frac{P_{T19}}{\eta}\right)_{nom}, \frac{\partial \eta}{\partial T_{T30}} \cdot \left(\frac{T_{T30}}{\eta}\right)_{nom},$$

and $\frac{\partial \eta}{\partial T_{T19}} \cdot \left(\frac{T_{T19}}{\eta}\right)_{nom}$.

Note that

$$\frac{\partial \eta}{\partial P_{T30}} \frac{P_{T30}}{\eta} = -\frac{\partial \eta}{\partial P_{T19}} \frac{P_{T19}}{\eta} = F_1\left(\frac{P_{T30}}{P_{T19}}, \frac{T_{T30}}{T_{T19}}, \bar{\gamma}, \eta\right) \tag{20}$$

$$\frac{\partial \eta}{\partial T_{T30}} \frac{T_{T30}}{\eta} = -\frac{\partial \eta}{\partial T_{T19}} \frac{T_{T19}}{\eta} = F_2\left(\frac{P_{T30}}{P_{T19}}, \frac{T_{T30}}{T_{T19}}, \bar{\gamma}, \eta\right) \tag{21}$$

Eqns. (20) and (21) can be used to compute influence coefficients for expected temperature and pressure ratio combinations at various compressor speeds and nominal efficiencies.

Table III contains pressure ratios (P_{T30}/P_{T19}), temperature ratios (T_{T30}/T_{T19}), and nominal efficiency values for 60 percent, 80 percent, and 100 percent design speed for normal compressor operating conditions at those speeds. Influence coefficients have been derived for this data using Eqns. (20) and (21) and assuming $\overline{\gamma} = 1.4$. Finally, the measurement errors given in Table I and the computed influence coefficients have been used in Eqns. (4) through (6) to yield the uncertainty in the efficiency calculation for the speeds in Table III.

Table III
COMPRESSOR EFFICIENCY VERSUS COMPRESSOR SPEED

% Design Speed	100	80	60
Pressure Ratio $\left(\dfrac{P_{T30}}{P_{T19}}\right)$	8.0	4.1	2.3
Temperature Ratio $\left(\dfrac{T_{T30}}{T_{T19}}\right)$	1.966	1.598	1.332
Nominal Efficiency (%)	84	83	81
Efficiency Uncertainty (%)	.79	1.04	1.57

Note that efficiency uncertainty for 60 percent speed is twice that for 100 percent. The conclusion to be derived from this example is that efficiency calculations at low pressure and temperature ratios require very careful measurements (low bias and precision errors) of inlet and

99

discharge pressures and temperatures, because the influence coefficients are relatively large at these operating conditions.

Also note that we have assumed that bias and precision errors (percent of reading) are the same for 80 and 60 percent speed as they were for 100 percent speed (i.e., the measurement errors in Table I have been used for all calculation results shown in Table III). This, in fact, is probably not a good assumption, because measurement error (percent of reading) is a function of where, in the transducer's range, the measurement occurs. Measurement error can be quite high as a percentage of the measured value at the low end of the transducer range, so the test engineer may be forced to change transducers to obtain the required data accuracy.

V. The Benefits of Using Uncertainty Analysis

We said in the introduction to this paper that measurement processes associated with an experiment will inevitably yield measurement error. If that is true, then a presentation of test data is incomplete without a statement concerning the accuracy of the data. Therefore, one of the major responsibilities of a test engineer is to establish data accuracy as part of the test requirements and then to report the accuracy after the test. Uncertainty analysis is the tool that the engineer uses to do this task. The test objectives and procedure, instrumentation layout, and calculation procedures together with the uncertainty analysis allow the engineer to determine the best test method <u>before</u> the test occurs. Then, following the test, the data can be compared to pre-test uncertainty estimates as a validity check and to identify problem areas. An important benefit from the effort expended in doing an uncertainty analysis is the careful test planning that is an integral part of the analysis. In most cases, this planning increases the probability of a successful test.

Also, the uncertainty analysis provides valuable insight into the test results.

VI. Conclusions

In this paper we have presented the fundamental concepts associated with uncertainty analysis and have used the results of an analysis that was done for a centrifugal compressor test to illustrate the following important points:

1. The precision error of a measured value is inversely proportional t the square root of the number of repeated (over a period of time) or redundant measurements of that value. Redundant instrumentation is very important for reducing measurement uncertainty.

2. The uncertainty of calculated values can be strongly influenced by the calculation procedure; if various procedures are available, the engineer should determine which procedure minimizes data uncertainty.

3. The uncertainty of a measured value can vary greatly depending on where, in the transducer's range, the measurement occurs. Normally, measurements at the low end of a transducer's range should be avoided.

4. The influence coefficients $\partial C_i / \partial M_j$ depend on measured values. Therefore, the uncertainty of a calculated value depends not only on the bias and precision of measured values used in the calculation, but also on the magnitude of the measured values. Influence coefficients must be recalculated for each set of measured data.

Finally, we have attempted to explain the importance of uncertainty analysis. Data accuracy should be specified as part of the test requirements, estimated using uncertainty analysis methods, and then reported after the test. The careful test planning that is an integral part of the analysis increases the probability that test objectives will be clearly defined and accomplished; that, in itself, is strong

justification for conscientious application of uncertainty analysis
techniques in testing.

Symbols

English Symbols

A	Area
B	Bias Limit – estimate of upper limit on unknown bias error
C_i	A computed value based on nominal values of all measured parameters
C_i'	A computed value based on nominal values of all measured parameters except one (which is one percent higher than its nominal value)
C_D	Discharge Coefficient
CRF	Compressor Research Facility
F_1, F_2	Functions
M	Mach number
M_j	A measured value
M_j'	A measured value one percent higher than M
n	Number of repeated or redundant measurements
N	Number of measurements represented in a frequency distribution
P_S	Static Pressure
P_T	Total Pressure
S	Precision Index (standard deviation of measurement frequency distribution)
t_{95}	95th percentile point for two-tailed Students "t" distribution
T_T	Total Temperature
U_{99}	Uncertainty in a calculation or measurement

W	Airflow
X	A measurement in the calculation of S
$\overline{X}$	The average of measurements in the calculation of S

Greek Symbols

α	Flow Swirl Angle
β	Bias Error
γ	Ratio of Specific Heats
$\overline{\gamma}$	Ratio of Specific Heats evaluated at $\dfrac{T_{T30} + T_{T19}}{2}$
η	Adiabatic Efficiency
σ	Precision Error

Subscripts

C_i	Pertaining to the ith computed value, C_i
M_j	Pertaining to the jth measured value, M_j
19,30,etc.	Pertaining to measurement stations shown in Figure 2

References

1. Mitchell, W. et al., "Development of a National Compressor Research Facility," AIAA Paper 77-911, presented at the 13th Propulsion Conference, Orlando, Florida, 11-13 July 1977.

2. Abernethy, R.B. and Thompson, J.W. Jr., Handbook, Uncertainty in Gas Turbine Measurements, AECD-TR-73-5, Feb 1973.

3. Holman, J.P., Experimental Methods for Engineers, McGraw-Hill, New York, 3rd Ed., 1978.

4. Kline, S.J. and McClintock, F.A., "Describing Uncertainties in Single-Sample Experiments," Mechanical Engineering, Jan 1953, pp. 3-8.

5. Abernethy, R.B., "Fluid Flow Measurement Uncertainty," Draft Revision of ISO/DIS 5168, Nov. 1981.

6. Shapiro, A.H., <u>The Dynamics and Thermodynamics of Compressible Fluid Flow</u>, Ronald Press, New York, 1953.

7. Oates, G., ed., <u>The Aerothermodynamics of Aircraft Gas Turbine Engines</u>, AFAPL-TR-78-52, July 1978.

SECTION III

Engineering Education

INTEGRATION OF AN AIRBORNE LABORATORY INTO
THE UNITED STATES AIR FORCE ACADEMY ACADEMIC CURRICULUM

Kent R. Crenshaw*

Abstract

The Department of Aeronautics at the United States Air Force Academy
has introduced a new special topics course -- Aero 495, Flight Test
Techniques -- into its academic curriculum for the Fall semester of 1982.
By using leased aircraft piloted by faculty members, the course attempts
to show students the relationship between the theory of flight mechanics
and actual aircraft performance and flying qualities (specifically,
stability and control). Each cadet enrolled in the course receives four
flights in a light, single-engine aircraft: two flights to determine
aircraft performance (i.e., turns, cruise, climbs and descents) and two
flights to evaluate aircraft flying qualities (i.e., static and dynamic
stability and stalls). Special cockpit instrumentation was designed and
built to measure static stability parameters. This instrumentation
consists of a force gauge, to determine stick force, and rudder pedal
pressure plates using strain gauges to measure rudder forces. The flying
program has been enthusiastically received by cadets and faculty, and its
potential for use in other courses and for research is enormous.

I.   Introduction

The facilities of the Department of Aeronautics Laboratory at the

USAF Academy are without a doubt some of the best in the country. The

subsonic and trisonic wind tunnel facilities, along with the engine test

cells, provide a vital link between classroom theory and real-life,

practical application of the principles of aeronautics. While the

instructional method currently used by the Department tries whenever

possible to link theory with reality, as in the aerodynamics and

propulsion areas of aeronautics instruction, a laboratory course has

always been needed to complement the study of flight mechanics. The

"Balsa Glider Lab," required in Aero 356, Flight Mechanics I, is currently

the only laboratory exercise offered to cadets in the field of flight

mechanics. The "Glider Lab," accomplished during the last quarter, allows

cadets to culminate their study of flight mechanics by applying basic

aircraft design principles to satisfy fundamental aircraft performance and

*Major, USAF, Associate Professor of Aeronautics, DFAN

stability-and-control (S & C) considerations. The balsa glider laboratory experience has always been enthusiastically received by both students and faculty.

Providing the student at the USAF Academy with actual experience in gathering performance and stability-and-control data in order to define these characteristics for a full-scale aircraft has been neglected. To meet this need, the Department of Aeronautics curriculum needed an Airborne Laboratory to link classroom theory with the knowledge of aircraft flight behavior gained from actual flight.

A. Background and Objectives

Attempts have been made in the past to introduce a course using an airborne laboratory into the curriculum. These attempts have involved an assortment of aircraft, including the U-10 Helio-Courier, the U-4, sailplanes, and the T-37B. None of these endeavors was successful, primarily because the aircraft were not available when we needed them. Other contributing factors included conflicts in scheduling, financial restraints, aircraft accidents, and, in general, failure to plan a comprehensive flying program that could be integrated with appropriate classroom instruction. Even though these attempts were failures, the students, faculty, and graduates were overwhelmingly in favor of such a course.

In order to find a solution to this old problem, we began in January 1982 to formulate an airborne laboratory program and to evaluate different aircraft to meet our program needs. Our objectives were to create a uniquely comprehensive curriculum, enhance student motivation and engineering experience, and develop and implement a program in time for the Fall 1982 semester.

B. Program Proposals

In planning our course of action, we examined existing
aeronautical education programs at other institutions around the country.
The United States Naval Academy, Pennsylvania State University,
Mississippi State University, the University of Arizona, and the United
States Military Academy, to name a few, were schools using airborne
laboratories in their curriculums. Out of all the programs we studied,
the United States Naval Academy program appeared to best suit our
requirements. In addition, the Navy's willingness to send us their
course materials, including specific descriptions of how they integrate a
flying laboratory into their Aeronautics education programs, was
particularly helpful.

After reviewing in detail the Naval Academy program, comparing it to
programs at other schools, and analyzing our own, we decided to formulate
a new course using a leased, FAA-certified passenger aircraft with our own
faculty members as pilots. In order to fully appreciate the context
within which this decision was made, some discussion of the program and
aircraft options we looked at is necessary.

The two program proposals presented to the head of the Department of
Aeronautics and his staff suggested the following alternatives:

1. Integration of the airborne laboratory into an existing course
   (Aero 356, 450, 457, or 464).

2. Creation of a new course, Aero 495, entitled "Flight Test
   Techniques for Flight Mechanics."

The first option, which added more material to courses already covering a
vast range of topics, was eliminated because the time required to
accommodate a flying program would detract from the main objectives of the
existing courses as well as those of the airborne laboratory itself.

In contrast, option 2 allowed us to develop a truly comprehensive new laboratory program. The potential scope of a new 495 course appeared to be more than adequate to make a semester course offering.

Our attention then turned to the problem of determining which aircraft to use in support of the laboratory. Criteria for selecting an aircraft, based on evaluations of safety, cost, convenience, and practicality, were finally established as follows:

1. an engine size of at least 180 horsepower

2. four-seat capacity

3. single engine

4. low wing

5. radio and transponder equipped

6. available spare aircraft of the same type

7. ability to base the aircraft at the USAFA Airfield, and

8. established fuel and maintenance support

The selection of an aircraft to meet these criteria was narrowed down to four possible options:

1. use of the Air Training Command (ATC) T-41C aircraft

2. use of the USAFA Aero Club aircraft

3. purchase of our own aircraft, and

4. lease of a commercial aircraft

Option 1 involved problems we have had in the past using somebody else's airplane in the midst of somebody else's flying program. The potential for scheduling conflicts and the amount of time ATC required for their attached pilots to check out and remain current in the T-41C eliminated that option.

Option 2, while attractive from a convenience and cost standpoint, was eliminated because of potential maintenance problems and lack of scheduling priority. The Aero Club, as a "Morale, Welfare, and Recreation

(MWR)" Program, would not give us priority in scheduling their aircraft, particularly if the aircraft we desired was scheduled by a club member for a cross-country flight. The flexibility that would be required on our part to use this option was thought to be detrimental to the continuity of our lab program. In addition, the Aero Club had only two available aircraft that satisfied our performance criteria: the Beech Sierra and the Piper Arrow. The Sierra, an older aircraft, was, and still is, plagued by both minor and major maintenance problems. Since the Piper Arrow is the club's primary cross-country aircraft, it is frequently unavailable. The other club aircraft, while more available, failed our performance criteria.

Option 3 offered us the most control of an aircraft, but it also gave us the most responsibility and added to our workload. In addition, the lead time necessary to coordinate acquisition of an aircraft with the Air Staff is measured in years. Since our objective was to make the Airborne Laboratory operational by the Fall 1982 semester, this option, for now at least, was also eliminated.

The most viable option, and the one used by most of the schools we contacted that have current airborne lab programs, was to lease a commercial aircraft. Hedrick Beechcraft at the Colorado Springs Municipal Airport had the type of aircraft we were looking for and more than just one of each type of aircraft. In addition, their maintenance and fuel support operations appeared to be outstanding. Hedrick had two Beech Bonanzas rated at 285 horsepower, two Beech Sierras at 200 horsepower, and four Beech Sundowners at 180 horsepower available for lease. While leasing from Hedrick would cost, on the average, $20.00 per hour more than leasing any of the Academy Aero Club aircraft, all but one of our aircraft criteria were satisfied by their service. The compromise here was not being able to operate out of the USAFA Airfield. In practice, this has

110

been less of a problem than anticipated. While the USAFA Airfield may be closed because of inclement weather or winds, the Colorado Springs airport is usually open (visual flight rule conditions) and has several more available runways. In addition, conflicts with USAF Academy T41 operations, particularly in the traffic pattern, are avoided.

The decision concerning the type of aircraft to lease from Hedrick was based on cost. The Bonanza, at $85.00 per hour, was eliminated from our planning because it was considered too expensive. The Sierra, at $55.00 per hour, was thought to offer an acceptable performance capability for our required flight operations. The Sundowner, at $40.00 per hour, was found to be adequate for the flying qualities phase of the laboratory. Both aircraft are aerodynamically the same; the Sundowner is the fixed-pitch-prop and fixed-gear version of the Sierra. Both are shown in Figure 1.

After receiving the approval of the Head of the Department of Aeronautics, the program proposal for a new Aero 495 course titled "Flight Test Techniques" and the proposal to lease aircraft from Hedrick Beechcraft was presented to the Dean and the Superintendent of the USAF Academy during February and March of 1982. The program was approved without revision by both, and the Dean supplied matching funds to finance the program through the end of FY82. At this point the decision was also made to enroll only ten cadets in the course for both the Fall and Spring semesters.

The following course description, including the assignment of credit and contact hours, was submitted to the Cadet Curriculum and Scheduling Office of the USAF Academy:

Aero 495. Flight Test Techniques. 1(2)

This course will cover fundamental flight test methods for gathering performance and flying qualities data for fixed-wing aircraft. The theory behind each flight test method will be studied using fundamental and

BEECHCRAFT Sundowner 180
C23 (M-1285 and After)

$S = 146 \text{ ft}^2$

$R = 7.5$

$\bar{c} = 52.7$ inches

BEECHCRAFT
Sierra C24R

$S = 146 \text{ ft}^2$

$R = 7.5$

Figure 1. Three Views of Beechcraft Sierra and Sundowner Aircraft

advanced principles of flight mechanics. Related topics will consist of pitot-static calibration, instrumentation, data reduction, and weight-and-balance. A light, single-engine aircraft is used as an airborne laboratory for obtaining data in flight. Final exam. Prerequisite: Completed Aero 356. Semester Hours: 3.

With this background on the evolution of our program in mind, it might be useful to provide a detailed description of the scope of the course, the instructional method that we intend to use, our scheduling plans, our instrumentation support, and the current status of the flying program.

II. Aero 495. Flight Test Techniques

A. Course Overview

Aero 495 is divided into two phases, performance and flying qualities, which are discussed more fully below. Each cadet enrolled receives four flights during the semester, two in each phase. The Beech Sierra is used in the performance phase and the Beech Sundowner during the flying qualities phase.

1. Performance

The performance phase is covered in lessons 1 through 23. The following topics are dealt with during this phase:

    a. the basics of performance flight testing,

    b. standard and non-standard atmospheric conditions,

    c. calibration and use of the pitot-static system,

    d. reciprocating engine mechanics and propeller theory,

    e. implication and analysis of aircraft weight and balance,

    f. the flight test techniques used in evaluation of each phase

       of an aircraft's typical flight profile (takeoff, climb,

       cruise, level turn, descent, and landing),

g. the analysis and importance of a test plan,

h. aircraft instrumentation and general cockpit layout, and

i. ground and in-flight safety

The primary text used in this part of the course is Light Aircraft
Performance for Test Pilots and Flight Test Engineers by Sean C. Roberts
of Flight Research, Inc., Mojave, California. Supplemental readings
consist of notes provided by the USAF Test Pilot School and by Mr. Ralph
D. Kimberlin of the University of Tennessee Space Institute at Tullahoma,
Tennessee. Excerpts taken from the Pilots' Operating Handbook for the
Beechcraft Sierra C24R are also used. The Roberts text is particularly
good since, in addition to covering most of the classroom topics in
detail, it provides formats for in-flight data cards and data reduction
procedures.

Of particular interest to the cadets is the propulsion aspect of the
course. While the cadets have had at least some exposure to most of the
classroom topics in the performance phase of Aero 495, they have had
little or no experience with propellers. All of our flight mechanics and
propulsion courses address gas-turbine engine technology only. This, of
course, is because most of the aircraft in the active Air Force inventory
are powered by gas turbines (jets).

The flying portion of the performance phase is conducted according to
a test plan, which has a format similar to that used at the Air Force
Flight Test Center. The test plan defines specific performance objectives
that must be met if the advertised performance of the test aircraft is to
be verified. Performance parameters that are evaluated include maximum
speed, range and rate-of-climb capability, service ceiling, and glide
ratio. The test plan also directs that the cadets be divided into two
separate test teams, as shown in Figure 2.

```
                    ┌─────────────────────────────┐
                    │  Department of Aeronautics   │
                    │     Professor and Head       │
                    │         Col. Daley           │
                    └─────────────────────────────┘
                                  │
            ┌─────────────────────┴──────────────────────┐
  ┌──────────────────────┐              ┌──────────────────────┐
  │      Aero 495         │              │     Operations        │
  │   Course Director     │              │  Hedrick Beechcraft   │
  │    Maj. Crenshaw      │              │    Mr. Eberhardt      │
  └──────────────────────┘              └──────────────────────┘
                                  │
                    ┌─────────────────────────────┐
                    │        Course Pilots         │
                    │        Maj. Crenshaw         │
                    │        Capt.Roberson         │
                    └─────────────────────────────┘
            ┌─────────────────────────────────────────────┐
     Test Team A                              Test Team B
   Project Engineers                        Project Engineers
```
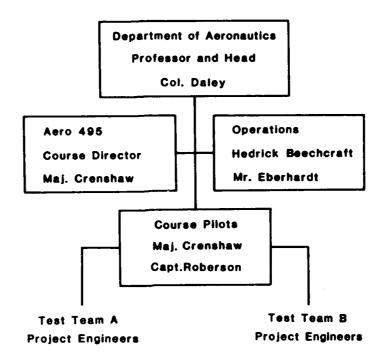
Figure 2.   Test Plan Organization

The cadets, functioning as project engineers under the supervision of a
test director, prepare data cards, prioritize the data to be collected,
and analyze the data after each test flight.   The test plan for the
"Sierra C24R Limited Performance Evaluation" is shown in Appendix A.

Both performance evaluation flights last one hour, with flight 1
dedicated to gathering aircraft cruise and turn performance data and
flight 2 to aircraft climb and descent data.   A "Flight Test Planning
Guide," modeled after the format used at the Naval Academy, is provided to
assist the cadets in their preparation for each flight.   Mission events,
pilot and student responsibilities, and post-flight data reduction
requirements are clearly defined.   In addition, data sheets, data
reduction sheets, and an "Initial Flight Test Report" form modeled after
the Air Force Flight Test Center (AFFTC) Form 365 are also used.

After each flight, the cadets submit for grading a flight report that
satisfies the requirements laid out in the "Flight Test Planning Guide."
Other graded events in the performance phase include a graded review and a
formal oral report presented by each test team on lesson 23.

2. Flying Qualities

The flying qualities phase of Aero 495 consists of lessons 24
through 41. Classroom topics include the following:

    a. a definition of the term and an explanation of the
importance of determining an aircraft's flying qualities,

    b. the study of flying qualities requirements for military
aircraft as defined in the Military Specification for
Flying Qualities of Piloted Airplanes (MIL-F-8785C), and

    c. the flight test techniques needed to evaluate the flying
qualities of an aircraft (lateral-directional static
stability, dynamic stability, longitudinal static stability,
stall characteristics, and maneuvering flight
characteristics).

The primary text for the Flying Qualities phase is another book by Sean C.
Roberts, titled Flying Qualities Flight Testing of Light Aircraft for
Test Pilots and Flight Test Engineers. A supplemental text is also
provided which includes chapters 4, 5, 6, and 7 of the United States Air
Force Test Pilot School notes.

The flying portion of the flying qualities phase is also conducted
according to a test plan. The objectives are to qualitatively and
quantitatively evaluate the Beech Sundowner 180 C23 as a primary trainer
for Class I as defined in MIL-F-8785C. The aircraft is evaluated for
compliance with selected paragraphs of MIL-F-8785C. The evaluation effort
is again organized as shown in Figure 2.

As in the performance phase, both flights in the flying qualities phase are for one hour. Flight 3 is dedicated to evaluating longitudinal and lateral-directional stability and control as well as maneuvering flight. Flight 4 concerns dynamic stability and stalls. A "Flight Test Planning Guide" that covers each flight is again provided to assist in cadet preparation for flying.

Graded events again include two flight reports, a graded review, and a formal oral report by each test team. The semester ends with a review and course evaluation on lesson 42 and a final exam worth 25 percent of the cadet's final grade.

For more detail on the actual test plans, planning guides, and data reduction techniques used in both phases of the course as well as sample calculations, refer to USAFA-TN-83-3.

B. Instructional Method

The instructional method used in Aero 495, shown in Figure 3, is modeled closely after the method used at the United States Air Force Test Pilot School.
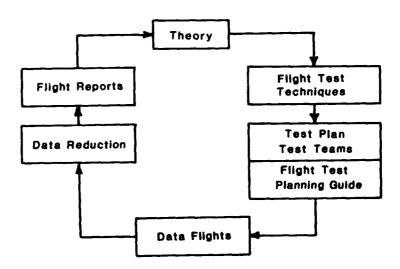

Figure 3. Instructional Method

Note that the flight test techniques are covered during classroom lectures as they apply to each area of study, i.e., cruise, climbs, longitudinal static stability, etc. While the techniques addressed are for light aircraft testing, other techniques for higher performance and multi-engine aircraft are also studied.

Data reduction for the first phase of the course involves standardizing performance data to standard aircraft weights and atmospheric conditions. During the flying qualities phase little data reduction is required. The data reduction schemes for both phases of the course are covered in lesson readings, class lectures, and, more specifically, in the flight test planning guides mentioned earlier.

The performance phase of the course lends itself very well to using computer routines for data reduction, since doing it by hand is a lengthy process. However, in the interest of the cadets learning the procedures by doing, they have not been provided with any computer codes to assist them in reducing data. Realizing and accepting the challenge, two cadets this semester have written data reduction programs for the performance phase of the course. Cadets will be permitted to use these programs in the future, but only as a basis for checking their work.

C. Instrumentation

In the performance phase of this course, the Beech Sierra had the standard cockpit gauges for gathering all necessary parameters. The only additional device required was a stopwatch for timing turns, climbs, and descents. Table I shows the parameters required for each performance data flight.

The flying qualities phase, for which the Beech Sundowner was used, required more than just the standard cockpit instruments. Special instrumentation and procedures were necessary. Stick force and

Table 1

PARAMETERS REQUIRED FOR PERFORMANCE DATA

Flight 1. Cruise and Turn Performance

Cruise Data

Indicated Airspeed
*Tach Time
Outside Air Temperature
Pressure Altitude
Manifold Pressure
Engine RPM
Fuel Flow

Turn Data

All items under
cruise data
Time to turn
360 degrees

Flight 2. Climb and Descent Performance

Climb Data

Indicated Airspeed
*Tach Time
Outside Air Temperature
Pressure Altitude
Manifold Pressure
Engine RPM
Fuel Flow
Vertical Velocity
Time to Climb

Descent Data

Indicated Airspeed
*Tach Time
Outside Air Temperature
Pressure Altitude
Vertical Velocity
Time to Descend

*Used to extrapolate aircraft weight at test points, since fuel
quantity gauges are not accurate.

displacement had to be measured as well as rudder force and displacement, an accelerometer or "g" meter had to be acquired, and a means of center of gravity control was nneeded.

A "g" meter was borrowed from the Academy's Soaring Branch of Airmanship and mounted on top of the aircraft glare shield, as shown in Figure 4.

Figure 4.   "G" Meter Installation

The various displacements and rotations of the controls that we needed were measured as follows: (1) longitudinal "stick" (control push rod) displacement was determined by using a tape measure, as shown in Figure 5, (2) a yardstick was used to measure rudder displacement, as shown in Figure 6, and (3) the rotation angle of the yoke was obtained by marking a reference line on top of the push rod and placing a scale on the instrument panel. This reference scale was marked off in increments of one-fourth from full left rotation to full right rotation. This arrangement is shown in Figure 7.

Figure 5. Measuring Stick Displacement
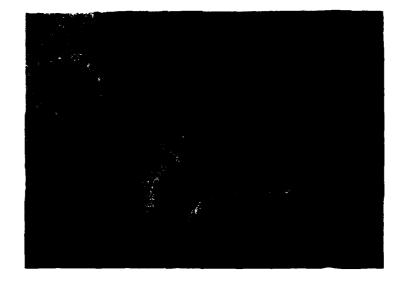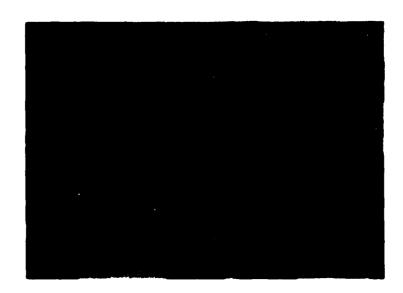

Figure 6. Measuring Rudder Displacement

Figure 7. Measuring Yoke Angle

These rather simple methods proved effective. However, we also needed to measure the force required to hold the "stick" and rudder pedals in various positions. The "stick" force was measured mechanically by a device mounted in the cockpit, as depicted in Figure 8.

Figure 8. Mechanical Force Gauge

The force gauge mounted on the "stick" was calibrated up to approximately 15 pounds. Rudder pedal force required more sophisticated instrumentation. Strain gauges installed in pressure plates mounted on the rudder pedals with velcro straps sent six-volt signals to two meters (one readout for each pedal) mounted in a box held by the cadet in the back seat. The system was powered by the aircraft electrical system (either 14 or 28 volts) through a voltage regulator using the cigarette lighter on the instrument panel. Rudder pedal force readings were calibrated up to 50 pounds. Figures 9 and 10 show the rudder pedal pressure plates and the six-volt readout system.
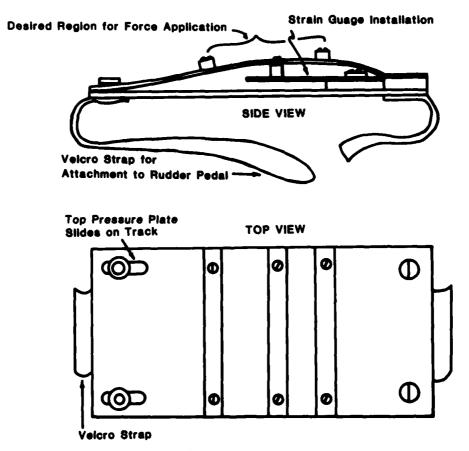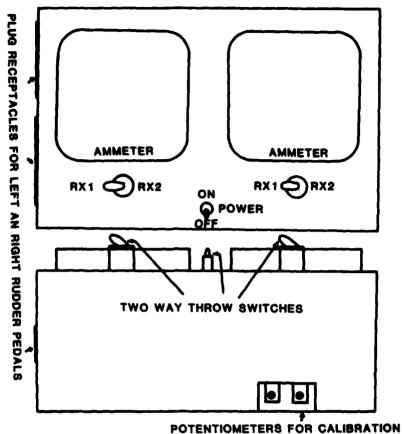
Figure 9. Rudder Pedal Pressure Plate

Notes:
1. R x 1 scale used for smaller, more sensitive force readings. R x 2 scale used for larger readings up to 50 lbs.
2. Ammeters read in milliamps converted to force in pounds from 5 to 50 lbs.

Figure 10. Rudder Force Readout System

Flight 3 required the cadets to gather longitudinal and maneuvering flight data with the center of gravity located first in a forward position and then later in an aft position. Center-of-gravity control was accomplished by using two fifty-pound lead weights secured in the baggage compartment. While cadets were required to check the center of gravity prior to each flight to insure that it was within flight manual limits, this became particularly important when lead ballast was carried.

Table II shows the parameters required for each flight in the flying qualities phase.

Table II

PARAMETERS REQUIRED FOR FLYING QUALITIES DATA

Flight 3. Longitudinal and Lateral Directional S & C;
Maneuvering Flight

Longitudinal Static
Stability Data:

  Indicated Airspeed
  Indicated Altitude
  Outside Air Temperature
*Tach Time
  Engine RPM
  Longitudinal Control
  Displacement ("Stick")
  Longitudinal Control
  Force ("Stick")

Maneuvering Flight Data

  Indicated Airspeed
  Indicated Altitude
  Outside Air Temperature
*Tach Time
  Engine RPM
  Aircraft Load Factor ("g" meter)
  Longitudinal Control
  Displacement ("Stick")
  Longitudinal Control
  Force ("Stick")

Lateral-Directional
Stability Data:

  Indicated Airspeed
  Indicated Altitude
  Outside Air Temperature
*Tach Time
  Engine RPM
**Aircraft Heading
  Bank Angle
  Longitudinal Control
  Force ("Stick")
  Rudder Force
  Yoke Angle
  Rudder Displacement

*Used to extrapolate aircraft weight at test points, since fuel
  quantity gauges are not accurate.
**The heading indicator, assuming an initial trimmed and coordinated
  flight condition, was used to measure sideslip angle.

Flight 4. Dynamic Stability; Stalls

Dynamic Stability Data:

  Indicated Airspeed
  Indicated Altitude
  Outside Air Temperature
*Tach Time
  Engine RPM
  Time Oscillations
  Roll Rates
  Bank Angle Changes

Stall Data:

  Indicated Airspeed
  Indicated Altitude
  Outside Air Temperature
*Tach Time
  Engine RPM

*Used to extrapolate aircraft weight at test points, since fuel
  quantity gauges are not accurate.

In summary, the instrumentation was crude, but it worked. As a spinoff, instrumentation to measure stick and rudder pedal forces is being designed by Engineering 430 students. The Sundowner, in its capacity as the Aero 495 flying qualities test bed, will be used to evaluate that equipment later this semester.

D. Cadet Scheduling and Transportation

With the ten cadets enrolled in Aero 495 making up two test teams and two cadets per flight, five data flights are flown for each of the four missions just discussed. Each of the test teams plans and flies two data flights (two/team) independently, while the fifth flight is a combined effort flown with both test directors to fill in gaps in the data gathered earlier by other test team members or to repeat selected data points. (See Figure 2 for Test Plan Organization.) While two cadets are flying, the other eight meet in the classroom for one hour to prepare for future flights, reduce data, or work on flight reports. Aero 495 is a two-contact-hour course and meets for two hours only during regularly scheduled classroom lecture periods. Cadets who are flying use the two hours of scheduled class time on the flight line, and their early morning military training time for traveling to the airport. Figure 11 shows the Daily Flying Schedule as arranged during the Fall 1982 semester.

Time	Event
0700	Military Taxi to Hedrick Beechcraft
0740	Military Taxi Arrives at Hedrick Beechcraft
0800	Takeoff and Fly Lab Mission
0900	Land and Debrief Lab Mission
0910	Transportation back to Fairchild Hall

Figure 11. Daily Flying Schedule

Approximately 80 minutes are spent on the road traveling to and from the
airport. Transportation to the airport is by military taxi, while return
transportation is provided by the Aero 495 pilot with whom the cadets
flew. Return travel time is used to debrief the flight. Cadets are
prebriefed in the classroom before flying on aircraft orientation and
safety. The safety and mission briefing is repeated again down at the
flight line. Incidentally, the faculty pilot normally arrives at the
flight line at least an hour prior to flying in order to preflight the
aircraft, check the weather, and install any necessary instrumentation.

    E. Flying Program to Data

       As this paper is being written, we are more than three quarters of
the way into the Fall 1982 semester, and the first three data missions
have been completed. Table III is a summary of our flying record to date.

<div align="center">

Table III

AERO 495 SORTIE SUMMARY
</div>

Instructor Only Sorties	7
*Cadet Sorties	16
Maintenance Cancellations	1
*Weather Cancellations	5
Total Sorties	23
Total Flying Hours	27.5

     *One flight air aborted due to weather.

Flexibility in the flying schedule to compensate for weather cancellations
and the single cancellation for maintenance we experienced was achieved by
flying four cadets per day using two airplanes and both course pilots. In
addition, during down time for weather, the classroom lecture schedule was
moved up, which allowed for makeup flying days in place of future class
meetings. Using more than one airplane per flying period worked well

during the performance phase, since no special instrumentation was
required. In the flying qualities phase, however, with only one set of
instrumentation, this option was not a good source of flexibility,
particularly for flight 3, which required the use of elevator and rudder
pedal force measuring devices. Flight 4, consisting of dynamic maneuvers,
rolls, and stalls, did not require special instrumentation other than a
means for measuring yoke angle and a stop watch for timing. The only two
workable options for flights 3 and 4 makeups were to adjust the classroom
lecture schedule and to arrange makeup flights on a volunteer basis during
cadet free time. The last option, however, was the least desirable and
was used only once during the first 15 flights. Our prime objective,
nonetheless, was that all cadets fly all the data flights for which they
were scheduled.

To summarize, the course has proceeded smoothly and as scheduled this
semester, weather and some minor instrumentation problems notwithstanding.
The scope and technical level of the course have been more than adequate
for an undergraduate level of study and the ratio of classroom to flying
time appears to be well-balanced. On a personal note, cadet comments on
the course have been uniformly positive.

F. Potential Improvement Areas

Both instructors and cadets have identified areas in which course
improvement is needed. For example, the aircraft performance envelope
that the cadets are evaluating needs to be increased. To accomplish this,
we would require a bigger, more powerful aircraft; the Beech Bonanza,
rated at 285 horsepower, is under consideration. With our current plan of
60 flights per year (40 cadet sorties and 20 pilot proficiency sorties),
another $2,000.00 per year added to our current budget of $3,500.00 would

cover the cost of using the Bonanza, possibly with three cadets per flight
instead of the usual two.

Another advantage of the airborne laboratory that should be pursued
is the use of this capability to allow cadets in other courses (Aero 499,
Aero 450, Engineering 420, etc.) to make actual engineering applications
of classroom theory to aircraft. This would probably require more
funding, but the potential seems enormous.

III. Conclusions

The Aeronautics Department has the beginnings of an ongoing airborne
laboratory program. The instructional method effectively links the
classroom theory to practical applications of flight mechanics. As a
laboratory for an academic course such as Aero 495 and as a future
research tool, the airplane is a significant addition to our engineering
curriculum. While the future development of our current program lies in
enrolling more cadets, in stimulating research by cadets and faculty, and
even in acquiring our own airplane; for now, at least, we have succeeded
in solving an old problem by leasing an aircraft and using our own faculty
members as pilots.

Appendix

USAF Academy, Department of Aeronautics
Aero 495 - Test Plan
Sierra C24R Limited Performance Evaluation
June 1982

Introduction

A limited performance evaluation of the Beech Sierra C24R will be
conducted at the U.S. Air Force Academy by Department of Aeronautics
(DFAN) faculty pilots and the students enrolled in Aero 495. Flight
testing will be conducted during the Fall 1982 semester from the fifth to

tenth week of classes. Results of the evaluation will be presented in a formal oral report given by each of the two student test teams.

Objectives

The objectives of this evaluation are to determine the Sierra C24R's general performance characteristics and to compare them to the contractor's Flight Manual. In addition, certain contractual guarantees are verified. Specific objectives follow.

A. Takeoff Performance

- determine takeoff power ground roll using the Flight Manual takeoff procedure

B. Climb Performance

- determine the full throttle maximum rate of climb

- determine the full throttle best angle of climb

- verify the climb performance predicted in the contractor's Flight Manual

C. Level Turn Performance

- determine the level sustained turn performance in cruise power at 2,700 rpm

- determine the speed for optimum sustained turn performance at the test altitude

D. Cruise Performance

- determine the airspeeds and rpm for maximum range and maximum endurance as derived from test data

- determine the aircraft drag polar

- compare test results with the contractor's Flight Manual

E. Descent Performance

- determine the propeller windmilling best no wind glide ratio

- determine the best glide speed and minimum sink speed with propeller windmilling

  - compare test results with the contractor's Flight Manual

    maximum glide configuration of 91 knots

F. Contractual Guarantees

  - maximum speed at sea level - 142 knots

  - cruise speed at 75 percent power, 10,000 feet - 137 knots

  - range with 45 minute reserve at 75 percent power at 10,000

    feet - 646 nautical miles

  - rate of climb at sea level - 927 fpm

  - service ceiling - 15,385 feet

  - glide ratio - 1.7 nautical miles per 1000 feet

Authority

    This test program will be conducted by Department of Aeronautics
faculty and students as an integral part of the curriculum for Aero 495, a
course in flight test techniques. The program has the approval of the
Superintendent, the Dean of the Faculty, the Head of the Department of
Aeronautics, and the Director of Flight Operation of Hedrick Beechcraft
Inc.

Test Team Organization

    Test team organization shown in Figure 1 will consist of two DFAN
faculty pilots and two student flight test engineer teams. Each test team
will be assigned to fly with one faculty pilot. A Test Director for each
team will be appointed to coordinate the entire evaluation effort. He
will in turn appoint individuals to be in charge of each test area (i.e.,
data monitors). It will be the data monitor's responsibility to specify
the tests to be flown in support of his test area. Test areas to be
assigned are takeoff, climb, turn, cruise and descent performance.

Scope/Schedule

    The evaluation will consist of sorties as specified in Table 1.

Table 1. Data Sorties

Test	Sorties Per Test Team	Flight Time Per Sortie
Flight #1 Takeoff Performance Cruise Performance Turn Performance	2.5	1.0
Flight #2 Takeoff Performance Climbs and Descents	2.5	1.0
*Total	5.0	

*One sortie will he shared by hoth test teams.

Flight #1 and #2 are scheduled as shown on the Integrated Academics and Flying Schedule for Aero 495. Mission time will not exceed 1.0 hour.

Limitations

The following limitations will be observed during this evaluation.

A. The aircraft will be operated in accordance with the Airplane Flight Manual, FAR Part 91 and all Beech Aero Club Operating Instructions.

B. All data sorties will be flown with one DFAN faculty pilot and two cadets.

C. Testing will only be accomplished under VFR daytime conditions at 10,000 ft MSL and below.

D. All testing will be accomplished within the local flying area of Colorado Springs

Test Aircraft Description

The Beechcraft Sierra C24R, manufactured by Beech Aircraft Corporation, is a six-place, retractable, general aviation aircraft powered by one fuel-injected, 4-cylinder, 200 HP Avco Lycoming engine. The propeller is a Hartzell constant-speed, two-blade, aluminum-alloy prop

with spinner. See Figure 2 for general dimensions and Table 2 for

Aircraft Limitations.

Table 2. Aircraft Limitations

	IAS Knots/mph
Never Exceed Speed (V)	168/193
Maximum Maneuvering Speed (V)	125/144
Maximum Cruising Speed in Turbulent Air (V)	143/165
1G Stall Speed Gear and Flaps Up (2,600 lbs) (power idle)	65/75
Maximum Ramp Weight	2,785 lbs
Maximum Takeoff Weight	2,750 lbs
Maximum Landing Weight	2,750 lbs
Flight Maneuvering Load Factor Flaps Up	+3.8 to -1.9G
Flight Maneuvering Load Factor Flaps Down	+1.9G
Maneuver, Bank Angles No More Than 60 Degrees	
Service Ceiling	15,385 feet
Test Plan Ceiling	10,000 feet

Flight Test Instrumentation

All test data will be hand recorded using standard cockpit
instrumentation. The only exceptions are the use of an accelerometer, a
stopwatch and a cassette tape recorder.

Weight and Balance

Detailed weight and balance records for each aircraft are available
at Hedrick Beechcraft. Prior to every data mission, student test
engineers will calculate aircraft weight and balance data for both takeoff
and landing.

Test Description/Procedures

Unless otherwise noted, all performance tests will be performed with
engine operating, landing gear and wing flaps retracted. All data will be
hand and voice recorded, and manually reduced to standard aircraft weight

and atmospheric conditions. Specific test techniques for each area will
be covered in classroom lectures and handouts from references 2, 3, and 4.

A. Takeoff Performance

The takeoff ground roll will be determined and hand recorded for
each sortie.

All takeoffs will be made with 15 degrees of flaps in accordance
with the Sierra C24R Airplane Flight Manual.

B. Climb Performance

Climb data at different airspeeds will be obtained using sawtooth
climbs. Data will be obtained at 2,700 rpm with mixture adjusted for best
power at test altitudes of 8,000, 8,500, 9,000 and 9,500 feet. Engine
operating limitations as specified in the Flight Manual will be followed.

C. Level Turn Performance

Turn performance for the Sierra will be determined from stabilized
turns at various altitudes and airspeeds. Data will be obtained at 2,700
rpm, or full throttle, between 7,000 and 10,000 feet.

D. Cruise Performance

Cruise performance will be evaluated using the P   versus V
test technique covered in references 2 and 4. Using the backside trim
shot technique, the aircraft will be stabilized at several altitude and
airspeed combinations. Data will be obtained at altitudes between 7,000
and 10,000 feet.

E. Descent Performance

Descent performance will be determined at various airspeeds at
test altitudes of 8,000, 8,500, 9,000 and 9,500 feet. The aircraft will
be operated with the throttle at idle and propeller at high pitch for
gathering descent data. The Flight Manual restriction concerning
prolonged idle settings will be observed.

Training

Both DFAN faculty pilots will have at least an FAA commercial pilot rating and be current in the Beech Sierra C24R in accordance with FAA and Hedrick Beechcraft Aero Club standards.

All cadets enrolled in Aero 495 will participate in the flying portion of the course as passengers only and will receive appropriate aircraft orientation andd safety instruction. All the performance flight tes: techniques required to gather test data will be covered during classroom lectures prior to the flights for which they will be used.

Crew Duties

A. Pilot

1. Check local flying weather.

2. Brief students on mission profile, and ground and in-flight safety.

3. Check maintenance status of aircraft and perform pre-flight.

4. Provide a stopwatch.

5. Provide the tachometer reading at which the aircraft was refueled and the quantity of fuel and oil on board.

6. Act as pilot in command of the aircraft and occupy the left front seat at all times.

B. Students

1. Bring data cards and a clipboard.

2. Complete aircraft weight and balance form.

3. Complete takeoff data using temperature and pressure altitude provided by the pilot.

4. Provide cassette tape player for each flight. (optional)

5. Record tachometer reading at which aircraft was refueled and the quantity of fuel and oil on board.

6. Cadets will be assigned to two man teams for purposes of taking flight test data. Flight crew duties will be rotated each flight. Along with the pilot, who will be primarily concerned with precisely flying the aircraft, both cadets will act as lookouts and notify the pilot immediately of any aircraft sighted. The cadet in the right front seat will act as data observer and timekeeper and the cadet in the rear seat will act as data recorder.

Safety

Flight personnel will adhere to the following while on the flightline and in and around the aircraft:

    a. Smoking is prohibited in or near the aircraft.

    b. Seat belts will be worn at all times.

    c. Flight personnel will be seated in the aircraft prior to engine start and will remain seated until the engine is stopped.

    d. Remain clear of the propeller area.

    e. Do not stand, walk, or lean on the aircraft except in designated areas.

    f. Do not open aircraft windows or doors in flight.

    g. Advise the pilot immediately upon observing another aircraft.

    h. Do not manipulate the aircraft flight controls or engine controls unless told to do so by the pilot.

    i. Advise the pilot of impending airsickness. Use the bag provided, your hat, your shoe, anything except the floor of the aircraft.

    j. Stay clear of taxiing aircraft and other flightline vehicles.

Command and Control

All testing to be accomplished will be for academic purposes only and will be performed within the restrictions of the Flight Manual, Part 91 of the Federal Aviation Regulations, Hedrick Beechcraft Aero Club Rules and the limitations imposed by this test plan.

All information with respect to this test plan is unclassified.

Test Plan Amendments

An amendment to this test plan is required if the flight test envelope is expanded or if any limitations in the test plan are made less restrictive. An amendment to the test plan must be reviewed and approved by the same authority who approved the basic plan.

References

1. Pilot's Operating Handbook and FAA Approved Airplane Flight Manual for the Beechcraft Sierra C24R, Beech Aircraft Corporation, Wichita, Kansas, November 1980.

2. Kimberlin, Ralph D., Performance Flight Testing Lecture Notes, The University of Tennessee Space Institute, Tullahoma, Tennessee, 1982.

3. Performance Theory and Flight Test Techniques, USAF Test Pilot School, Edwards AFB, California, FTC-TIH-79-1, 1 August 1979.

4. Roberts, Sean C., Light Aircraft Performance for Test Pilots and Flight Test Engineers, Flight Research, Inc., Mojave, California, 1980.

SECTION IV

Aeronautical History

HISTORY OF THE HIGH ALTITUDE RECONNAISSANCE AIRCRAFT

Ben R. Rich*

Editor's Note

Mr. Ben R. Rich has been involved in aircraft design since 1950, when he joined Lockheed Corporation. At Lockheed he worked with the legendary C.L. "Kelly" Johnson and was involved in the development of all of the Lockheed high altitude reconnaissance aircraft including the U-2 and SR-71. Since 1975 he has been the director of Lockheed's "Skunk Works" organization, which is noted for developing advanced aircraft. The evolution of these aircraft is described in the following paper presented to the faculty and cadets of the United States Air Force Academy on November 16, 1982.

It is indeed a great pleasure to address the cadets and faculty of the United States Air Force Academy. Today I would like to discuss the four kinds of aircraft development that I have observed at Lockheed's Advanced Development Projects Division or, as it is more commonly known, the "Skunk Works."

First, there is what I call technology push. This is design progression due to technological advances -- in aerodynamics, propulsion, materials, avionics, etc. -- resulting in increased capability in speed, altitude, maneuverability, payload, persistence, and endurance. The evolution of the World War I Spad into today's F-15 is a prime example of technology push; at the Skunk Works I've seen the P-80s develop into the F-104s.

Second, there is progressive growth or the improvement of a particular model with time. Douglas' A-4, for example, advanced through a number of stages before the final product, Model N, was achieved. We had a similar experience at the Skunk Works with the F-94 series, from the A model to the D model.

Third, there is what I call requirement pull: this occurs when an aircraft is designed to meet a special purpose or requirement. Good

---

*Vice President and General Manager, Advanced Development Projects, Lockheed-California Company.

examples are the U-2 and the SR-71, which were developed to meet reconnaissance needs.

Fourth, there is the breakthrough. Examples of this include the jet engine and, more currently, the "low observable" or stealth aircraft.

At the Skunk Works all four kinds of aircraft development occur. I could tell you stories dating from the time of the XP-38 all the way up to the present, but today I will restrict my talk to the evolution of the different Blackbirds -- all developed since I joined the Skunk Works in 1954.

When President Eisenhower's "Open Skies Policy" was rejected by the Russians in 1954, Kelly Johnson, the father of the Skunk Works and my predecessor, made an unsolicited proposal to the Department of Defense to develop a high-altitude aircraft: the U-2A. This aircraft is shown in Figure 1.
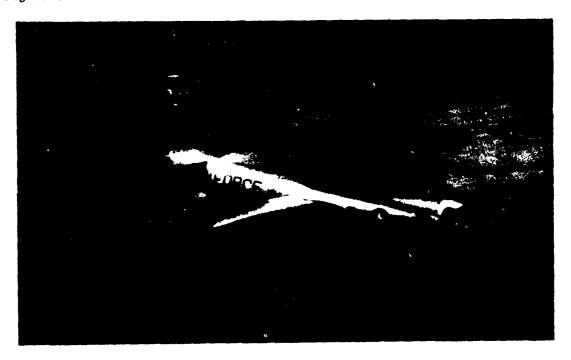

Figure 1. Lockheed U-2A

The U-2A was a 17,000-pound aircraft with an 80-foot wing span powered by a single, modified J-57 Pratt & Whitney turbojet engine -- in effect, a powered glider. This extremely successful aircraft carried only photographic equipment. With time more equipment was added, resulting in an altitude loss of approximately 5,000 feet. To compensate for this loss we retrofitted a larger engine, the Pratt & Whitney J-75 turbojet, modifying the inlet and exit to handle the larger airflow. The fuselage was able to accommodate the larger engine without modification. When electronic intelligence (Elint) and communication intelligence (Comint) gathering equipment were added to the payload, the aircraft weight grew to 24,000 pounds. The added engine thrust, however, more than made up for the added weight, and the airplane more than regained the lost altitude. This airplane was designated the U-2C and is shown in Figure 2.
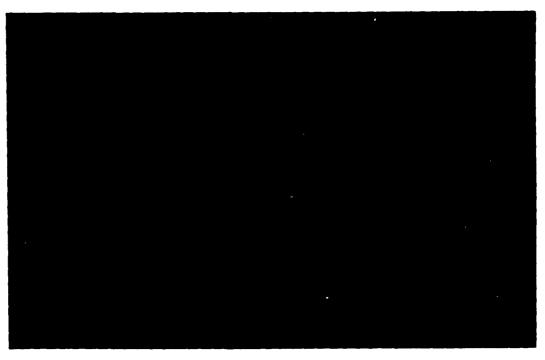

Figure 2. Lockheed U-2C

There was, however, a mismatch between the aerodynamics and propulsive thrust of this aircraft. At altitudes above 70,000 feet the airplane had a cruise speed envelope of four knots. If the airplane flew too fast, it went into Mach buffet; if it flew too slowly, it went into stall buffet. Even with this shortcoming, however, the aircraft was very successful. From 1956 through the eventful May Day of 1960, when a U-2 was eventually shot down by the Russians, we overflew Russia regularly, taking photographs at will. These U-2s were sometimes followed by as many as 35 Russian fighter aircraft flying 20,000 feet below. This annoyed our pilots, since this aluminum shield obstructed their photographs.

In late 1965 Kelly Johnson decided to design a wing for the U-2 that would match the aircraft's thrust. We looked at a variety of fancy wings, such as the Whitcomb supercritical wing, but since none of them could match the lift-to-drag (L/D) ratio of the basic wing at the high values of coefficient-of-lift required, we simply added 40 percent more area to the existing U-2 wing. The resulting aircraft was the U-2R shown in Figure 3.
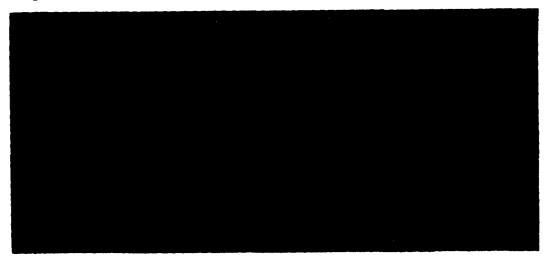

Figure 3. Lockheed U-2R

By now the U-2s were doing all types of real time reconnaissance (i.e.,
the results of the reconnaissance were immediately available), such as
photo, Elint, and Comint. We added the slipper tanks and large wing pods
that are still used today, until the gross weight of the aircraft reached
40,000 pounds. Figure 4 shows a comparison of the U-2C to the U-2R.
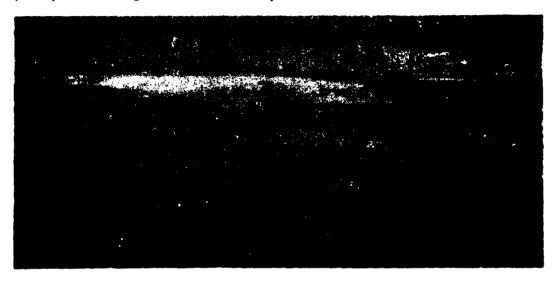
Figure 4. A Side-by-Side Comparison of the U-2C and the U-2R

U-2 production ended in 1968 -- and the 25,000 tools were hidden in five
different places so that some idiot wouldn't have them cut up to sell as
scrap. This shortsighted policy was supposed to save money for the United
States government.

In 1977 Kelly and I met with General David Jones to discuss the
potential of the U-2 as a tactical reconnaissance vehicle. As a result,
General Jones set up a joint Air Force/Army tactical reconnaissance study
which selected the updated U-2 as the best vehicle for this job. In 1979
the tactical version of the U-2 (renamed the TR-1) went back into
production. Since then, six aircraft have been delivered, five to Beale
Air Force Base and one (designated an ER-2) to NASA Ames. Figure 5 is a
photograph of the TR-1.

Figure 5.   Lockheed TR-1

In 1975 the Skunk Works and Sperry/Salt Lake made a proposal to the
Air Force to build a U-2 RPA. An RPA (remotely piloted airplane) differs
from an RPV (remotely piloted vehicle) in that the vehicle can be either
manned or unmanned. The control could be developed with man-in-loop
during early flights; during later flights the pilot could operate the
vehicle from the ground. This system, called the Sperry Flight System, is
now used on the F-102 drones. The RPA could be highly effective in these
days of large, expensive drones with very expensive black boxes;
unfortunately, we never sold the concept.

In 1958, when Russian aircraft began to fire air-to-air rockets at
the U-2s, we began the design of the first of four supersonic Blackbirds,
the A-11* shown in Figure 6. This was a Mach 3+, over-80,000-foot-
altitude, single-place, reconnaissance (recce) aircraft. Its first flight
occurred on April 26, 1962. The A-11 was followed in 1964 by the
interceptor version shown in Figure 7 and in 1965 by the two-place current
reconnaissance aircraft, the SR-71, shown in Figure 8. The latter was
originally named the RS-71, but when President Johnson goofed and called
it the SR-71 we had to change all our drawings.

---

*The term A-12, which is the correct airplane number, is also used. The
 aircraft became known as the A-11 because of an Air Force Press release.

Figure 6. Lockheed A-11

Figure 7. Interceptor Version of Lockheed A-11
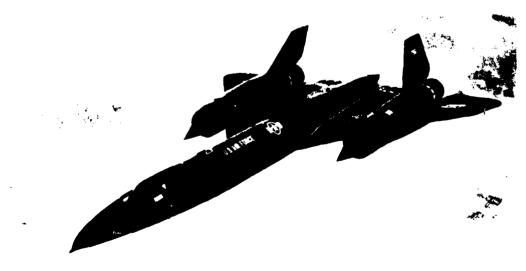
Figure 8. Lockheed SR-71 (Originally Named the RS-71)

145

At the same time we developed a Mach 3+ drone called the D-21. At first, the D-21 was carried on top of the SR-71. This arrangement is shown in Figure 9.

Figure 9. Lockheed D-21 Drone Mounted on SR-71

I believe that this was the first supersonic biplane. The drone was launched at cruise speed above Mach 3. After several successful launch flights, the D-21 had an engine unstart, causing it to bank about 30 degrees. It collided with the carrier, resulting in the loss of both aircraft. Since McNamara and his colleagues had ordered us to cut up the SR-71 tools and sell them as scrap at $.07 a pound, we couldn't afford to lose any more SR-71s. We found that, with the addition of a big booster rocket, the D-21 could be successfully launched from the B-52. A photograph of two D-21s attached to a B-52 is shown in Figure 10.

Figure 10. Two D-21s Attached to B-52

These aircraft became operational in 1969, and we stationed them at Beale
Air Force Base.   Seventeen of the D-21s are currently stored at
Davis-Monthan Air Force Base.

Not everything that we do at the Skunk Works is successful.   Figure
11 shows that we have had some failures too.   But remember, Jesus Christ
was only 91.5 percent perfect: he missed on one of his twelve apostles.

SKUNK WORKS PROJECTS

DEVELOPED BY KELLY JOHNSON

TYPE	APPROX GROSS WT.	COST PERFORM.	SUCCESS	FAILURE	REASON FOR FAILURE
F-80 & F-80A	8600-15,000	EXCEL.	X		
T-33	15,000	EXCEL.	X		
F-94A	17,500	GOOD	X		
F-94C	19,000	EXCEL.	X	X	LOW CRIT. MACH N
XFV-1	13,500	EXCEL.		X	BAD POWER PLANT
SATURN	17,000	GOOD		X	DC-3 PRICE ⅓ OF SAT
CONSTITUTION*	184,000	GOOD		X	GOOD PWR PLT. NOT A
XF-90	22,500	FAIR		X	POOR SPEC & ENGIN
X-7	2,500	EXCEL.	X		
R7V-2	140,000	POOR(MATL)		X	NO PROD. ENGINE
T2V	16,500	GOOD	X		
XF-104	15,500	EXCEL.	X		
YC-130*	110,000	GOOD	X		
U-2	17,500	EXCEL.	X		
JETSTAR	37,500	EXCEL.	X		
CL-400	75,000	GOOD		X	POOR CONCEPT
MODEL A	SECRET	GOOD	X		
YF-12A	SECRET	EXCEL.	X		
SR-71	SECRET	EXCEL.	X		
MODEL D	SECRET	EXCEL.	X		
MODEL R	SECRET	EXCEL.	X		

* PARTIAL SKUNK WORKS METHOD

Figure 11.   A List of Projects at the Skunk Works

Let me expand on one of our boo-boos.   We called this bird, shown in
Figure 12, the CL-400. It was a Mach 2.5, 100,000-foot-altitude,
hydrogen-powered reconnaissance aircraft.

Figure 12. The Proposed Lockheed CL-400

When the Russians brought their liquid hydrogen (LH2) expert Peter Kapitsa out of prison camp in 1955, we thought they were building a hydrogen airplane to shoot down the U-2. So the following year we received a contract to build 16 LH2 recce aircraft. It was to be powered by a new type of engine: a hydrogen expansion engine designed by Pratt & Whitney. Both Pratt & Whitney and the Skunk Works learned how to handle tons of liquid hydrogen -- all before the great space age. The CL-400 carried a quarter of an acre-foot of LH2. Its stable or equilibrium temperature as a liquid is 20 degrees C above absolute zero temperature -253 degrees C (-420 degrees F). One version of the airplane was about two-thirds the length of a football field with the fuselage diameter of a

widebody jet (20 feet) and the wings of an F-104. (In those days we
didn't know too much about blended wing bodies.) The engine's TSFC
(thrust specific fuel consumption, the engine's mass flow rate of fuel
divided by its thrust) was supposed to be 0.6 at Mach 2.5, 100,000 feet;
it turned out to be 0.8. So between the low L/D and high TSFC we had an
airplane with a 1900 nautical mile range with no possible future
improvement.

Even though Pratt & Whitney had the engine running well, and we had
produced 15 miles of metal extrusion, we were going to turn out a
"wide-body" dog (failure). What would happen if the airplane landed at
Mt. Home Air Force Base or Pease Air Force Base? Where would the Air
Force get liquid hydrogen? If it went operational overseas, where could
we find LH2 in Turkey, for example? So Kelly Johnson and Perry Pratt
spoke to either General Irvine or General LeMay and recommended that we
cancel the program. As it turned out, this was a wise decision. If we
had built the 16 airplanes, we would have used one-quarter of the natural
gas coming into Los Angeles -- right in the middle of the 1974 energy
crisis. By the way, we found out why the Russians brought Kapitsa out of
prison when they launched the Sputnik with a LH2-fueled rocket in 1957.

Unfortunately, I cannot tell you what we have been doing for the past
10 years. We seem to score a breakthrough at the Skunk Works every
decade, so if you invite me back in 10 years I will be able to tell you
what we are doing now. I can tell you about a contract that we recently
received for the vehicle shown in Figure 13. The Skunk Works has been
assigned the task of getting "E.T."** back home.

**Extra-Terrestrial (from the movie of the same name)

Figure 13. A Lockheed Vehicle for E.T.

SECTION V

The Engineer's Bookshelf

THE ENGINEER'S BOOKSHELF:
CLASSICS OF CONTEMPORARY SCIENCE WRITING AND THE NUCLEAR DEBATE:
SOME SUGGESTED READING

James M. Kempf*

In the last issue of the Aeronautics Digest I asserted that the best writing on technical and scientific subjects often concerns the impact of technology on human society. The books I am recommending in this essay do too. The writers I call "classics" of contemporary scientific literature all demonstrate wide-ranging knowledge and a stubborn allegiance to a singular belief: that no matter how technical and specialized our contemporary culture has become, true science confirms an age-old faith in the interdependence of knowledge as discovered by the world's only creative and thinking species, man.

As many writers have argued in modern times, a major deficiency of contemporary education is its increasingly narrow training in both intellectual disciplines and professional vocations. The sad result of this narrowed training is the arrogant and ignorant temperament it produces in the technocratic, bureaucratic personalities that thrive in modern institutions. The fear of complexity, of dissent, of inquiring minds, and of the questioning of values often paralyzes contemporary institutions. This timid habit of mind leads to the stifling of free intellect, or more commonly to the division of knowledge into narrowly-focused concerns, so that we lose our sense of the whole and the purpose of education itself, which should be the search not just for facts but for wisdom. By separating the quest for knowledge about things from a quest for the values we require to shape our use of knowledge, modern education too often is satisfied with routine mental exercise, not the more difficult task of building a just civilization.

---

*Assistant Professor of English, USAF Academy

But the concerns of the writers I wish to bring to your attention in this essay and the most widely discussed public issue of this past year concerning technology -- the issue of nuclear weapons -- illustrate the impossibility of separating discussion of technology from the broad issues of social debate. All these writers argue, often from quite different perspectives, that if we are to accurately understand our technically complex civilization, we must understand how science, philosophy, art, politics, history, economics, moral values, and methodology as well as psychology interact and affect our perception of "reality" as well as of truth. I begin by recommending the works of several writers who are, or were, distinguished scientists, and who are also distinguished writers.

Few scientists illustrate better than Lewis Thomas how an expansive mind is a necessary complement of a technical researcher whose focus, on the surface, is the most minute subject of natural science. Thomas is a microbiologist who has spent his life studying biological organisms and systems that the human eye can't even discern. Yet his essays, in two lucid, beautifully written volumes, The Lives of a Cell: Notes of a Biology Watcher (Viking, 1974) and The Medusa and the Snail: More Notes of a Biology Watcher (Viking, 1979), demonstrate a mind that ranges all across the phenomena of human society. Thomas writes about everything, it seems, from the ways in which our advertising industry can misinform the public about the dangers of bacterial organisms to how the fear of genetic manipulation (as well as ignorance of biology) leads to unwarranted political passions that fabricate unnecessary restrictions on recombinant DNA research. Thomas is at ease discussing how disease, death, computers, and public health practices are fruitfully analyzed not only by the techniques of scientists but also by the imaginative perceptions of the Argentinian novelist Jorge Luis Borges. He is, in short, a science writer whose work "educates by delight," an old adage about good art as well as

good science. It is perhaps indicative of his skill that The Lives of a Cell was honored by the publishing industry in 1975 with a National Book Award -- for belles-lettres, not science.

Another equally instructive and learned scientist was the late paleontologist Loren Eiseley. In a number of books about human evolution and history, Eiseley brought to his studies a poetic prose style and a grand historical perspective. His essays range from discussion of ancient paleontology to meditations on the "naturalist" explorations of American writers such as Henry David Thoreau. The best introduction to Eiseley's thought is a volume of selected essays and poetry taken from a lifetime of his work. Titled The Star Thrower (Harcourt Brace Jovanovich, Harvest Books, 1978), this volume reveals Eiseley to be a profound thinker and scientist, one whose writing demonstrates lucid intelligence and familiarity with subjects as diverse as aesthetic philosophy and the "artistic" skills which Cro-Magnon man demonstrated thousands of years ago. Eiseley's essay "The Illusion of Two Cultures" might serve as a representative example of his work. In this essay he angrily denounces the "trade union" habits of much modern science and meditates on his discovery that the most practical tools of ancient man were decorated or designed as works of art. He also shows how the symbolic constructs of human imagination have often become the basis of later scientific theory. Eiseley may well have been an anachronism, since his commanding scientific concern for the multiple dimensions of human society and his sensitive appreciation for the wonder of nature made him turn to poetry as well as science to express himself. His achievement was unique, for among his many professional involvements and awards was his election to the National Institute of Arts and Letters, an almost unheard of honor for a scientist.

Fred Alan Wolf is a physicist and educator who won the American Book Award in 1982 for the outstanding paperback book published the previous

year in science. His book describing the revolutionary concepts of
twentieth-century particle physics and quantum mechanics, Taking the
Quantum Leap, (Harper and Row, 1981), is a pleasurable excursion through
the history of modern physics. The effect of that revolution on our
understanding of natural philosophy and the structure of the universe is a
collateral theme of Wolf's book. By discussing concepts such as
Heisenberg's uncertainty principle and Niels Bohr's and Max Planck's
analyses of wave mechanics and the quantum nature of light, Wolf connects
this history of physics to the concurrent modern revolutions in
psychology, epistemology, and art, which all exploded during the early
part of this century. The virtue of Wolf's book is his ability to
discuss wiith ease and insight the connection between such apparently
disparate subjects as wave mechanics, perceptual psychology, irrational
thought processes, and Dadaist art. Taking the Quantum Leap is a book
well worth reading.

Men like Thomas and Eiseley gently but firmly have warned in several
essays that science itself is too often endangered by rigidity of mind,
hostility to new theory and evidence, and abuse of the prestige which
modern society has bestowed on it. No better example exists of these
dangerous tendencies than Stephen Jay Gould's book, The Mismeasure of
Man (Norton, 1981), which won the National Book Critics Circle Award for
nonfiction in 1981. A science writer of increasing prominence, Gould
traces the scandalous ways in which, in the name of science, such quackery
as phrenology, rigged intelligence testing, and downright falsified data
have been used by so-called scientists over the past century.
Intelligence tests, Gould demonstrates, are often really inspired by
political and economic motives to suppress racial minorities and
economically underprivileged classes of people. His book begins with an
epigraph from Darwin's Voyage of the Beagle:

> If the misery of our poor be caused not by the laws of
> nature, but by our institutions, great is our sin.

It is a curious comment, one calling for moral judgment, by a scientist
often erroneously cited by "social darwinists" as support for social and
economic exploitation. The ways in which the "sins of science" have
fostered social oppression is the subject of Gould's marvelous,
stimulating history of intelligence testing and scientific fraud.

The fact that modern science has been viewed as a subversive threat
to religion and has been antagonistic to religious and mythological world
views for four centuries is a common theme of intellectual history. In a
recent book by one of our finest living scientist-writers, Robert Jastrow,
the director of NASA's Goddard Space Flight Center, this history is shown
to have come full circle. Jastrow's little book God and the
Astronomers (Norton, 1978) briefly describes the history and biographies
of the men who revolutionized modern astronomy and developed the so-called
"Theory of the Expanding Universe." In short discussions of men like
Vesta Melvin Slipher, the astronomer who in 1913 discovered the
"red-shift" of the retreating motion of galaxies, and Edwin Hubble, who
first used Slipher's data and Einstein's relativity theory to postulate
the "Law of the Expanding Universe," Jastrow concludes with a startling
theme. The implications of modern astronomy have led scientists to
conclude that the universe began with a "big bang" and is expanding on a
scale that boggles the mind. The result of this new cosmology is to show
that, instead of conflicting with religious doctrine, the theories of
modern scientific astronomy may in fact be congruent with the religious
views of the origin of the universe. Two other popular books by Jastrow
that show how interdependent the disciplines of both science and
humanistic study have become are Until the Sun Dies (Norton, 1977) and
Red Giants and White Dwarfs (Warner Books, 1967/1979).

Perhaps no recent public debate demonstrates so clearly the
impossibility of trying to isolate science and technology in an artificial
vacuum freed from social implications as the debate the past year over
nuclear weapons policy and technology. That discussions of nuclear policy
are not constrained only by technical questions is evident in the Great
Nuclear Debate of 1982, which touched on a variety of related issues,
including religious values and morality, foreign and military policy and
strategy, economic and political values, and the psychological as well as
biological and physical damage to the western alliance caused by present
military strategy and tactics. For anyone who wishes to know more about
this debate I have listed below a number of articles and books that should
be informative.

Several works in particular are useful starting points if one wishes
to understand the context of the current debate. Two English authors,
E.P. Thompson and Mary Kaldor, have written influential essays and books
that explain the position and attitude of the leaders of Europe's nuclear
disarmament movement. Kaldor's essay "Nuclear Weapons and the Atlantic
Alliance" (in the January 1982 issue of democracy magazine) outlines not
only the European movement's desire to achieve a nuclear weapons-free
continent, but explains the political thrust of the movement, which
includes "an explicit rejection of current relations of power." Tracing
the nuclear policies of the United States and NATO to Cold War history,
Kaldor argues that European political and economic interests have diverged
from the United States, and the problem for Europe is to free itself from
its hostage relationship to both the United States and the Soviets. In
another article, "Beyond 'No First Use': What the Peace Movement Really
Means," (The Nation, June 26, 1982), Kaldor reaffirms the disarmament
movement's position that its real demand is for "changing political

relations" so that Europe does not become the theatre for limited nuclear
war.

Thompson's ideas are summarized in his article "Letter to America,"
The Nation (January 24, 1981), and in two books: Beyond the Cold War: A
New Approach to the Arms Race and Nuclear Annihilation (Pantheon 1981),
and Protest and Survive, co-edited with Dan Smith (Monthly Review Press,
1981). A good analysis of the views of these leaders of Europe's nuclear
disarmament movement is Alan Wolfe's essay "Europe in Search of
Autonomy," The Nation (February 27, 1982).

The reasons behind America's nuclear freeze movement are most
clearly articulated by Randall Forsberg in her essay "A Bilateral
Nuclear-Weapon Freeze," Scientific American (November, 1982). Forsberg
wrote the April 1980 document, "Call to Halt the Nuclear Arms Race," which
led to the June 1982 anti-nuclear rally in New York's Central Park and,
eventually, to the numerous freeze resolutions on the ballot in many
states during the November 1982 elections. The article cited above
outlines the rationale of the freeze campaign, particularly its attempt to
prevent production of new "counterforce weapons" and to freeze current
force levels at a relative position of "parity." The article is
accompanied by excellent charts of the comparative levels of weapon
systems and warheads possessed by the United States and the U.S.S.R.

An equally influential work of the American anti-nuclear movement is
Jonathan Schell's book The Fate of the Earth (Avon, 1982). Schell has
been widely criticized, as well as praised, for his idealistic view that
we must undergo a change of consciousness to save the earth from what he
believes is an increasing risk of nuclear holocaust. Though strongly
criticized for his unrealistic idealism, the virtue of his book is its
delineation of the known facts about nuclear detonations. The dramatic
scene he paints is culled from unclassified government reports, studies of

the National Academy of Sciences, and research data compiled by
biologists, physicists, and medical personnel from experiments conducted
to test nuclear radiation, blast, and heat phenomena. His book has flaws,
but it has succeeded in forcing the general public to think conceptually
about the real consequences of nuclear warfare. That alone is no small
achievement.

Finally, a response to the anti-nuclear movement written in the
spring of 1982 by four members of America's defense and foreign policy
establishment generated wide discussion. The essay "Nuclear Weapons and
the Atlantic Alliance" by McGeorge Bundy, George F. Kennan, Robert S.
McNamara, and Gerard Smith in Foreign Affairs (Spring 1982) describes
these men's proposal for changing America's military strategy to a "no
first use" doctrine. They view their tactic as a way of both allaying
growing public unrest over nuclear policy and reuniting, under a common
policy, the fragmenting forces within NATO. A no first use policy would
"neutralize the highly disruptive" debate and fear in Europe that the
United States wants to fight a limited nuclear war in Europe.

In response to these various positions which I have outlined, scores
of articles and books have been pouring forth from the presses to weigh in
on the debate over western military and nuclear weapons policy. I have
merely tried to list below a number of these essays and books. They
represent the opinions of a large number of influential policy makers,
scholars, and military strategists. They also represent diverse political
viewpoints and, consequently, quite divergent responses to the issue of
nuclear strategy. Many of these authors respond to the ideas of the
authors I have briefly summarized in the preceding paragraphs.

Leon Wieseltier, "Nuclear War, Nuclear Peace: The Great Nuclear Debate,"
The New Republic (January 10 and 17, 1983); Albert Gore, Jr., "The Fork
in the Road: A New Plan for Nuclear Peace," The New Republic (May 5,

1982); Charles Krauthammer, "The Real Way to Prevent Nuclear War," The New Republic (April 28, 1982);

William J. Perry and Cynthia A. Roberts, "Winning Through Sophistication: How to Meet the Soviet Military Threat," Technology Review (July 1982); Lynn R. Sykes and Jack F. Everden, "The Verification of a Comprehensive Nuclear Test Ban," Scientific American (October 1982);

Edward N. Luttwak, "How to Think about Nuclear War," Commentary (August 1982); and Edward Jay Epstein, "Disinformation: Or Why the CIA Cannot Verify an Arms-Control Agreement," Commentary (July 1982);

George Kennan, "Cease This Madness: Our Collision Course with the U.S.S.R.," The Atlantic (January 1981) and "America's Unstable Soviet Policy," The Atlantic (November 1982), and The Nuclear Delusion (1982);

"The Nuclear Debate," Part I by Fred Kaplan, "Russian and American Intentions," Part II by Jerome B. Wiesner, "Russian and American Capabilities," The Atlantic (July 1982); and Peter H. Stone, "The Bomb: The Last Epidemic," The Atlantic (February 1982).

Two influential foreign policy journals have published a continuing series of essays on the nuclear-military policy debate. Foreign Affairs has published the following essays during the past year:

"Nuclear Weapons in the 1980s" (Winter 1981/82) included essays by Spurgeon M. Keeny, Jr. and Wolfgang K.H. Panofsky, "Mad vs. Nuts: The Mutual Hostage Relationship of the Superpowers"; Christopher Bertram, "The Implications of Theatre Nuclear Weapons in Europe"; and Stanley Hoffman, "NATO and Nuclear Weapons."

"Military and Political Policy" (Summer 1982) included essays by Robert W. Komer, "Maritime Strategy vs Coalition Defense"; General Bernard Rogers, "The Atlantic Alliance"; and Karl Kaiser et al., "Nuclear Weapons and the Preservation of Peace: A German Response to No First Use."

The Fall 1982 issue of Foreign Affairs included the essays, "Toward an Overall Western Strategy for Peace, Freedom and Progress," by Hans-Dietrich Genscher; Stansfield Turner and George Thibault. "Preparing for the Unexpected: The Need for a New Military Strategy"; and Francois de Rose, "Inflexible Response."

A similar series of essays has been run by Foreign Policy magazine and includes the following essays:

"Future of Arms Control" (Fall 1981) includes essays by Leon V. Sigal, "Kennan's Cuts"; Peter D. Zimmerman, "Quota Testing"; and David A. Andelman, "Space Wars."

"The Great Strategic Debate" (Winter 1981-82) includes essays by John Steinbrunner, "Nuclear Decapitation"; Robert J. Einhorn, "Treaty Compliance"; and Lawrence Freedman, "NATO Myths."

"The Nuclear Jumble" (Fall 1982) includes essays by Jonathan Dean, "Beyond First Use"; Leon V. Sigal, "Warming to the Freeze"; Jan M. Lodal, "Finishing Start"; and L. Bruce van Voorst, "The Critical Masses."

Two military journals have run continuing analyses of the nuclear debate. The Naval War College Review has recently published the following articles:

Peter D. Zimmerman and G. Allen Greb, "The Bottom Rung of the Ladder: Battlefield Nuclear Weapons in Europe" (November-December 1981);

Donald M. Snow, "Strategic Uncertainty and Nuclear Deterrence," (November-December 1981);

Lt.-Commander T. Wood Parker, "Theater Nuclear Warfare and the U.S. Navy" (January-February 1982).

Several essays in the Naval War College Review issue of September-October 1982 are especially useful:

Laurence Martin, "National Security in an Insecure Age"; Michael Mandelbaum, "The Future of Nuclear Weapons"; Robert Komer, "Is Conventional Defense of Europe Feasible."

The book considered the "classic" study of military strategy in the age of nuclear technology is Bernard Brodie's Strategy in the Missile Age (Princeton University Press, 1959). A good discussion of this book's relevance to current debate and American military strategy is included in Major Leslie J. Hamblin's "Deterrence: After the Golden Age," Air University Review (January-February 1982).

The Air University Review also recently published these useful essays:

Stephen M. Millett, "Soviet Perceptions of Nuclear Strategy and Implications for U.S. Deterrence" (March-April 1982);

Group Captain R. A. Mason, "Western Deterrence: Posture and Rationale"; John Borowski, "Theater Nuclear Arms Control and Forward-Based Systems" (May-June 1982).

There are scores of other articles and books on this issue, and the bibliography expands each week. But the list above should be sufficient

to get anyone who is interested started on reading about the most urgent

issue of technology and policy confronting us today.

FILM
6